1 **Copernicus Atmosphere Monitoring Service - Regional Air Quality Production System v1.0**

2 Augustin Colette[1], Gaëlle Collin[2], François Besson[2], Etienne Blot[2], Vincent Guidard[2,14], Frédérik Meleux[1], Adrien Royer[2],
3 Valentin Petiot[2,14], Claire Miller[2], Oihana Fermond[2], Alizé Jeant[2], Mario Adani[5,16], Joaquim Arteta[14], Anna Benedictow[10],
4 Robert Bergström[11], Dene Bowdalo[8], Jorgen Brandt[4], Gino Briganti[5], Ana. C. Carvalho[11], Jesper Heile Christensen[4], Florian
5 Couvidat[1], Ilia D'Elia[5], Massimo D'Isidoro[5], Hugo Denier van der Gon[12], Gaël Descombes[1], Enza Di Tomaso[3, 8], John
6 Douros[13], Jeronimo Escribano[8], Henk Eskes[13], Hilde Fagerli[10], Yalda Fatahi[9], Johannes Flemming[3], Elmar Friese[6], Lise Frohn[4],
7 Michael Gauss[10], Camilla. Geels[4], Guido Guarnieri[5], Marc Guevara[8], Antoine Guion[1], Jonathan Guth[14], Risto Hänninen[9], Kaj
8 Hansen[4], Ulas Im[4], Ruud Janssen[12], Marine Jeoffrion[2], Mathieu Joly[14], Luke Jones[3], Oriol Jorba[8], Evgeni Kadantsev[9], Michael
9 Kahnert[11], Jacek W. Kaminski[7], Rostislav Kouznetsov[9], Richard Kranenburg[12], Jeroen Kuenen[12], Anne Caroline Lange[6],
10 Joachim Langner[11], Victor Lannuque[1], Francesca Macchia[8], Astrid Manders[12], Mihaela Mircea[5], Agnes Nyiri[10], Miriam Olid[8],
11 Carlos Pérez García-Pando[8,15], Julia Palamarchuk[9], Antonio Piersanti[5], Blandine Raux[1], Miha Razinger[3], Lennard Robertson[11],
12 Arjo Segers[12], Martijn Schaap[12], Pilvi Siljamo[9], David Simpson[10], Mikhail Sofiev[9], Anders Stangel[9], Joanna Struzewska[7],
13 Carles Tena[8], Renske Timmermans[12], Thanos Tsikerdekis[13], Svetlana Tsyro[10], Svyatoslav Tyuryakov[9], Anthony Ung[1],
14 Andreas Uppstu[9], Alvaro Valdebenito[10], Peter van Velthoven[13], Lina Vitali[5], Zhuyun Ye[4], Vincent-Henri Peuch[3], Laurence
15 Rouïl[1, ^a]

16 [1]INERIS: Institut National de l'Environnement Industriel et des Risques, Verneuil en Halatte, 60550, France

17 [2]Météo-France, Saint-Mandé, 94165, France

18 [3]ECMWF: European Centre for Medium-Range Weather Forecasts, Reading, RG2 9AX, United Kingdom

19 [4]Aarhus University: Roskilde, 4000, Denmark

20 [5]ENEA: Italian National Agency for New Technologies, Energy and Sustainable Economic Development, Bologna, 40129,
21 Italy

22 [6]Forschungszentrum Jülich GmbH, ICE-3, Institute of Climate and Energy Systems - Troposphere, 52428 Jülich, Germany

23 [7] IEP-NRI: Institute of Environmental Protection - National Research Institute, Warsaw, 00-001, Poland

24 [8]BSC: Barcelona Supercomputing Center, Barcelona, 08034, Spain

25 [9]FMI, Finnish Meteorological Institute, Helsinki, 00-001, Finland

26 [10]MET Norway: Norwegian Meteorological Institute, Oslo, 0372, Norway

27 [11]SMHI: Swedish Meteorological and Hydrological Institute. Norrköping, SE-601 76, Sweden

28 [12]TNO: Netherlands Organisation for applied scientific research, Utrecht, 3584, The Netherlands

29 [13] KNMI: Royal Netherlands Meteorological Institute, De Bilt, 3730, The Netherlands

30 [14]: Centre National de Recherches Météorologiques - UMR 3589 CNRS/Météo-France, Toulouse, 31000, France

31 [15]. Catalan Institution for Research and Advanced Studies (ICREA), 08010, Barcelona, Spain

32 [16] Centro Euro-Mediterraneo sui Cambiamenti Climatici, 40127 Bologna, Italy

33 ^a: now at: ECMWF: European Centre for Medium-Range Weather Forecasts, Reading, RG2 9AX, United Kingdom

34 *Correspondence to*: Augustin Colette (augustin.colette@ineris.fr)

Abstract

The Copernicus Atmosphere Monitoring Service (CAMS) delivers a range of full, free and open products in relation to atmospheric composition at global and regional scales. The CAMS Regional Service produces daily forecasts, analyses, and reanalyses of air quality in Europe. This Service relies on a distributed modelling production by eleven teams in ten European countries: CHIMERE (France), DEHM (Denmark), EMEP (Norway), EURAD-IM (Germany), GEM-AQ (Poland), LOTOS-EUROS (The Netherlands), MATCH (Sweden), MINNI (Italy), MOCAGE (France), MONARCH (Spain), SILAM (Finland). The project management and coordination of the service is devoted to a Centralised Regional Production Unit. Each model produces every day 24h analyses for the previous day and 97h forecasts for 19 chemical species over a spatial domain at 0.1x01. degree resolution (approximately 10km x 10km) with 420 points in latitude and 700 in longitude and 10 vertical levels. Six pollen species are also delivered for the surface forecasts. The eleven individual models are then combined into an ENSEMBLE median. In total, more than 82 billion data points are made available for public use on a daily basis.

The design of the system follows clear technical requirements in terms of consistency in the model setup and forcing fields (meteorology, surface anthropogenic emission fluxes, and chemical boundary conditions). But it also benefits from a diversity of in the description of atmospheric processes through the design of the eleven European Chemistry Transport Models (CTM) involved.

The present article aims to provide a comprehensive technical documentation, both for the setup as well as for the diversity of CTM involved in the Service. We also include an overview of the main output products, their public dissemination and the related evaluation and quality control strategy.

1   Introduction

The Copernicus Atmosphere Monitoring Service (CAMS, atmosphere.copernicus.eu/) is the core global and regional atmospheric environmental service operated by the European Centre for Medium-Range Weather Forecast (ECMWF) within the European Union Copernicus Earth Observation Programme. It provides a range of full, free, open, and quality assured products in relation to global and regional air quality, inventory-based emissions, observation-based surface fluxes of greenhouse gases and from biomass burning, solar energy, ozone and UV radiation, and climate forcings (Peuch et al., 2022).

We focus here on the regional production service (https://atmosphere.copernicus.eu/european-air-quality-forecast-plots/) which provides daily 4-day forecasts of the main air quality species and analyses of the day before, as well as posterior re-analyses using the latest observation datasets available for assimilation. It constitutes today the reference air quality forecasting system at European scale by building upon a distributed production of eleven chemistry transport models operated in ten European countries, with a Centralised Regional Production Unit to ensure a consistent implementation. Such a comprehensive air quality forecasting system operated at continental scale has no equivalent in the world.

Air quality monitoring and forecasting constitute an essential activity to improve the knowledge of atmospheric composition and air pollution patterns and identify short and long-term mitigation strategies. In the European legislation, the Directive (Ec, 2008) on ambient air quality and cleaner air for Europe of the European Parliament and of the European Council, defines limit and target values for regulatory ambient air concentrations and improvement of ambient air quality to avoid, prevent or reduce harmful effects on human health and the environment. To this end, it sets out the methodological requirements for the assessment of ambient air quality in Member States which are based on the implementation of adequate monitoring systems, typically relying on reference and standardised instruments operated at air quality monitoring stations whose data are reported to the Air Quality e-reporting database maintained by the European Environment Agency (which subsequently makes the data publicly available). A revision of the Ambient Air Quality Directive was adopted by the European Council in October 2024, the revision includes amongst other features, a stronger emphasis on the use of air quality models as well as an explicit reference to the Copernicus Atmosphere Monitoring Service as a trusted source of information products and supplementary tools to support reporting activities in relation to forecasting and management of air pollution episodes.

Modelling comes as a complementary information on ambient air quality. Fitness for forecasting purposes of air quality modelling has been widely documented (Zhang et al., 2012a, b), but air quality models are also essential to produce exposure maps through data assimilation or data fusion. In such processes, the prior modelled estimates of surface air concentrations of the main air pollutants are combined with in situ or remote sensing observations to produce improved mapping of air pollution, typically for use in health impact assessment or epidemiological studies (Shaddick et al., 2020). Air quality modelling and reanalyses are also typically used to anticipate ex-ante and assess ex-post the effectiveness of policy mitigation strategies. The

84 projections and hindcasts performed in the framework of the Convention on Long Range Transboundary Air Pollution
85 (CLRTAP) of the United Nations Economic Commission for Europe Geneva Air Convention and its Gothenburg Protocol
86 constitute a good example of atmospheric modelling activities in support of policy decisions at European scale (Maas and
87 Grennfelt 2016).

88 Whereas several European countries or selected metropolitan areas operate their own air quality modelling system, there is
89 also a need to produce air quality forecasts and analyses over the whole European continent: to provide background data for
90 those local systems (chemical boundary conditions), for the areas not covered by any national system, or just as complementary
91 information. The Copernicus Atmosphere Monitoring Service has played that role since 2015. It builds upon the earlier
92 research and development phases initiated since 2005 through European collaborative research and innovation projects: GEMS
93 (Hollingsworth, 2008) and MACC, MACC-II, and MACC-III (Marécal et al., 2015; Peuch et al., 2014).

94 The unique setup of the system allows it to reach an unprecedented level of quality and robustness by relying on a set of
95 stringent common requirements combined with a large variety of Chemistry-Transport Models (CTMs). Since 2022, an
96 ensemble of eleven CTMs have been used: CHIMERE (INERIS, France), DEHM (Aarhus Univ., Denmark), EMEP (Met
97 Norway), EURAD-IM (Forschungszentrum Juelich, Germany), GEM-AQ (IEP-NRI, Poland), LOTOS-EUROS (TNO and
98 KNMI, The Netherlands), MATCH (SMHI, Sweden), MINNI (ENEA, Italy), MOCAGE (Météo-France, France),
99 MONARCH (BSC, Spain), SILAM (FMI, Finland). Using an ensemble of CTMs allows at the same time to minimize the risk
100 of failure in the daily operational production, and to increase the skill of the forecast (Galmarini et al., 2013). But consistency
101 in the implementation is key to ensure the continuous improvement of the system, hence the crucial role of the CAMS Regional
102 Central Production Unit led by Météo-France and INERIS.

103 Each model delivers every day 24h analyses and 97h forecast for 19 chemical species over a spatial domain at 0.1x0.1 degree
104 resolution (approximately 10km x 10km) with 420 points in latitude and 700 in longitude and 10 vertical levels. Additionally,
105 surface forecasts of six pollen species are delivered. With the 11 individual models and one ENSEMBLE median, it is a total
106 of almost 82 billion data point made available for public use every day.

107 The results of the CAMS Regional Service are made publicly available as quick looks on the website
108 atmosphere.copernicus.eu/european-air-quality-forecast-plots and the numerical outputs are disseminated on the Copernicus
109 Atmosphere Data Store: ads.atmosphere.copernicus.eu. The typical use of the forecasts is as background information used by
110 national and local air quality agencies, in addition to their knowledge about specific local air pollution sources. This can be
111 done either qualitatively by the consultation of available online viewers, or by using the numerical data to feed downstream
112 chemistry-transport, gaussian, or machine-learning models. The use of reanalyses is rather for policy applications (for

113 regulatory reporting obligations or to assess the impact policy interventions through trends analyses) or exposure assessment
114 in health impact studies.

115 The aim of the present article is to provide a transparent and detailed documentation to serve as a reference for the user of
116 CAMS Regional Air quality Products. It constitutes an update of the previous similar article devoted to the MACC regional
117 forecast system (Marécal et al., 2015), whereas the system was still in research mode at the time and not fully operational. A
118 focus on regional activities within the overall CAMS portfolio was also described in (Peuch et al., 2022). The CAMS Regional
119 production system has evolved continuously over the past. In the present article, we provide a detailed description of the system
120 as it stands in 2024. But since the near real time production of forecast and analysis remains available for public use with a 3-
121 year retention time, and reanalysis data remain available since the beginning of the production, we also provide some
122 information about the major evolutions in the recent past.

123 The main characteristics of the centralised production system are introduced in Section 2. This section covers the overall
124 production workflow, but also the common features and requirements which apply to the distributed production of individual
125 modelling teams such as the common external forcing data. Since the use of an ensemble of eleven different chemistry transport
126 models is an important specificity of the service, we devote a large part of the paper in Section 3 to summarize the formulation
127 of each model and how they adapt specifically to the requirement of the CAMS Regional Production System. The post-
128 processing as well as some elements regarding the evaluation and quality control or the main uses of the production are
129 presented in Section 4. In the conclusion (Section 5) we refer to the short and long-term development priorities to ensure the
130 performance and sustainability of the system over the long term.

2 Centralised Regional Production Unit

2.1 Organisation of the production system

The CAMS regional production relies on a quite unique ensemble of 11 individual models whose daily operation is distributed amongst 11 modelling centres in ten European countries. The coordination is handled by the Central Regional Production Unit (CRPU) which is led by Météo-France, with the support of INERIS for model development matters and reanalysis production (Figure 1).

The CRPU defines the design of the regional production system under the auspices of ECMWF. This includes setting the guidance and requirements for the implementation of individual models as well as continuous evolution in order to maintain the system within the state of the art. The CRPU is also in charge of contractual matters and relations with the providers of input data as well as the delivery of model results to the Atmosphere Data Store for public use (Section 4.3).

In earlier MACC phases and the first CAMS regional project, only 7 models were contributing to the distributed operational production: CHIMERE, EMEP, EURAD-IM, LOTOS-EUROS, MATCH, MOCAGE, and SILAM. As of October 2019, DEHM and GEM-AQ joined the operational system. As of June 2022, MINNI and MONARCH joined the production.

144
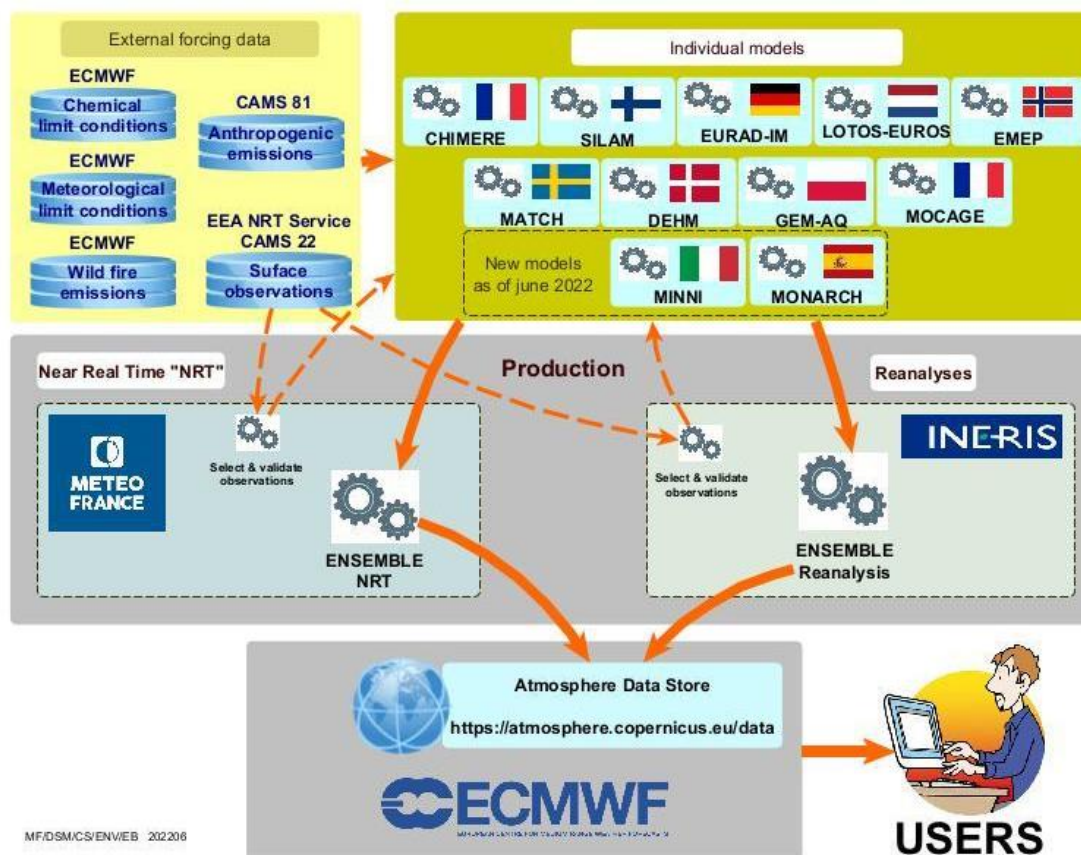
Figure 1: Schematic of the CAMS Regional Production workflow. Top-left the external forcings (anthropogenic emissions, meteorology, boundary conditions) and in-situ observations for assimilation and evaluation. Top right: eleven regional chemistry-transport model operated in ten European countries. Middle: Meteo-France (for the near real time) and INERIS (for the reanalysis) centralise the individual productions. Bottom: the results are disseminating to the Atmosphere Data Store.

2.2 Modelling products

The CAMS regional system includes both daily 4-days forecasts and several analysis products. All of them are provided from both eleven individual CTMs results and an ENSEMBLE product which is constituted by the median of individual models at each grid point.

Hourly near-real time forecasts (NRT/FC) are released every day with a 4 days horizon (from 0 to 96hrs forecasts). They rely on chemistry-transport outputs, some of which are initialised on the basis of the previous analysis (see details in Section 3). The ENSEMBLE NRT/FC fields are made available publicly each day at 08:00 UTC for forecast horizon 0 to 48hrs (day 1 and day 2), and at 10:00 UTC for forecast horizon 49 to 96hrs (day 3 and days 4).

157   As of January 2024, the list of species in the NRT/FC includes the following gases: ozone (O_3), nitrogen oxide (NO), nitrogen

158   dioxide (NO_2), carbon monoxide (CO), sulphur dioxide (SO_2), glyoxal (CHOCHO), formaldehyde (HCHO), ammonia (NH_3),

159   total Non-Methane Volatile Organic Compounds (NMVOC), total Peroxy-Acetyl Nitrates (PANs). Particulate matter (PM)

160   are included as : $PM_{2.5}$ (smaller than 2.5µm), PM_{10} (smaller than 10µm). The following tracers in the $PM_{2.5}$ fraction are also

161   provided: secondary inorganic aerosols (SIA), total elemental carbon (EC), EC fraction related to residential emissions, total

162   organic matter. In the PM_{10} fraction, the tracers include desert dust, sea salt and wildfires. In addition, six pollen species are

163   included: birch, olive, grass, alder, mugwort and ragweed.

164   Hourly near-real time analysis (NRT/AN) are released each day by 12:00 UTC for the previous day. Here, each individual

165   model is corrected to minimise error with observed air pollutant concentrations over Europe. For the latest reanalysis available

166   on the ADS as of January 2024 (covering the year 2021), the list of species is: for O_3, NO, NO_2, CO, NH_3, NMVOC, PM_{10},

167     $PM_{2.5}$, PM_{10} wildfires, PM_{10} dust, EC total, EC residential, PAN, SIA, SO_2. For earlier years, not all of these species are

168   available, and in the future the list will continue expanding to catch up with the full species set in the daily forecast production.

169   Note that observations are not available for all of those species, individual components contributing to the total PM_{10} or $PM_{2.5}$

170   mass are scaled according to the assimilation of total PM_{10} or $PM_{2.5}$ measurements, and pollen species are not assimilated.

171   The daily analyses products are supplemented by an interim reanalysis (IRA) and a validated reanalysis (VRA). Both rely on

172   the same modelling tools as the NRT production, including assimilation strategy. But the observations taken into account

173   differ. Acknowledging that for the NRT/AN production some observations can be missing or not validated, daily analyses are

174   reproduced with a 20 days delay in the IRA. This time gap is considered sufficient to fix most failures in NRT data flows and

175   maximise the number of available measurement data. The interim reanalysis is subsequently consolidated and delivered in the

176   first months of Y+1. Since all observations are only definitively validated by European member states by the end of the

177   following year (Y+1), the full year Y is reprocessed in Y+2 to produce the VRA of the corresponding year.

178   **2.3   Air quality observations**

179   The gathering, filtering and selection of observations is centralised by the CRPU and subsequently disseminated to individual

180   modelling teams which apply different assimilation algorithms even though the exact same stations are assimilated by each

181   model (see details in Section 3). All observation data are obtained from the Air Quality e-reporting database[1] maintained by

182   the European Environment Agency where near real time "up-to-date" (UTD) and validated observations are reported, in

183   particular for countries of the European Union which are expected to do so with respect to the European Directives.

---

[1] https://www.eea.europa.eu/data-and-maps/data/aqereporting-9, last accessed 30/10/2024

184   An important step lies in the filtering and selection of data, where an objective classification is applied based upon the temporal

185   variability patterns of the air pollutant concentrations to differentiate background and proximity stations (Joly and Peuch,

186   2012). Traffic and industrial sites are excluded from the assimilation strategy, but since November 2020 stations falling in

187   classes 1-7 of the Joly & Peuch classification are included, which means broadly that urban background sites are taken into

188   account, whereas earlier than November 2020, only suburban and rural sites were included. This way, even if the spatial

189   resolution of the CAMS Regional Production is 10x10km, we ensure the relevance of the modelling setup to capture urban

190   background air quality.

191   Approximately 2-third of the stations' data are distributed by the CRPU for assimilation (both for NRT/AN and IRA&VRA),

192   while the rest of the data are kept for evaluation (see Section 4.2).

193   At present there is no centralisation of the dissemination of any satellite observation of atmospheric composition even if many

194   individual modelling teams already assimilate satellite data, and this is expected to further develop in the coming years (See

195   details in the presentation of individual models in Section 3).

2.4   Modelling domain

197   The modelling domain covers Europe within 25°W to 45°E longitude and 30°N to 72°N latitude at a 0.1°x0.1° resolution.

198   Whereas in earlier phases of the project some individual models were operating at slightly lower resolution (about 0.2°), today

199   all models operate on a native resolution of about 0.1°. Covering the whole region is a strong requirement, and all models

200   deliver data over the entire domain, which means that some of them perform the forecast on a slightly larger domain in order

201   to include a buffer area or cope with differing geographic projection (see details in Section 3). The spatial extent has evolved

202   marginally in recent years, it was only reaching up to 70°N until June 2019.

203   The strategy for the vertical discretisation is left open for individual contributing models, but there is a common requirement

204   in the delivery of model results on common vertical levels. As of January 2024, the complete list of vertical levels is: surface,

205   50m, 100m, 250m, 500m, 750m, 1000m, 2000m, 3000m, and 5000m above ground. This has evolved substantially in recent

206   years, only surface concentrations were provided in the earlier phases of CAMS, and different lists of vertical levels have been

207   archived in the past for near real time forecast, analyses, and reanalysis products.

2.5   Meteorology and chemical boundary conditions

209   The meteorological fields used to force the individual operational CTMs are from the operational IFS (Integrated Forecasting

210   System) daily meteorological forecasts of the European Centre for Medium-Range Weather Forecasts (ECMWF). The spatial

211   resolution of the IFS forecast has increased in time, it is about 9km as of 2024. The exact list of meteorological parameters

212 used to drive the individual CTMs differs depending on the models (see details in Section 3). Most of them use the forecast

213 starting at 12:00 UTC on D–1 but there might also be some deviations to account for operational constraints.

214 The chemical boundary conditions are also obtained from ECMWF but using the configuration of the IFS including chemistry

215 (Flemming et al., 2015; Rémy et al., 2019) operating at approximately 40km spatial resolution. This configuration of the IFS

216 model runs forecasts twice daily from 00 and 12 UTC and the data are available every hour (for surface fields) and every 3

217 hours (for model- and pressure-level fields). The model results are made available for further use as boundary conditions of

218 regional models through different dissemination routes including the MARS archive server of ECMWF, a dedicated ftp access

219 for the regional CAMS operational models and the atmosphere data store (ADS) of Copernicus.

220 The list of species used as boundary conditions for the regional CAMS models is given in Table 2. Further details are available

221 through the CAMS User Support website[2] and (Morcrette et al., 2009). All aerosol species are provided as dry PM, except for

222 sea salt, whose mass and size is provided at a relative humidity of 80%. The mass of the corresponding dry sea salt is 1/4.3

223 smaller and the radius is half of the sea salt at relative humidity of 80%.

2.6 Surface emissions

2.6.1 Anthropogenic emissions

226 Using identical anthropogenic emissions in all the eleven individual models is essential for the consistency of the CAMS

227 Regional products. The so-called TNO-MACC-III (Kuenen et al., 2014) emission inventory was used for several years in the

228 past. Since June 2019, it has been replaced by the CAMS-REG emissions inventory, which is regularly updated (Kuenen et

229 al., 2022). The CAMS-REG inventory is based on official national totals of air pollutant emissions reported in compliance

230 with the European Directive on National Emission Reduction Commitments (2016/2284/EU) and the Gothenburg Protocol of

231 the LRTAP Convention. Additional processing is applied to ensure consistency in the dataset by making corrections and

232 performing some gap-filling where information is missing. A consistent spatial distribution for gridded emission datasets is

233 applied at $0.05° \times 0.1°$ resolution. Since June 2021, the CAMS Regional production has used an improved version of the

234 CAMS-REG inventory which substituted national estimates of wood burning emission in order to cope with a well-established

235 inconsistency in the reporting of condensable emissions (Denier Van Der Gon et al., 2015).

236 The use of officially reported emissions induces a subsequent delay in the successive updates of the emission datasets. The

237 Emissions for year Y, are reported in March Y+2. Then they undergo verification, gap filling and spatialisation before being

---

2   https://confluence.ecmwf.int/display/CKB/CAMS%3A+Global+atmospheric+composition+forecast+data+documentation
(last accessed 30/10/2024)

238   considered for implementation in the CAMS Regional production. The emissions being used for the day-to-day forecasts are
239   thus generally based on national emissions reported about 3 years earlier. In order to cope with this limitation, the CAMS-
240   REG emission inventory developed a proxy inventory for the recent years, still based on the officially reported emissions. This
241   way, the emission implemented in late 2023 in the regional production could be based on an estimate for the year 2022.

242   Only the spatialised annual fluxes of NO_x, SO_x, non-methane volatile organic compounds, (NMVOCs), NH_3, CO, PM_{10} and
243   $PM_{2.5}$ emissions are prescribed for all models. The subsequent disaggregation required in CTMs in terms of (i)
244   hourly/daily/weekly/monthly profiles, (ii) vertical injection height, and (iii) mapping towards model chemical species is left
245   open for individual modelling teams. Default information is nevertheless provided regarding the temporal disaggregation
246   (Guevara et al., 2021) as well as the ventilation of total VOC or total PM on individual VOC species or aerosol species,
247   respectively.

2.6.2   Biogenic, natural and wildfire emissions

249   Biogenic emissions are left to the choice of individual operational models, most of which include their own online calculation
250   of emissions from vegetation and other natural sources. They include soil emissions for (i) mineral dust resuspension, (ii) soil
251   NOx or even (iii) sea salt within the European domain.

252   The only coordination regarding ecosystem emissions concerns wildfires where all models are expected to use the Global Fire
253   Assimilation System (GFAS) product (Kaiser et al., 2012) provided by CAMS. GFAS is based on fire radiative power retrievals
254   from data of the Moderate Resolution Imaging Spectroradiometer (MODIS) instruments aboard the Terra and Aqua satellites.
255   GFAS provides hourly emission data with a 8-hr delay compared to real time. Each individual modelling team retrieves GFAS
256   emission when initiating their forecast. As the individual forecasts are initiated between 12:00 D-1 and 03:00 D+0 depending
257   on the regional systems, the only full day where GFAS wildfire emissions are available is D-2, and some systems also include
258   part of D-1 emissions. Each system therefore reconstructs a 24hr cycle of emission based either on D-2 only or also including
259   part of D-1 emissions. This cycle is used by all models for their analysis of D-1. For the forecast, persistence of this daily cycle
260   of emission is only maintained for D+0 and D+1 considering that the vast majority of wildfires in Europe are not persisting
261   for longer time periods.

2.6.3   Pollen emission and dispersion

263   The following pollen species are included in the CAMS Regional production: birch, grass, olive, ragweed, alder, and mugwort.
264   Their implementation in the individual operational CAMS models is more uniform than for the air pollutants as they all rely
265   on the documentation of (Sofiev et al., 2013). The pollen species differ in terms of their geographic distribution (source masks),
266   total amount of available pollen grains, start and end date of the season (heatsum thresholds), and the shape of the season

267   (source strength as function of time). The alder pollen emission model is similar to that of birch and olive, while the mugwort

268   source is a variation of the grass source. However, mugwort is implemented as five different sub-species, each with its own

269   spatially gridded start and end dates of the flowering season. Ragweed pollen follows the method described in (Prank et al.,

270   2013).

271   Once emitted, pollen species are advected in the model in the same way as other chemically inert species and are subject to

272   gravitational settling over time.

3 Individual Model Description

3.1 CHIMERE

3.1.1 Model Overview

CHIMERE is a multi-scale CTM developed jointly by INERIS and CNRS (Menut et al., 2021). Its development was initiated in the early 2000s (Bessagnet et al., 2004; Vautard et al., 2005) and it has since then pioneered operational national air quality forecasting in France (Rouïl et al., 2009). It is also extensively used for long-term simulations for emission control scenarios (Colette et al., 2013; Meleux et al., 2007; Colette et al., 2015). It runs over a range of spatial scale from the hemispheric to the urban scale, with resolutions from 100km to 1km (Colette et al., 2014; Bessagnet et al., 2017). The exact model version used since June 2021 in the CAMS Regional Production is CHIMERE v2020r1.

3.1.2 Model geometry

For the CAMS regional forecasts, CHIMERE uses a regular latitude-longitude grid with a 0.1°x0.1° resolution which covers 25°W to 45°E and 30°N to 72°N and 9 vertical levels, extending from the surface up to 500 hPa, a lowermost layer about 20m deep and about 7 layers below 2 km. No vertical downscaling is applied and concentrations in the lowermost model layer are considered representative of the surface.

3.1.3 Forcing Meteorology

The forcing meteorology is retrieved from the IFS model vertical layers covering the CHIMERE vertical extent on a 0.2°x0.2° horizontal grid resolution with a temporal resolution of 3 hours. The forecast released at 00:00UTC of the previous days is used. The three-dimensional meteorological parameters included to force the CHIMERE forecast are horizontal wind components, temperature, specific humidity, orography, rain water/snow mixing ratios, cloud liquid and ice water contents. The 2D variables included are: surface temperature, surface pressure, large scale and convective precipitations, boundary layer height, sensible and latent heat fluxes at surface, surface solar radiation downwards, soil parameters (water and temperature) for 4 layers (0-7 cm, 7-28 cm, 28-100 cm, 100-255 cm), sea ice cover, snow depth.

3.1.4 Chemical initial and boundary conditions

Lateral and top boundary conditions are taken from chemical species available in the global IFS forecast model of the previous day at 3hr temporal resolution. The full list of species used from the IFS model is given in Table 2. The forecasts are initialised by the CHIMERE forecasts of the previous day.

3.1.5   Emissions

The common annual anthropogenic emissions CAMS-REG are implemented as explained in Section 2.5.1. Temporal disaggregation is based on TNO time profiles provided with CAMS-REG. Chemical disaggregation for VOCs is based on (Passant, 2002). PM components are speciated using the splits provided with the CAMS-REG database.

Biogenic VOC emissions are computed online with the MEGAN 2.10 algorithm (Guenther et al., 2012) implemented in CHIMERE and using high spatiotemporal data LAI (30 arcsec every 8 days) generated from MODIS (Yuan et al., 2011). Biogenic emission factors are estimated based on the 30 arcsec USGS (US Geophysical Survey) land-use database and the emission factors provided for each functional type by (Guenther et al., 2012).

The hourly GFAS wildfire emission for D-2 (i.e. the last full day available when launching the forecast system) are used for the analysis (D-1) and the first two days of the forecast (D+0 and D+1). Fire emissions are set to zero for the remainder of the forecast horizon.

Dust production within the European domain is included (Alfaro and Gomes, 2001). It is based on a scheme for saltation and a vertical flux estimate using cohesion kinetic energies scheme (Marticorena and Bergametti, 1995).

3.1.6   Solver, advection and mixing

The numerical time solver is based on a splitting operator which solves separately transport (including deposition and emissions), chemistry and aerosol formation.

Advection is based on the Piecewise Parabolic Method 3d order scheme (Colella and Woodward, 1984). Vertical turbulent mixing takes place only in the boundary layer. The formulation uses K-diffusion parameterisation (Troen and Mahrt, 1986), without counter-gradient term.

3.1.7   Deposition

Dry deposition of gaseous and particle species is parameterised as a downward flux out of the lowest model layer where the deposition velocity is described through a resistance analogy (Wesely, 1989). Wet deposition of particles and gases are computed by using a polydisperse distribution of rain droplets based on (Willis and Tattelman, 1989) and by computing the efficiency of the collision. Below-cloud scavenging of gases is assumed irreversible and is therefore only accounted for the most soluble compounds (HNO_3, H_2O_2, HCl, SO_2 and NH_3). In-cloud scavenging is accounted for all gases by computing the gaseous and aqueous phases partitioning based on Henry's law constants and the pH of the clouds. Scavenging by snow is also accounted for and is based on (Chang, 1984) for gases and on (Wang et al., 2014) for particles.

3.1.8 Chemistry and aerosols

In order to optimise computing time, the reduced MELCHIOR2 mechanism with 44 species and about 120 reactions is derived from the full mechanism MELCHIOR (Derognat et al., 2003). The sectional aerosol module accounts for 7 species and 10 bins from 10nm to 40µm (primary particle material, nitrate, sulphate, ammonium, biogenic secondary organic aerosol SOA, anthropogenic SOA and water). Photolytic rates are attenuated using liquid water and relative humidity. The aerosol module is described in great details in (Couvidat et al., 2018) and accounts for condensation, nucleation, and condensation/evaporation. Aerosol thermodynamic equilibrium is achieved using the ISORROPIA model version 2.1. The secondary organic aerosol formation mechanism used in the operational forecasting version of CHIMERE is described in (Bessagnet et al., 2008).

3.1.9 Assimilation system

The CHIMERE assimilation for operational purposes relies on a kriging based approach to assimilate hourly concentration values for correcting the raw model results. For the analysis period, linear regression between a selected set of observations (excluding mountain and proximity sites) and the raw CHIMERE model is performed (in moving neighbourhood). The experimental variogram of the regression residuals is then computed and a variogram model is fitted; the model adequacy is checked by cross validation. Ultimately, observations are kriged with the CHIMERE model as external drift (in moving neighbourhood). This method is applied for O_3 and NO_2. For PM_{10} and $PM_{2.5}$, an ordinary co-kriging of the observations (main variable) and CHIMERE (secondary variable) is applied to ensure consistency between both pollutants. Only in-situ surface observations are used.

Further evolution of the CHIMERE assimilation system using an ensemble Kalman Filter approach is under development, in particular to pave the way for assimilation of satellite data. It is has however not yet demonstrated to provide better skill score than the geostatistical method.

3.2 DEHM

3.2.1 Model Overview

The Danish Eulerian Hemispheric Model (DEHM) is a 3-dimensional, offline, large-scale, Eulerian, atmospheric chemistry transport model developed to study long-range transport of air pollution in the Northern Hemisphere. DEHM was originally developed in the early 1990's in order to study the atmospheric transport of sulphur-dioxide and sulphate into the Arctic (Christensen, 1997; Heidam et al., 2004). The model has been modified, extended and updated continuously since then and now includes a flexible setup with the possibility for nested domains with higher resolutions over targeted areas (Brandt et al., 2012; Geels et al., 2021). Apart from standard air pollution components and pollen, the DEHM model also includes mercury (Christensen et al., 2004), CO_2 (Lansø et al., 2019) and POPs (Hansen et al., 2008).

3.2.2 Model geometry

The horizontal domain is defined on a regular latitude-longitude grid of 0.1° resolution with grid centre points covering longitude 24.95˚W to 44.95˚E and latitude 30.05˚N to 71.95˚N. The vertical discretization is defined on 29 terrain-following sigma levels up to about 100hPa. The 12 lowest layers are within the lowest 1 km of the atmosphere and the thickness of the lowest layer is about 20m. The model includes an option for downscaling to the surface, but this is not applied in the operational setup.

3.2.3 Forcing Meteorology

The forcing meteorology is retrieved from the IFS model vertical layers covering the DEHM vertical extent on a 0.2°x0.2° horizontal grid resolution with a temporal resolution of 3 hours. The forecast released at 12:00 UTC of the previous days is used. The meteorological parameters included to force the DEHM forecast are: 3D fields of the horizontal wind components (U,V), temperature, specific humidity, cloud liquid water contents, cloud ice water contents, rain water contents, snow water contents and fraction of cloud cover. The 2D fields are land-sea mask, surface pressure, geopotential height, skin temperature, Ustar, large scale and convective rain, snow depth, sensible heat flux, latent heat flux, net solar radiation, boundary layer height, 2 m temperature, 2 m dew point temperature, 10 m wind (U,V), albedo, sea ice area fraction and surface roughness.

3.2.4 Chemical initial and boundary conditions

Lateral and top boundary conditions are taken from chemical species available in the global IFS forecast model of the previous day at 3 hr temporal resolution. The full list of species used from the IFS model is given in Table 2. The DEHM forecasts are initialised by the DEHM forecasts of the previous day.

3.2.5 Emissions

The common annual anthropogenic emissions CAMS-REG are implemented as explained in Section 2.5.1. Originally the temporal disaggregation was based on the GENEMIS tables, using a GNFR to SNAP matrix. From 2021 the new CAMS-TEMPO (Guevara et al., 2021) profiles for annual, monthly, weekly and daily distribution of emissions have been included in the operational version of DEHM. PM components are speciated using the splits provided with the CAMS-REG emissions. The speciation of VOCs from the emission input of total non-methane VOCs is based on the global speciated NMVOC emission database EDGAR 4.3.2 (Huang et al., 2017).

Natural emissions of the Biogenic Volatile Organic Compounds (BVOCs) isoprene and monoterpenes are estimated in the DEHM model based on the MEGAN model (Zare et al., 2012). The production of sea salt aerosols at the ocean surface is based on two parameterisation schemes describing the bubble-mediated sea spray production of smaller and larger aerosols. In each time step, the production is calculated for 10 size bins and thereafter summed up to give an aggregated production of fine (with dry diameters <1.3 um) and coarse (with dry diameters ranging 1.3-6um) aerosols (Soares et al., 2016). Soil and lightning NOx emissions are based on data from the Global Emissions Inventory Activity (Yienger and Levy, 1995).

The hourly GFAS wildfire emissions are retrieved as soon as they are available (i.e. with a 8-hr delay from real time) in order to obtain a recent 24hr cycle spanning over D-2 and D-1. This cycle is used for the analysis (D-1) and the first two days of the forecast (D+0 and D+1). Fire emissions are set to zero for the remainder of the forecast horizon. Hourly injection heights are calculated based on the hourly data of 'Mean altitude of maximum injection' and 'Altitude of plume top'.

3.2.6 Solver, advection and mixing

The horizontal advection is solved numerically using the higher order Accurate Space Derivatives scheme, documented to be very accurate (Dabdub and Seinfeld, 1994), especially when implemented in combination with a Forester filter (Forester, 1977). The vertical advection as well as the dispersion sub-models is solved using a finite elements scheme (Pepper et al., 1979)for the spatial discretization. For the temporal integration of the dispersion, the q-method (Lambert, 1991) is applied and the temporal integration of the 3-dimensional advection is carried out using a Taylor series expansion to third order. Time integration of the advection is controlled by the Courant-Friedrich-Lewy (CFL) stability criterion. A wind adjustment is included in order to ensure mass conservation.

The vertical diffusion is configured by Kz profiles (Hertel et al., 1995), based on Monin-Obukhov similarity theory for the surface layer. This Kz profile is extended to the whole boundary layer by using a simple extrapolation, which ensures that Kz is decreasing in the upper part of the boundary layer. The planetary boundary layer (PBL) height is obtained directly from the IFS meteorology.

3.2.7 Deposition

Gaseous and aerosol dry-deposition velocities are calculated based on the resistance method for 16 different land-use types and are configured similar to the EMEP model (Emberson et al., 2000b; Simpson et al., 2003), except for the dry deposition of species on water surfaces, where the deposition depends on the solubility of the chemical species and the wind speed (Hertel et al., 1995).

Wet deposition includes in-cloud and below-cloud scavenging and is calculated as the product of scavenging coefficients and the concentration of gases and particles in air (Simpson et al., 2003). The in-cloud scavenging coefficients are dependent on Henry's law constants and the rate at which precipitation is formed.

3.2.8 Chemistry and aerosols

The basic chemical scheme in DEHM now includes 74 different species and 158 reactions. It is based on the original scheme by (Strand and Hov, 1994). The original Strand and Hov scheme has been modified in order to improve the description of, amongst other things, the transformations of nitrogen containing compounds. The chemical scheme has been extended with a detailed description of the ammonia chemistry through the inclusion of ammonia (NH_3) and related species: ammonium-nitrate (NH_4NO_3), ammonium bisulphate (NH_4HSO_4), ammonium sulphate (($NH_4)_2SO_4$) and particulate nitrate (NO_3) formed from nitric acid (HNO_3) using an aerosol equilibrium approach with reaction rates dependent on the equilibrium (Frohn, 2004). Furthermore, reactions concerning the wet-phase production of particulate sulphate have been included. The photolysis rates are calculated by using a 2-stream version of the Phodis model (Kylling et al., 1995). The original rates for inorganic and organic chemistry have been updated with rates from the chemical scheme applied in the EMEP model (Simpson et al., 2003). SOA formation is included via a VBS-based approach (Bergström et al., 2012b; Zare et al., 2014). In total, DEHM includes nine classes of particulate matter ($PM_{2.5}$, PM_{10}, TSP, seasalt< 2.5 mm, sea-salt >2.5 mm, smoke from wood stoves, fresh black carbon, aged black carbon, and organic carbon).

3.2.9 Assimilation system

Since the system upgrade in November 2020, the assimilation in DEHM has been based on an updated version of the comprehensive 3D-var data assimilation scheme previously described in (Silver et al., 2016). The NMC method (Kahnert, 2008; Parrish and Derber, 1992) is used to estimate the background error covariance matrix. Two 1-year runs of DEHM using analysed and forecasted ECMWF weather data are performed and their differences are used to estimate the background errors in spectral space for O_3, NO_2, SO_2, CO, $PM_{2.5}$, and PM_{10}. For the analysis and reanalysis runs, surface in-situ observations of the six species are assimilated at an hourly basis in DEHM.

3.3 EMEP

3.3.1 Model Overview

The EMEP MSC-W (European Monitoring and Evaluation Programme Meteorological Synthesizing Centre-West) model is a chemical transport model developed at the Norwegian Meteorological Institute under the EMEP programme of the United Nations Geneva Convention on Long-range Transboundary Air Pollution. The EMEP MSC-W model system allows several options with regard to the chemical schemes used and the possibility of including aerosol dynamics. (Simpson et al., 2012) described an early version of the EMEP MSC-W model in detail, while updates to the model since 2012 have been documented and evaluated in the annual status reports of EMEP (see (Emep, 2023) and references therein). The forecast version of the EMEP MSC-W model (EMEP-CWF) has been in operation since June 2006. The scheduled model updates in CAMS ensure that the model version stays as close as possible to the official EMEP Open Source version[3]. Nevertheless, the EMEP-CWF results and performances in CAMS might differ from those presented in the annual EMEP Status Reports, because of different input data (emissions and meteorological driver) and model configurations (Forecast in EMEP-CWF versus Hindcast in EMEP Status Reports).

3.3.2 Model geometry

The EMEP-CWF covers the European domain [30°N-76°N] x [30°W-45°E] on a geographic projection with a horizontal resolution of 0.1° x 0.1° (longitude-latitude). Vertically the model uses 20 levels defined as sigma coordinates. The 10 lowest model levels are within the PBL, and the top of the model domain is at 100 hPa. The lowermost layer has a thickness of approximately 50 meters. Vertical downscaling is used to derive surface concentrations at 3 meters altitude, as described in (Simpson et al., 2012).

3.3.3 Forcing Meteorology

The forcing meteorology is retrieved from the IFS model vertical layers covering the EMEP vertical extent on a 0.1°x0.1° horizontal grid resolution with a temporal resolution of 3 hours. The forecast released at 12:00UTC of the previous days is used. The meteorological parameters included to force the EMEP forecast are: 3D fields of the horizontal wind components (U,V), potential temperature, specific humidity, and cloud fraction. The 2D fields are land-sea mask, surface pressure, friction velocity (u*), large scale and convective precipitation, soil water, snow depth, fraction of snow cover, fraction of ice cover, sensible heat flux, latent heat flux, sea surface temperature, 2m temperature and 2m relative humidity. The IFS forecasts do not include 3D precipitation, which is needed by the EMEP-CWF model. Therefore, a 3D precipitation estimate is derived from large-scale precipitation and convective precipitation (surface variables).

---

[3] https://github.com/metno/emep-ctm (last accessed 30/10/2024)

3.3.4   Chemical initial and boundary conditions

Boundary conditions are taken from chemical species available in the global IFS forecast model of the previous day at 3hr temporal resolution (Table 2). In cases where IFS chemical boundary conditions are not available, default boundary conditions are specified for O_3, CO, NO, NO_2, CH_4, HNO_3, PAN, SO_2, isoprene, C_2H_6, some VOCs, Sea salt, Saharan dust and SO_4, as annual mean concentrations along with a set of parameters for each species describing seasonal, latitudinal and vertical distributions. The EMEP forecasts are initialised by the EMEP 3D VAR analysis of the previous day.

3.3.5   Emissions

The common annual anthropogenic emissions CAMS-REG are implemented as explained in Section 2.5.1. Temporal disaggregation is based on CAMS-REG-TEMPO v4.1. Chemical disaggregation for PM species follows the tables that come with CAMS-REG while VOC emissions are speciated for each source-sector based on a lumped-species approach as described in (Simpson et al., 2012; Bergström et al., 2022) .

The hourly GFAS wildfire emission for D-2 (i.e. the last full day available when launching the forecast system) are used for the analysis (D-1) and the first two days of the forecast (D+0 and D+1). Fire emissions are set to zero for the remainder of the forecast horizon.

The mineral dust source in the EMEP model is based on (Alfaro and Gomes, 2001; Fécan et al., 1998; Gomes et al., 2003; Marticorena and Bergametti, 1995; Marticorena et al., 1997).

Natural emissions of Biogenic Volatile Organic Compounds (BVOCs) are based on Table 3 of (Simpson et al., 2012).

3.3.6   Solver, advection and mixing

The numerical solution of the advection terms of the continuity equation is based on the scheme of (Bott, 1989). The fourth order scheme is utilized in the horizontal directions. In the vertical direction, a second order version applicable to variable grid distances is employed.

The turbulent diffusion coefficients (Kz) are first calculated for the whole 3D model domain on the basis of local Richardson numbers. The planetary boundary layer (PBL) height is then calculated using methods described in (Simpson et al., 2012). For stable conditions, Kz values are retained. For unstable situations, new Kz values are calculated for layers below the mixing height using the O'Brien interpolation.

3.3.7 Deposition

Parameterisation of dry deposition is based on a resistance formulation. The deposition module makes use of a stomatal conductance algorithm which was originally developed for ozone fluxes, but which is now applied to all gaseous pollutants when stomatal control is important (Emberson et al., 2000a; Simpson et al., 2003; Tuovinen et al., 2004). Non-stomatal deposition for NH_3 is parameterised as a function of temperature, humidity, and the molar ratio SO_2/NH_3.

Both gaseous and particulate nitrogen species are scavenged in the EMEP model according to their wet scavenging ratios and collection efficiencies listed in Table S20 of (Simpson et al., 2012). In-cloud and sub-cloud scavenging ratios are considered for gases and in-cloud scavenging ratios and sub-cloud scavenging efficiencies for particles.

3.3.8 Chemistry and aerosols

The EmChem19 chemical scheme couples the sulphur and nitrogen chemistry to the photochemistry and organic aerosol formation using about 200 reactions between ca. 1300 species (Bergström et al., 2022; Simpson et al., 2020b; Andersson-Sköld and Simpson, 1999). The standard model version distinguishes 2 size fractions for aerosols, fine aerosol ($PM_{2.5}$) and coarse aerosol ($PM_{2.5-10}$). The aerosol components presently accounted for are SO_4, NO_3, NH_4, anthropogenic primary PM, organic aerosols, and sea salt. Also aerosol water is calculated. Dry deposition parameterisation for aerosols follows standard resistance-formulations, accounting for diffusion, impaction, interception, and sedimentation. Wet scavenging is treated with simple scavenging ratios, taking into account in-cloud and sub-cloud processes. For secondary organic aerosol (SOA) a volatility-basis set approach (Simpson et al., 2012) is used, which is a somewhat simplified version of the mechanisms discussed in detail by(Bergström et al., 2012a). The EmChem19a scheme also has explicit toluene and benzene with different SOA yields to the o-xylene surrogate that was used previously.

3.3.8.1 Assimilation system

The EMEP data assimilation system (EMEP-DAS) is based on the 3D-Var implementation for the MATCH model (Kahnert, 2008). The background error covariance matrix is estimated following the NMC method (Parrish and Derber, 1992). Recent changes involved increased computational efficiency, tuning of model and observation representation uncertainties, and improved impact of the assimilation in the vertical.

The EMEP-DAS delivers analyses of yesterday (driven by the operational IFS forecast of 00UTC of yesterday) assimilating O_3, NO_2, CO, $PM_{2.5}$, and PM_{10} surface observations. For NO_2, satellite observations from OMI used to be assimilated up to 2021 too.

3.4 EURAD-IM

3.4.1 Model Overview

The EURAD-IM (European Air pollution Dispersion - Inverse Model) system consists of 5 major parts: the meteorological driver WRF (Weather Research and Forecasting[4]), the pre-processors EEP and PREP for preparation of anthropogenic emission data and observations, the EURAD-IM Emission Model EEM, and the chemistry transport model EURAD (Hass et al., 1995; Memmesheimer et al., 2004). EURAD-IM is a Eulerian meso-scale chemistry transport model involving advection, diffusion, chemical transformation, wet and dry deposition and sedimentation of tropospheric trace gases and aerosols. It includes 3d-var and 4d-var chemical data assimilation (Elbern et al., 2007) and is able to run in nesting mode.

3.4.2 Model geometry

To cover the CAMS domain from 25°E to 45°W and 30°N to 72°N, two lambert conformal projections subdomains with respectively 45 km (199x166 grid boxes) and 9 km horizontal resolution (581x481 grid boxes) are used. The model domain with the finer resolution covering the entire European part of the CAMS domain is nested within the halo domain with the coarser resolution.

Variables are horizontally staggered using an Arakawa C grid. Vertically, the atmosphere is divided by 23 terrain-following sigma coordinate layers between the surface and the 100 hPa pressure level. About 15 layers are within the first 2 km of the atmosphere The thickness of the lowest layer is about 35 m. No vertical downscaling is used to derive surface concentrations from the first model level.

3.4.3 Forcing Meteorology

The Weather Research and Forecast (WRF) model is used for the calculation of meteorological fields needed to drive the EURAD-IM CTM. Initial and boundary values for the WRF simulations are derived from 3-hourly IFS meteorological fields. The main motivation to use WRF is to improve the spatial and temporal interpolation of IFS fields towards the EURAD-IM geometry.

3.4.4 Chemical initial and boundary conditions

---

[4] https://www.mmm.ucar.edu/models/wrf, last accessed 30/10/2024

537   The CAMS Global IFS 00:00 UTC forecast for the previous day is extracted from the MARS archive at ECMWF using 36

538   model levels with a temporal resolution of 3 hours. The full list of species used from the IFS model is given in Table 2. Sea

539   salt concentrations from IFS are divided by the constant 4.3 for the conversion from wet to dry mass.

540   **3.4.5   Emissions**

541   The common annual anthropogenic emissions CAMS-REG are implemented as explained in Section 2.5.1. The VOC and PM

542   split, the vertical distribution of area sources, and the emission strength per hour are calculated within the EURAD-IM CTM

543   with the distribution profiles provided with the CAMS-REG-AP_v6.1/2019 inventory (Kuenen et al., 2022). The VOC and

544   PM split depends on source category and country, the vertical distribution only depends on the source category. The CAMS-

545   TEMPO v4.1 (Guevara et al., 2021) profiles are used for the annual, monthly, weekly and daily distribution of emissions.

546   Biogenic emissions and NO_x emissions from soil are calculated within the EURAD-IM CTM with the Model of Emissions of

547   Gases and Aerosols from Nature (MEGAN) (Guenther et al., 2012). Fire emissions are taken into account using hourly data

548   from the Global Fire Assimilation System Version 1.2 (GFASv1.2) product (Kaiser et al., 2012). Zero fire emissions are

549   assumed for D+2 and D+3 forecasts.

550   **3.4.6   Solver, advection and mixing**

551   The positive definite advection scheme of (Bott, 1989), implemented in a one-dimensional realisation, is used to solve the

552   advective transport. An operator splitting technique is employed (Mcrae et al., 1982) to handle the varying numerical

553   specificities of processes to be solved.

554   An Eddy diffusion approach is used to parameterize the vertical sub-grid-scale turbulent transport. The calculation of vertical

555   Eddy diffusion coefficients is based on the specific turbulent structure in the individual regimes of the planetary boundary

556   layer (PBL) according to the PBL height and the Monin-Obukhov length (Holtslag and Nieuwstadt, 1986). A semi-implicit

557   (Crank-Nicholson) scheme is used to solve the diffusion equation.

558   The sub-grid cloud scheme in EURAD-IM was derived from the cloud model in the EPA Models-3 Community Multiscale

559   Air Quality (CMAQ) modelling system (Roselle and Binkowski, 1999). Convective cloud effects on both gas phase species

560   and aerosols are considered.

561   **3.4.7   Deposition**

562   The gas phase dry deposition modelling follows the method proposed by (Zhang et al., 2003). Dry deposition of aerosol species

563   is treated size dependent, using the resistance model of (Petroff and Zhang, 2010) with consideration of the canopy. Dry

564   deposition is applied as lower boundary condition of the diffusion equation.

565 Wet deposition of gases and aerosols is derived from the cloud model in the CMAQ modelling system (Roselle and Binkowski,
566 1999). The wet deposition of pollen is treated according to (Baklanov and Sørensen, 2001).

567 Size dependent sedimentation velocities are calculated for aerosol and pollen species. The sedimentation process is
568 parameterized with the vertical advective transport equation and solved using the fourth order positive definite advection
569 scheme of (Bott, 1989).

3.4.8 Chemistry and aerosols

571 In the EURAD-IM CTM, the gas phase chemistry is represented by an extension of the Regional Atmospheric Chemistry
572 Mechanism (RACM) (Stockwell et al., 1997) based on the Mainz Isoprene Mechanism (MIM) (Geiger et al., 2003). A 2-step
573 Rosenbrock method is used to solve the set of stiff ordinary differentials equations (Sandu and Sander, 2006). Photolysis
574 frequencies are derived using the FTUV model (fast TUV) according to (Tie et al., 2003). The radiative transfer model therein
575 is based on the Tropospheric Ultraviolet-Visible Model (TUV) developed by (Madronich and Weller, 1990).

576 The modal aerosol dynamics model MADE (Ackermann et al., 1998) is used to provide information on the aerosol size
577 distribution and chemical composition. To solve for the concentrations of the secondary inorganic aerosol components, a
578 FEOM (fully equivalent operational model) version, using the HDMR (high dimensional model representation) technique
579 (Nieradzik, 2005; Rabitz and Aliş, 1999), of an accurate mole fraction based thermodynamic model (Friese and Ebel, 2010) is
580 used. The updated SORGAM module (Li et al., 2013) simulates secondary organic aerosol formation.

3.4.9 Assimilation system

582 The EURAD-IM assimilation system (Elbern et al., 2007) includes (i) the EURAD-IM CTM and its adjoint, (ii) the formulation
583 of both background error covariance matrices for the initial states and the emission, and their treatment to precondition the
584 minimisation problem, (iii) the observational basis and its related error covariance matrix, and (iv) the minimisation including
585 the transformation for preconditioning. The quasi-Newton limited memory L-BFGS algorithm described in (Liu and Nocedal,
586 1989; Nocedal, 1980) is applied for the minimisation.

587 Currently assimilated in the EURAD-IM analysis and interim re-analysis are surface in-situ observations of O_3, NO_2, SO_2, CO,
588 $PM_{2.5}$, PM_{10}.

589

590

3.5 GEM-AQ

3.5.1 Model Overview

GEM-AQ is a numerical weather prediction model where air quality processes (gas phase and aerosols) are implemented on-line in the host meteorological model, the Global Environmental Multiscale (GEM) model, developed at Environment and Climate Change Canada (Côté et al., 1998a). The model is used for operational air quality forecasting in Poland. Also, it is used in a research project to investigate air quality in different environmental conditions (Struzewska and Kaminski, 2008, 2012; Struzewska et al., 2015; Struzewska et al., 2016). Application of the GEM-AQ to modelling of satellite retrieved NO2 column was carried out by (Szymankiewicz et al., 2014) and (Kawka et al., 2021).

3.5.2 Model geometry

The GEM-AQ model can be configured to simulate atmospheric processes over a broad range of scales, from the global scale down to the meso-gamma scale. An arbitrarily rotated latitude-longitude mesh focuses resolution on any part of the globe. In the CAMS regional production, the model is run in the limited area mode with a resolution of 0.1° x 0.1° on a spherical coordinate system. The coordinates are the following: lower-left (17.4N / 22.1W), upper-right (58.6N/ 86.6E),and are generated internally based on lower-left corner, grid extent and the numerical equator location. In the vertical, GEM-AQ uses the generalised sigma vertical coordinate system. It has terrain-following sigma surfaces near the ground that transform to pressure surfaces higher in the atmosphere. The model top is set at 10 hPa.

3.5.3 Forcing Meteorology

The operational IFS model provides meteorological fields for initial and boundary conditions used by the meteorological part of the GEM-AQ model. The GEM-AQ model is started using the 12-hour forecast (valid at 00:00 UT of the following day) as initial conditions. The IFS data are used as boundary conditions with a nesting interval of 3 hours. The IFS meteorological fields are computed from spectral coefficients for the target GEM-AQ grid. Meteorological fields, within the GEM-AQ model domain, are constrained and relaxed to the IFS global model every 3 hours. Thus, the meteorological fields are 'dynamically interpolated' by the GEM meteorological model to the required transport and chemistry time steps.

3.5.4 Chemical initial and boundary conditions

Chemical species of the CAMS Global IFS forecast for the previous day are used with a temporal resolution of 3 hours (Table 2). For dust aerosols, the three available size bins from the IFS model are distributed uniformly over the 10 corresponding bins in GEM-AQ. For organic matter aerosol, black carbon and sulphates, the same log-normal based profile was applied. For organic aerosol and black carbon, hydrophobic and hydrophilic components were summed as "total organic aerosol" and "total black carbon aerosol" before applying size-bin distribution profiles.

3.5.5 Emissions

620

621 The common annual anthropogenic emissions CAMS-REG are implemented as explained in Section 2.5.1. In those emissions,

622 the following fields are available: SO_2, NOx, CO, NMVOC, NH_3, PM_{10} and $PM_{2.5}$. Based on this information, emission fluxes

623 for 15 gaseous species (9 hydrocarbons and 6 inorganics) and 4 aerosol components (primary organic aerosol, black carbon,

624 sulphates, nitrates) are derived using factors provided by TNO. Total emission fluxes for each aerosol component are

625 distributed into 12 bins in the GEM-AQ aerosol module.

626 Anthropogenic emissions are distributed within the 7 lowest model layers (up to 1350 m) with injection height profiles for

627 each of the GNFR sectors re-mapped for the GEM-AQ levels. Temporal profiles modulating annual and diurnal variation of

628 emission fluxes for each GNFR are used.

629 For biogenic emissions, a monthly averaged MEGAN-MACC (Guenther et al., 2012) dataset valid for 2010 was used in order

630 to avoid short-term variability of reactive biogenic VOC generated on-line in the model.

3.5.6 Solver, advection and mixing

631

632 The set of non-hydrostatic Eulerian equations (with a switch to revert to the hydrostatic primitive equations) maintains the

633 model's dynamical validity right down to the meso-gamma scales. The time discretization of the model dynamics is fully

634 implicit, 2 time-level (Côté et al., 1998b; Côté et al., 1998a). The spatial discretization for the adjustment step employs a

635 staggered Arakawa C grid that is spatially offset by half a mesh length in the meridional direction. It is second-order accurate,

636 whereas the interpolations for the semi-Lagrangian advection are of fourth-order accuracy.

637 Deep convective processes are handled by Kain-Fritch convection parameterisation (Kain and Fritsch, 1990). The vertical

638 diffusion of momentum, heat and tracers is a fully implicit scheme based on turbulent kinetic energy (TKE) theory.

3.5.7 Deposition

639

640 The effects of dry deposition are included as a flux boundary condition in the vertical diffusion equation. Dry deposition

641 velocities are calculated from a `big leaf' multiple resistance model (Wesely, 1989; Aamaas et al., 2013) with aerodynamic,

642 quasi-laminar layer, and surface resistances acting in series. The process assumes 15 land-use types and takes snow cover into

643 account. Wet deposition takes into account cloud scavenging for soluble gas species and aerosols.

3.5.8 Chemistry and aerosols

644

645 The gas-phase chemistry mechanism currently used in the GEM-AQ model is based on a modification of version 2 of the Acid

646 Deposition and Oxidants Model (ADOM) (Venkatram et al., 1988), derived from the condensed mechanism of (Lurmann et

al., 1986). The ADOM-II mechanism comprises 47 species, 98 chemical reactions and 16 photolysis reactions. In order to account for background tropospheric chemistry, 4 species (CH_3OOH, CH_3OH, CH_3O_2, and CH_3CO_3H) and 22 reactions were added. All species are solved using a mass-conserving implicit time stepping discretization, with the solution obtained using Newton's method. Heterogeneous hydrolysis of N_2O_5 is calculated using the on-line distribution of aerosol. Although the model meteorology is calculated up to 10 hPa, the focus of the chemistry is in the troposphere where all species are transported throughout the domain. To avoid the overhead of stratospheric chemistry in this version (a combined stratospheric/tropospheric chemical scheme is currently being developed), both the ozone and NOy fields are replaced with a climatology above 100 hPa after each transport time step. Ozone fields are taken from the HALOE (Halogen Occultation Experiment) climatology (Hervig et al., 1993), while NOy fields are taken from the CMAM (Canadian Middle Atmosphere Model). Photolysis rates (J values) are calculated on-line every chemical time step using the method of (Landgraf and Crutzen, 1998). In this method, radiative transfer calculations are done using a delta-two stream approximation for 8 spectral intervals in the UV and visible applying pre-calculated effective absorption cross sections. This method also allows for scattering by cloud droplets and for clouds to be presented over a fraction of a grid cell. The host meteorological model provides both cloud cover and water content. The J value package used was developed for MESSy (Jöckel et al., 2006) and is implemented in GEM-AQ.

The current version of GEM-AQ has 5 size-resolved aerosol types, viz. sea salt, sulphate, black carbon, organic carbon and dust as well as nitrates. The microphysical processes that describe the formation and transformation of aerosols are calculated by a sectional aerosol module (Gong et al., 2003). The particle mass is distributed into 12 logarithmically spaced bins from 0.005 to 10.24-micron radius. This size distribution leads to an additional 60 advected tracers. The following aerosol processes are accounted for in the aerosol module: nucleation, condensation, coagulation, sedimentation and dry deposition, in-cloud oxidation of SO_2, in-cloud scavenging, and below-cloud scavenging by rain and snow.

3.5.9   Assimilation system

Data assimilation in the GEM-AQ modelling system is done with Optimal Interpolation method (Robichaud and Ménard, 2014) and is applied to the forecast. Error statistics are computed with the Hollingsworth - Lönnberg (HL) method (Hollingsworth and Lönnberg, 1986). It estimates the correlation length and the ratio of observation to model error variances by a least-square fit of a correlation model against the sample of the spatial autocorrelation of observation-minus-model residuals.

Currently, data assimilation is done at each forecast hour for O_3, NO_2, SO_2, CO, PM_{10} and $PM_{2.5}$, using surface observations.

3.6 LOTOS-EUROS

3.6.1 Model Overview

The LOTOS-EUROS model is a 3D chemistry transport model aimed to simulate air pollution in the lower troposphere. The model has been used in a large number of studies for the assessment of particulate air pollution and trace gases (e.g. O_3, NO_2) (Hendriks et al., 2016; Schaap et al., 2013; Thürkow et al., 2021; Timmermans et al., 2022). A detailed description of the model is given in (Manders et al., 2017). At present the version used in the production is v2.2.009.

3.6.2 Model geometry

The domain of LOTOS-EUROS is the CAMS regional domain from 25°W to 45°E and 30°N to 72°N. The projection is regular longitude-latitude, at 0.1°x0.1° grid spacing. In the vertical and for the forecasts there are currently 12 model layers and 2 more reservoir layers at the top, defined by coarsening in a mass conservative way the first 77 model levels of the IFS. For the analyses there are 4 dynamic layers up to 5km agl and a surface layer with a fixed depth of 25 m. The lowest dynamic layer is the mixing layer, followed by 3 reservoir layers. The heights of the reservoir layers are determined by the difference between the mixing layer height and 5 km. For output purposes, the concentrations at measuring height (usually 2.5 m) are diagnosed by assuming that the flux is constant with height and equal to the deposition velocity times the concentration at height z. This applies for several of the gaseous species, namely O_3, NO, NO_2, HNO_3, N_2O_5, H_2O_2, CO, SO_2 and NH_3. For aerosols, the same approach is utilized, only sedimentation velocity is used instead of deposition velocity.

3.6.3 Forcing Meteorology

The forcing meteorology is retrieved from the 00:00 and 12:00 UTC runs of the IFS model at hourly (surface fields) or 3-hourly temporal resolution (model layer fields). The meteorological data is retrieved on a regular horizontal resolution of about 15 km and for all layers covered by the model's vertical extent. The meteorological variables included are 3-hourly 3D fields for wind direction, wind speed, temperature, humidity and density, substantiated by hourly 2D gridded fields of mixing layer height, surface wind and temperature, precipitation rates, heat fluxes, cloud cover and surface variables snow depth, sea ice cover and volumetric soil water.

3.6.4 Chemical initial and boundary conditions

The lateral and top boundary conditions for trace gases and aerosols are obtained from the CAMS-global daily forecasts (see Table 2). LOTOS-EUROS uses a bulk approach for the aerosol size distribution differentiating between a fine and a coarse fraction, but for dust and sea salt there are 5 distinct size classes: ff: 0.1-1 μm, f:1-2.5 μm, ccc: 2.5-4 μm, cc: 4-7 μm, c:7-10 μm. When the chemical boundary conditions from IFS are missing, the model uses climatological boundary concentrations derived from IFS data. The forecasts are initialised with the LOTOS-EUROS forecast of the previous day.

704

3.6.5 Emissions

The common annual anthropogenic emissions CAMS-REG are implemented as explained in Section 2.5.1. Injection height distribution from the EuroDelta study is implemented, which is per SNAP (or more recently, GNFR) category. Time profiles used are defined per country and GNFR emission category type.

Biogenic NMVOC emissions are calculated online using actual meteorological data and a detailed landuse and tree species database including emission factors from (Köble and Seufert, 2001). The isoprene emissions follow the mathematical description of the temperature and light dependence of the isoprene emissions, proposed by (Guenther et al., 1993). Sea salt emissions are parameterised following (Martensson et al., 2003; Monahan, 1986) from the wind speed at 10-meter height.

The fire emissions are taken from the near real-time GFAS fire emissions database. For the forecast, we assume persistence, so that the latest downloaded emission for the specific hour is used. When the hourly emission is more than 3 days old, it is set to zero.

Mineral dust emissions within the modelling domain are calculated online based on the sand blasting approach by (Marticorena and Bergametti, 1995) with soil moisture inhibition as described by (Fécan et al., 1998). Finally, a parameterization using land cover and temperature is used for handling soil NOx emissions, based on (Yienger and Levy, 1995).

3.6.6 Solver, advection and mixing

The transport consists of advection in 3 dimensions, horizontal and vertical diffusion, and entrainment/detrainment. The advection is driven by meteorological fields (u,v), which are input every 3 hours. The vertical wind speed w is calculated by the model as a result of the divergence of the horizontal wind fields. A linear advection scheme is used to ensure tracer mass conservation, which also allows more efficient parallelization and reduced model complexity. This scheme uses piece-wise linear functions to define sub-grid concentrations, which is sometimes referred to as MUSCL ("Monotonic Uwind-centered Scheme for Conservation Laws") following (Van Leer, 1984).

Vertical diffusion is described using the standard K_z theory. Vertical exchange is calculated employing the new integral scheme by (Yamartino et al., 2007). For the forecasting set-up with 12 layers, atmospheric stability values and functions, including Kz values, are derived based on the surface heat fluxes from ECMWF meteorology and similarity profiles following the IFS approach (Ecmwf, 2021) to adapt for land-use specific conditions. For the 5-layer version in the assimilation, a correction is made for the vertical diffusion to correct for the height difference between surface and mixing layer.

3.6.7   Deposition

The dry deposition in LOTOS-EUROS is parameterised following the resistance approach. The laminar layer resistance and the surface resistances for acidifying components are described following the EDACS system (Van Zanten et al., 2010), the deposition velocities for particles are based on (Zhang et al., 2001). Wet deposition is divided between in-cloud and below-cloud scavenging. The in-cloud scavenging module is based on the approach described in (Seinfeld and Pandis, 1998) and (Banzhaf et al., 2012).

3.6.8   Chemistry and aerosols

LOTOS-EUROS uses the TNO CBM-IV scheme, which is a modified version of the original CBM-IV (Gery et al., 1989). N_2O_5 hydrolysis is described explicitly based on the available (wet) aerosol surface area (using $\gamma = 0.05$) (Schaap et al., 2004). Aqueous phase and heterogeneous formation of sulphate is described by a simple first order reaction constant (Barbu et al., 2009; Schaap et al., 2004). Inorganic aerosol chemistry is represented using ISORROPIA II (Fountoukis and Nenes, 2007) and secondary organic aerosols formation based on a VBS scheme (Bergström et al., 2012a; Zare et al., 2014) will be included in the operational forecast version at the end of 2023.

3.6.9   Assimilation system

The LOTOS-EUROS model is equipped with a data assimilation package with the ensemble Kalman filter technique (Curier et al., 2012). The ensemble is created by specification of uncertainties for emissions (NOx, VOC, NH_3 and aerosol), ozone deposition velocity, and ozone top boundary conditions. Currently, data assimilation is performed for O_3, NO_2, PM_{10} and $PM_{2.5}$ surface observations, OMI NO_2 is also assimilated.

3.7   MATCH

3.7.1   Model Overview

The Multi-scale Atmospheric Transport and Chemistry model (MATCH) (Robertson et al., 1999) is an off-line chemical transport model (CTM) with a flexible design, accommodating different weather data forcing on different resolutions and projections, and a range of alternative schemes for deposition and chemistry.

3.7.2   Model geometry

The model geometry is taken from the input weather data. The vertical resolution is reduced with respect to the ECMWF operational model by combining pairs of IFS layers; hybrid vertical coordinates are used. The horizontal geometry of the MATCH simulation is the same as the meteorological forcing (currently a lat-lon grid with 0.1° resolution). The lowest 76 layers of the ECMWF model are lumped in 26 levels, which then are used for the air quality simulations. The model top is at about 8000 m height. The model domain covers the area between 28.8° W to 45.8° E and 29.2° N to 72.0° N. The grid is an Arakawa C-grid with staggered wind components. The current operational system uses various tiles of physiography derived from CLC/SEI inventory[5] (Simpson et al., 2012).

3.7.3   Forcing Meteorology

The forcing meteorology is retrieved from the 12:00 UTC run of the IFS modelling system on a 0.1°×0.1° spatial grid and with a temporal resolution of one hour. For the analyses, the 00:00 UTC analysis of the IFS is used at 0.2°×0.2° resolution. The meteorological variables included are 3D fields of the horizontal wind components (U, V), temperature, specific humidity, cloud cover, cloud water content, cloud ice water content, and surface fields of surface pressure, logarithm of surface pressure, surface temperature, sea surface temperature, snow depth, albedo, roughness height, total cloud cover, precipitation, and volumetric soil water at the surface.

3.7.4   Chemical initial and boundary conditions

The lateral boundary conditions for trace gases and aerosols are obtained from the IFS global forecasts at 3-hourly resolution for the following species: O_3, CO, HCHO, NO, NO_2, SO_2, HNO_3, PAN, CH_4, C_5H_8, o-xylene, sulphate and C_2H_6 (see Table 2). When the chemical boundary conditions from IFS are missing, the model uses seasonal climatological boundary concentrations instead.

---

[5] www.sei.org/projects/sei-european-land-cover-map (last accessed 30/10/2024)

3.7.5 Emissions

The common annual anthropogenic emissions CAMS-REG are implemented as explained in Section 2.5.1. Temporal disaggregation is based on the GENEMIS tables (Ebel et al., 1997), using a GNFR to SNAP matrix. The vertical distribution of the emissions depends on the sector. Near-surface emission sources (SNAP 2,6,7,8,10) are distributed in the lowest 90 m; for other sectors the emissions are allocated over varying model levels up to a maximum of about 1100 m height. According to the sector, the anthropogenic VOC emissions are split into the MATCH chemical mechanism surrogate species: C_2H_6, NC_4H_{10}, C_2H_4, C_3H_6, OXYLENE, BENZENE, TOLUENE, CH_3OH, C_2H_5OH, HCHO, CH_3CHO, $CH_3COC_2H_5$; the particulate matter components elemental carbon, organic matter, anthropogenic dust (other than soil and road dust) are allocated to two bins ($PM_{2.5}$ and PM-coarse), as well as the road dust estimated according to (Schaap et al., 2009) and (Omstedt et al., 2005), and the teluric dust calculated according to (Zender et al., 2003).

Biogenic emissions of isoprene, monoterpenes and sesquiterpenes are calculated following (Simpson et al., 2012; Simpson et al., 1995; Bergström et al., 2012a), taking into account temperature at 2 m, radiation fluxes and the vegetation cover. Exception is made for the isoprene oxidation for which the chain of reactions is following the Carter-1 chemical mechanism, which has proven to give the comparable results with fewer reactions (Carter, 1996; Langner et al., 1998).

The dimethyl sulphide - DMS – emissions from the Ocean and Baltic Sea are also considered; whereas the particulate matters from sea salt are calculated according to the parameterisation proposed by (Sofiev et al., 2011).

The GFAS biomass burning emissions are taken into the model mapping the following species into the MATCH chemical mechanism: NOx, SO_2, CO, CH_4, C_2H_4, C_2H_6, C_3H_6, C_4H_{10}, C_8H_{10}, benzene, toluene, CH_3OH, C_2H_5OH, formaldehyde, acetaldehyde, OC, BC, $PM_{2.5}$, and PM_{10}. Half of these grid emissions are vertically distributed between the surface and the top of the plume (GFAS parameter) according to a parabolic curve, and the other half is uniformly distributed among the same levels.

3.7.6 Solver, advection and mixing

Mass conservative transport schemes are used for advection and turbulent transport. The advection is formulated as a Bott-like scheme (Robertson et al., 1999). A second order transport scheme is used in the horizontal as well as the vertical. The vertical diffusion is described by an implicit mass conservative first order scheme, where the exchange coefficients for neutral and stable conditions are parameterized following (Holtslag and Nieuwstadt, 1986). In the convective case the turbulent Courant number is directly determined from the turnover time in the boundary layer.

Part of the dynamical core is the initialisation and adjustment of the horizontal wind components. This is a very important step to ensure mass conservative transport. The initialisation is based on a procedure proposed by (Heimann and Keeling, 1989),

804   where the horizontal winds are adjusted by means of the difference between the input surface pressure tendency, and the
805   calculated pressure tendency assumed to be an error in the divergent part of the wind field.

806   Boundary layer parameterisation is based on surface heat and water vapour fluxes as described by (Van Ulden and Holtslag,
807   1985) for land surfaces, and (Burridge, 1977) for sea surfaces. The boundary layer height is calculated from formulations
808   proposed by (Zilitinkevich and Mironov, 1996) for the neutral and stable case, and from (Holtslag et al., 1995) for the
809   convective case. These parameterisations drive the formulations for dry deposition and vertical diffusion.

3.7.7   Deposition

811   Dry deposition of gases and aerosols is modelled using a resistance approach (based on the scheme in (Simpson et al., 2012)),
812   which includes stomatal and non-stomatal pathways for vegetated surfaces. MATCH uses 3D-precipitation (estimated in the
813   model, based on the surface precipitation and 3D cloud water information from the IFS forecast) and separates wet scavenging
814   into in-cloud and sub-cloud scavenging. For most gaseous components the scavenging is assumed to be proportional to the
815   precipitation intensity (with higher scavenging ratios in-cloud than sub-cloud). For the particulate components in-cloud
816   scavenging is also treated using simple scavenging ratios while the sub-cloud scavenging is treated using a scheme based on
817   (Berge, 1993) with size dependent collection efficiencies (as in (Simpson et al., 2012)).

3.7.8   Chemistry and aerosols

819   The photochemistry scheme is based on the EMEP MSC-W chemistry scheme (Simpson et al., 2012), with a modified scheme
820   for isoprene, based on the so-called Carter-1 mechanism (Carter, 1996; Langner et al., 1998). The SOA description is based
821   on (Hodzic et al., 2016).

3.7.9   Assimilation system

823   The model for data assimilation is an integrated part of the MATCH modelling system. The data assimilation scheme as such
824   is a variational spectral scheme (Kahnert, 2008), implying that the background covariance matrices are modelled in spectral
825   space. The limitation is that covariance structures are described as isotropic and homogeneous. The advantage is that the
826   background error matrix becomes block diagonal, and there are no scale separations as the covariance between spectral
827   components are explicitly handled. The block diagonal elements are the covariance between wave components at model layers
828   and chemical compounds.

829   Modelling the background error covariance matrices is the central part in data assimilation. This is conducted by means of the
830   so-called NMC approach (Parrish and Derber, 1992). The CTM (MATCH) is run for a 3-month period for photochemistry and
831   aerosols with analysed and forecasted ECMWF weather data. The differences are assumed to mimic the background errors,

832 and the statistics in spectral space are generated for different combinations of the model compounds: O_3, NO_2, NO, SO_2, CO,

833 $PM_{2.5}$, PM_{10}.

834 The scheme is fully intermittent in hour-by-hour steps and the above-listed components are assimilated from in-situ

835 measurements. The analysed components are propagated by chemistry and transport into unobserved components as

836 NMVOCs, PAN and NH_3.

837

3.8 MINNI

3.8.1 Model Overview

MINNI (Italian Integrated Assessment Modelling System for supporting the International Negotiation Process on Air Pollution and assessing Air Quality Policies at national/local level; (D'elia et al., 2021; Mircea et al., 2014) has been developed to support the Italian Ministry for Environment and Territory and Sea. The core of the modelling system is the 3-dimensional offline Eulerian CTM FARM (Flexible Air quality Regional Model, (Silibello et al., 2008) that accounts for the transport, chemistry and removal of atmospheric pollutants.

3.8.2 Model geometry

For the CAMS regional forecast, the model is configured with a regular latitude-longitude grid of 0.15° * 0.10° resolution. The domain spans from -25° to 45.05° degree East and from 30° to 72° degree North. The model uses z-level terrain following mesh with the first central grid point at 20 m AGL (above ground level) and the last one at 6290 m AGL. No vertical downscaling is applied to extrapolate concentrations from 20 meters above the ground to the surface.

3.8.3 Forcing Meteorology

The forcing meteorology is retrieved from the 12:00 UTC run of the IFS modelling system on a 0.1°x0.1° spatial grid and with a temporal resolution of one hour. The meteorological variables included are 3D fields such as temperature, relative humidity, pressure and wind velocity and 2D fields such as boundary layer height, roughness length, albedo, sea surface temperature, total cloud cover and precipitation.

3.8.4 Chemical initial and boundary conditions

The lateral and top boundary conditions for trace gases and aerosols are obtained from the CAMS-global daily forecasts with a 3-hr temporal resolution (see Table 2). The initial condition is taken from the previous forecast of the MINNI model.

3.8.5 Emissions

The common annual anthropogenic emissions CAMS-REG are implemented as explained in Section 2.5.1. Point emissions are summed up to diffuse emissions for each GNFR sector, since no information was available about the characterization of the point sources in terms of injection height. Conservative mass horizontal interpolation has been applied to map the emissions on the actual model domain. Vertical splitting has been applied for each GNFR sector adapting the vertical injection profiles provided by TNO to the actual model levels. Temporal emission profiles for each GNFR sector, as they were provided by TNO, have been applied considering local hour (i.e. the time zones shift has been taken into account).

865

PM$_{2.5}$ has been speciated following the TNO table as a function of country and sector and AERO3 (Binkowski and Shankar, 1995; Binkowski, 1999) species size fractions below 2.5µm. The coarse component (PM$_{10}$-PM$_{2.5}$) was associated to non-speciated coarse mode since MINNI dispersion model considers all the secondary aerosol fraction as PM$_{2.5}$. This method leaves the detailed chemical speciation out but ensures mass conservation.

The NMVOC speciation originated from the TNO table as a function of country and sector obtaining the v01-v25 species. The mapping among the v01-v25 species to SAPRC99 species has been done in agreement with the choices made and tested in the frame of EURODELTA III intercomparison exercise (Colette et al., 2017).

Biogenic emissions are computed with the MEGAN model v.2.04 (Guenther et al., 2006), and NOx emissions from soil following (Williams et al., 1992) approach.

Erosion and resuspension of the dust are calculated by means of method proposed by (Vautard et al., 2005). Road dust emissions are parameterized following (Zender et al., 2003).

Fire emissions are taken into account using hourly data from the GFAS database considering emissions from D-1 for AN (D-1) and FC (D+0 and D+1, zero for the remaining days).

3.8.6   Solver, advection and mixing

FARM is a 3-dimensional Eulerian model with first order turbulence closure. Physical and chemical processes influencing the concentration fields within the modelling domain are described by a system of partial differential equations (PDE). The numerical integration of the above system of PDEs is performed by a method that splits the multi-dimensional problem into time dependent one-dimensional problems, which are then solved sequentially over the time step.

Partial differential equations involved in horizontal and vertical advection-diffusion operators are solved in FARM using the schemes employed in CALGRID model (Yamartino et al., 1992). In particular, horizontal advection-diffusion operators are solved using a finite elements method based on Blackman cubic polynomials. The coefficients of a cell-centered cubic polynomial are constrained to maintain high-accuracy and low-diffusion characteristics and to avoid undesirable negative concentrations. In addition, a filter is used for filling undesired short wavelength minima. The numerical integration of the vertical diffusion equation is performed in a hybrid way employing a hybrid semi-implicit Crank-Nicholson / fully implicit scheme (Yamartino et al., 1992).

891   The calculation of horizontal diffusion coefficients is based on Stress tensor formulation of (Smagorinsky, 1963) also including

892   a dependence on the local stability class and wind speed. For the calculation of vertical diffusion coefficients, the (Lange,

893   1989) approach to boundary layer scaling regimes is used. Mixing due to deep convection is not explicitly taken into account.

894   Two different schemes to compute the PBL scaling parameters are used. In the daytime, the (Maul et al., 1980) version of

895   (Carson, 1973)encroachment method is used. During night-time, the minimum value between (Nieuwstadt, 1981) and

896   (Venkatram, 1980) is used.

897   3.8.7   Deposition

898   The dry deposition velocities are modelled following a resistance analogy approach, as an inverse sum of a series of 3

899   resistances: the aerodynamic resistance, the quasi-laminar layer resistance and the surface resistance. Aerodynamic resistance

900   is dependent on surface characteristics and atmospheric stability conditions (described through friction velocity and Monin-

901   Obukhov length). Quasi-laminar layer resistance is parameterised using (Hicks et al., 1987). Surface resistance is approximated

902   as a set of parallel resistance associated with leaf stomata, leaf cuticles, lower canopy and surface soil, litter and water (Wesely,

903   1989). Deposition to water surfaces is based on (Slinn et al., 1978) work.

904   The deposition velocity of particulate species also depends on particle size distribution and density because of gravitational

905   settling. Sedimentation velocity acts in parallel to the other resistances. Hygroscopic growth is considered over water for

906   particles less than 2 µm. For particles ranging from 0.1 to 1 µm deposition velocity is computed as the inverse of the resistance

907   computed from canopy height, friction velocity and Monin-Obukhov length.

908   The parameterization of wet deposition follows the (Simpson et al., 2012) approach, including in-cloud and below-cloud

909   scavenging of gas and particles.

910   3.8.8   Chemistry and aerosols

911   The gas-phase chemical mechanism used for CAMS forecast is SAPRC-99 with the inclusion of Polycyclic aromatic

912   hydrocarbons (PAHs) and Mercury chemistry; moreover, a simplified aqueous phase mechanism is included for SO_2 oxidation

913   and chemical processes involving Mercury in both gas and aqueous phases.

914   A simple approach is used to estimate photolysis rates based on look-up tables to calculate the rate constants for photolysis

915   reactions (Nenes et al., 1998). Photolysis rates are computed and adjusted according to local solar zenith angle using an

916   empirical formula based on (Peterson, 1976) data.

917   The aerosols module is AERO3 (Binkowski and Shankar, 1995; Binkowski, 1999). In AERO3 the representation of the particle

918   size is three-modal (Aitken, accumulation and coarse), following lognormal distributions. The aerosol dynamics takes into

919   account nucleation, condensation and coagulation processes. The gas/particle mass transfer is implemented by means of

920   ISORROPIA v1.7 (Nenes et al., 1998) and SORGAM (Schell et al., 2001a) for secondary inorganic and organic aerosol,

921   respectively.

3.8.9   Assimilation system

923   The assimilation scheme used in CAMS is optimal interpolation: the correlation function is factorized in vertical and horizontal

924   components. The horizontal component has pollutant dependent fixed correlation length with a terrain-following exponential

925   decay. The vertical component is modelled with a Cressman function dependent on the boundary layer height. The system

926   assimilates NO_2, O_3, SO_2, CO, PM_{10} and $PM_{2.5}$. In case of aerosol components, the correction applied to each of them is

927   proportional to their content in PM. At present, only data from surface stations are assimilated. More details are available in

928   (Adani and Uboldi, 2023).

929

3.9 MOCAGE

3.9.1 Model Overview

The MOCAGE 3D multi-scale Chemistry and Transport Model has been designed for both research and operational applications in the field of environmental modelling. Since 2000, MOCAGE has been allowing to cover a wide range of topical issues ranging from chemical weather forecasting, tracking and backtracking of accidental point source releases, transboundary pollution assessment, assimilation of remote sensing measurements of atmospheric composition, to studies of the impact of anthropogenic emissions of pollutants on climate change.

3.9.2 Model geometry

For the CAMS Regional Service, MOCAGE operates on a regular latitude-longitude grid at 0.1 resolution covering the 28° to 72° North and 26°W to 46°E domain, for both forecast and assimilation. The products delivered for the CAMS service are issued from the regional domain only. In the vertical, 47 hybrid levels go from the surface up to 5 hPa, with approximately 8 levels in the Planetary Boundary Layer (i.e. below 2km), 16 in the free troposphere and 24 in the stratosphere. The thickness of the lowest layer is about 40 m. There is no downscaling applied to surface concentration.

3.9.3 Forcing Meteorology

The forcing meteorology is retrieved from the IFS model vertical layers covering the MOCAGE vertical extent on a 0.1°x0.1° horizontal grid resolution with a temporal resolution of one hour for the 3 first forecast days and 3 hours for the last forecast day. The forecast released at 12UTC of the previous days is used. The meteorological parameters used are: horizontal and vertical winds, temperature, humidity, cloud fraction and surface pressure.

3.9.4 Chemical initial and boundary conditions

Chemical initial values in the regional domain are provided by MOCAGE 24h forecast from the day before. The boundary conditions are taken from global CAMS operational suite for the species (chemical and aerosols) that are distributed (see Table 2). For aerosols, the 2 or 3 bins from IFS are summed to get total concentration and then distributed onto the 6 MOCAGE bins considering Mean IFS bin size as emission modes. A factor 4.3 is applied to convert Sea Salt from wet to dry fractions. Aerm03 (of diameter larger than 10µm) is only marginally distributed within MOCAGE PM_{10} sea salt because of the matching between bins and log-normal modes. For the species not included in Table 2, the concentrations from the MOCAGE global domain are used, which helps to introduce smoothly, on the horizontal as well as on the vertical, these chemical boundary conditions into the CAMS regional domain.

3.9.5 Emissions

The common annual anthropogenic emissions CAMS-REG are implemented as explained in Section 3.2. Temporal disaggregation is based on the GENEMIS tables (Ebel et al., 1997), using a GNFR to SNAP matrix. Chemical disaggregation for PM species and VOCs is based on sector and country-dependent split factors proposed by TNO.

Isoprene biogenic emissions are computed online using MEGAN model (Guenther et al., 2012), while other biogenic emissions are computed from CAMS global biogenic emission inventory (version 3.1). NOx soil emissions are taken from the CAMS-GLOB-SOILv2.2 emission inventory.

Concerning biomass burning sources, GFAS emissions are emitted according to an 'umbrella' profile, with a maximum injecting height climatologically determined. GFAS "near real time" observation-based fire emissions are made available with a 8-hr delay. So that when the forecast system is initiated, most GFAS emission cover Day-2 of the forecast to be produced. As a consequence, the 2-day persistence is interpreted in a way that fire emissions are only applied for D+0.

3.9.6 Solver, advection and mixing

Concerning physical and chemical parameterisations, an operator splitting approach is used. Parameterisations are called alternatively in forward and reverse order, with the objective to reduce systematic errors.

Meteorological forcings are read every 3 hours from IFS input data, and are linearly interpolated to yield hourly values, which is the time-step for advection; smaller time-steps are used for physical processes and chemistry, but the meteorological variables are kept constant over each hour. MOCAGE is based upon a semi-lagrangian advection scheme (Williamson and Rasch, 1989), using a cubic polynomial interpolation in all 3 directions.

For sub-gridscale transport processes, vertical diffusion is treated following (Louis, 1979) and transport by convection is from (Bechtold et al., 2001). Scavenging within convective clouds is following (Mari et al., 2000), allowing to compute wet removal processes directly within the convective transport parameterisation. Wet deposition in stratiform clouds and below clouds follows (Giorgi and Chameides, 1986).

3.9.7 Deposition

A description of MOCAGE surface exchanges module is presented in (Michou et al., 2005). The dry deposition parameterisation relies on a fairly classical surface resistance approach (Wesely, 1989), but with a refined treatment of the stomatal resistance, similar to the one used in Meteo-France numerical weather prediction models (Noilhan and Planton, 1989). Sedimentation of aerosol follows (Nho-Kim et al., 2004).

3.9.8 Chemistry and aerosols

The MOCAGE configuration for CAMS comprises 118 species and over 300 reactions and photolysis. It is a merge of reactions of the RACM scheme (Stockwell et al., 1997) with the reactions relevant to the stratospheric chemistry of REPROBUS (Lefevre et al., 1994). Aqueous chemistry for the formation of sulphate is represented, following (Ménégoz et al., 2009). Detailed heterogeneous chemistry on Polar Stratospheric Clouds (types I, II) is accounted for, as described in (Lefevre et al., 1994). Other heterogeneous chemistry processes are currently not included.

Photolysis is taken into account using a multi-entry look-up table computed off-line with the TUV software version 4.6 (Madronich, 1987). Photolysis depends on month (including monthly aerosol climatologies), solar zenith angle, ozone column above each cell (as the model extends to the mid-stratosphere, it is actually the ozone profile computed by MOCAGE which is used at every time step), altitude and surface albedo in the UV. They are computed for clear-sky conditions and the impact of cloudiness on photolysis rates is applied afterwards.

The aerosol module of MOCAGE includes the primary species dusts, black carbon, sea salts, organic carbon, and the secondary inorganic species sulphate, nitrate and ammonium. The formation and the multi-phasic equilibrium of inorganic secondary aerosols are modelled by the ISORROPIA-II module. Details on MOCAGE aerosol simulation evaluation can be found in (Martet et al., 2009) for dusts, in (Nho-Kim et al., 2005) for black carbon, and in (Sič et al., 2015) for the latest version of MOCAGE primary aerosol module. The implementation and the evaluation of secondary inorganic aerosols in MOCAGE are described by (Guth et al., 2016). Further improvements of the representation of aerosols in MOCAGE are expected in the future with on-going work regarding organic secondary aerosols.

3.9.9 Assimilation system

MOCAGE operations for CAMS use the assimilation system based upon MOCAGE and PALM (Lahoz et al., 2007). As a first approximation, background error standard deviations are prescribed as proportional to background amounts. In order to spread assimilation increments spatially, background error correlations are modelled using a generalized diffusion operator (Weaver and Courtier, 2001). Several assimilation strategies are available in PALM but for CAMS MOCAGE uses a 3D-VAR technique, with an assimilation window that is 1h every hour.

For surface analyses (NRT, IRA and VRA), MOCAGE assimilates O_3, NO_2, CO, PM_{10} and $PM_{2.5}$ in-situ surface observations. The species are assimilated independently every hour without any cross-species covariances, and then the increments per species are added to the analysis that serves at initial condition for computing the background of the next hour of the assimilation process, in this reanalysis mode.

1012   An hourly assimilation cycle is also used to update the atmospheric state of aerosols, with the assimilation of French lidars

1013   (mini-MPL) and some ceilometers from the European network E-profile in the regional domain of MOCAGE. The quantity

1014   modified during the assimilation process is the 3D field of total mass of all aerosol types and all sizes all together. The split

1015   per aerosol type and particle size is not modified during the assimilation. This hourly assimilation cycle is the backbone and

1016   every day at 00 UTC, the +96h forecast is initialised from this assimilation cycle.

1017

3.10 MONARCH

3.10.1 Model Overview

The MONARCH model is a fully online multiscale chemical weather prediction system for regional and global-scale applications (Badia and Jorba, 2015; Badia et al., 2017; Jorba et al., 2012; Klose et al., 2021; Pérez et al., 2011). The system is based on the meteorological Nonhydrostatic Multiscale Model on the B-grid (NMMB; (Janjic and Gall, 2012)), developed and widely verified at the National Center for Environmental Prediction (NCEP). The model couples online the NMMB with the gas-phase and aerosol continuity equations to solve the atmospheric chemistry processes in detail. The model is designed to account for the feedbacks among gases, aerosol particles and meteorology. Currently, it can consider the direct radiative effect of aerosols while ignoring cloud–aerosol interactions.

3.10.2 Model geometry

The hybrid pressure-sigma coordinate is used in the vertical direction and the Arakawa B-grid is applied in the horizontal direction. The regional model is formulated on a rotated longitude–latitude grid, with the Equator of the rotated system running through the middle of the integration domain, resulting in more uniform grid distances. In the operational regional CAMS forecasts, the model is configured for a regional domain covering Europe and part of northern Africa with a regular horizontal grid spacing on the rotated projection of 0.15° (lower-left corner at 16.37ºN 22.14ºW, upper-right corner at 58.56ºN 88.18ºE) and the top of the domain is set at 50hPa using 24 vertical layers. Surface concentrations of gases and aerosols are derived directly from the first model level; no particular vertical downscaling is implemented. The depth of the first vertical layer of the model is around 45 m and about 7 layers are set below 2 km.

3.10.3 Forcing Meteorology

The forcing meteorology is retrieved from the IFS model on a 0.125°x0.125° horizontal grid resolution with a temporal resolution of 6 hours and dynamically interpolated to the final chemistry grid and time steps using the meteorological component of MONARCH. The IFS forecast released at 12:00UTC of the previous days is used. The meteorological variables obtained from IFS are: Skin temperature, Soil temperature, Soil moisture, Snow depth, Sea-ice mask, Sea-level pressure, U component of the wind, V component of the wind, Temperature, Geopotential height, Relative humidity or specific humidity, Cloud water content.

3.10.4 Chemical initial and boundary conditions

The variables used from chemical species available in the global IFS forecast model are detailed in Table 2. Note that CH_4 is not used from IFS because the MONARCH chemical mechanism considers a constant CH_4 concentration of 1.85 ppmv. A

1046   remapping has been applied to couple the modal distribution of the IFS aerosols with the aerosols distribution of the

1047   MONARCH model (see Table 2). The forecasts are initialised by the model results of the previous day.

1048   **3.10.5   Emissions**

1049   The common annual anthropogenic emissions CAMS-REG are implemented as explained in Section 2.5.1. The High-Elective

1050   Resolution Modelling Emission System version 3 (HERMESv3; (Guevara et al., 2019)) is used to pre-process the

1051   anthropogenic, ocean and biomass burning emissions for the MONARCH model. HERMESv3 is an open source, parallel and

1052   stand-alone multiscale atmospheric emission modelling framework that processes gaseous and aerosol emissions for use in

1053   atmospheric chemistry models.

1054   CAMS_REG-AP NMVOC and $PM_{2.5}$ emissions are speciated using the sector and country-dependent split factors proposed

1055   by TNO. In terms of NOx, a fraction of 90% NO and 10% NO_2 is considered for all sectors except for road transport, in which

1056   the following fractions are applied: (i) 95% NO, 4.2% NO_2 and 0.8 HONO for gasoline road transport and (ii) 70% NO, 28.3%

1057 NO_2 and 1.7% HONO for diesel road transport (Rappenglück et al., 2013). The vertical distribution of anthropogenic emissions

1058   is performed following the sector-dependent profiles proposed by TNO. The temporal distribution follows the gridded CAMS-

1059   REG-TEMPO v4.1 profiles (Guevara et al., 2021).

1060   The biogenic emissions for NMVOC and NO are computed on-line within the MONARCH model using the Model of

1061   Emissions of Gases and Aerosols from Nature version 2.04 (MEGANv2.04; (Guenther et al., 2006)), while monthly oceanic

1062   emissions of DMS are obtained from the CAMS-GLOB-OCEA v3.1 dataset (Granier et al., 2019; Lana et al., 2011).

1063   Mineral dust emissions can be calculated online using one of the schemes described in (Klose et al., 2021). For sea salt aerosol

1064   emissions, multiple source functions are available (Spada et al., 2013).

1065   Finally, biomass burning emissions (forest, grassland and agricultural waste fires) of organic carbon, black carbon, SO_2, and

1066   DMS are taken from the GFASv1.3 dataset. This product reports hourly emissions at a horizontal gridded resolution of 0.1° x

1067   0.1°. The vertical allocation of GFAS emissions is done using the maximum fire plume injection height and distributing

1068   uniformly all the emissions across the layers below this height. The persistence of the fires in forecast mode is set to 2 days,

1069   afterwards biomass burning emissions are set to zero.

1070   **3.10.6   Solver, advection and mixing**

1071   Different chemical processes were implemented following a modular operator splitting approach to solve the advection,

1072   diffusion, emission, dry and wet deposition, and chemistry processes. In order to maintain consistency with the meteorological

1073   solver, the chemical species are advected and mixed at the corresponding time step of the meteorological tracers following the

principles described in (Janjic and Gall, 2012) and references therein. The advection scheme is Eulerian, positive definite and monotone, maintaining a consistent mass conservation of the chemical species within the domain of study. Lateral diffusion is formulated following the Smagorinsky non-linear approach, while vertical diffusion is based on the Mellor–Yamada–Janjic level 2.5 turbulence closure scheme.

The convective mixing, however, is treated differently for aerosols and gases. The scheme implemented for aerosols is described in detail in (Pérez et al., 2011) and follows a relaxation approach similar to the Betts-Miller-Janjic convective parameterization of the NMMB. On the other hand, the convective mixing of gases is solved following the sub-grid cloud scheme of (Foley et al., 2010) as described in (Badia et al., 2017).

3.10.7 Deposition

The deposition processes implemented in the MONARCH model are dry deposition, in-cloud grid-scale, and in-cloud subgrid-scale scavenging for gases and aerosols, and below cloud scavenging for aerosols only.

For gases, the dry deposition scheme follows the classical deposition velocity analogy, enabling the calculation of deposition fluxes from airborne concentrations. The canopy resistance is simulated following (Wesely, 1989). The cloud-chemistry processes are included in the system considering both the sub-grid and grid-scale scheme described in (Foley et al., 2010). The processes included are the scavenging, vertical mixing and wet-deposition. Only in-cloud scavenging is considered in the current implementation (Badia et al., 2017).

Regarding aerosols, the parameterization of the aerosol dry deposition is based on (Zhang et al., 2001) which includes simplified empirical parameterizations for the deposition processes of Brownian diffusion, impaction, interception and gravitational settling. Wet scavenging of aerosols by precipitation is computed separately for convective and grid-scale (stratiform) precipitation. The model includes parameterizations for in-cloud scavenging, and for below cloud scavenging. Detailed description of the schemes can be found in (Pérez et al., 2011).

3.10.8 Chemistry and aerosols

A gas-phase module combined with a hybrid sectional-bulk mass-based aerosol module is implemented in the MONARCH model. The gas-phase chemical mechanism used is the Carbon Bond 2005 chemical mechanism (CB05; (Yarwood. G. et al., 2005)) extended with Chlorine chemistry (Sarwar et al., 2012). The rate constants were updated based on evaluations from (Atkinson et al., 2004; Sander et al., 2006). The photolysis scheme used is the Fast-J scheme (Wild et al., 2000). It is coupled with physics of each model layer (e.g., aerosols, clouds, absorbers as ozone) and it considers grid-scale clouds from the atmospheric driver.

The aerosol module in MONARCH model solves the life cycle of sea salt, dust, organic matter (both primary and secondary), black carbon, sulphate, and nitrate aerosols. While a sectional approach is used for dust and sea salt, a bulk description of the other aerosol species is adopted. A simplified gas–aqueous–aerosol mechanism accounts for sulphur chemistry (Spada, 2015). The production of secondary nitrate–ammonium aerosol is solved using the thermodynamic equilibrium model EQSAM (Metzger et al., 2002). The coarse nitrate production is computed with an uptake reaction of HNO_3 on dust and sea salt coarse particles. The formation of SOA is considered using a simple non-volatile scheme accounting for the contribution of anthropogenic, biomass burning, and biogenic formation (Pai et al., 2020). Hygroscopic growth is considered for all aerosol components except mineral dust.

3.10.9   Assimilation system

The MONARCH assimilation system (MONARCH-DA) is based on a Local Ensemble Transform Kalman Filter (LETKF) scheme (Di Tomaso et al., 2022; Di Tomaso et al., 2017; Escribano et al., 2022; Hunt et al., 2007; Miyoshi and Yamane, 2007; Schutgens et al., 2010) coupled to the model through I/O routines. MONARCH ensemble is created by perturbing anthropogenic, biomass burning, soil and ocean emissions that are pre-processed by HERMESv3 or that are modelled by MONARCH via a physically-based scheme for dust aerosol. For analysis production in CAMS, MONARCH ensemble is run at a horizontal resolution of 0.2° latitude × 0.2° longitude in a rotated grid and initialised by the ensemble forecast of the previous day.

Hourly surface observations from in-situ measurements are currently assimilated operationally for O_3, NO_2, SO_2, CO, PM_{10}, $PM_{2.5}$. For near-real time operational analysis production, previous-day observations are combined with a MONARCH 24-hour ensemble forecast initialised at 12 UTC of the previous day.

3.11 SILAM

3.11.1 Model Overview

The System for Integrated modeLling of Atmospheric coMposition SILAM (silam.fmi.fi) is a global-to-sub-km chemistry transport model developed for a wide range of atmospheric composition and air quality assessment tasks (Sofiev et al., 2015b), emergency decision support applications (Sofiev et al., 2008), and data assimilation and source inversion problems (Vira and Sofiev, 2015; Sofiev et al., 2013). The model incorporates Eulerian and Lagrangian dispersion frameworks (the Eulerian transport routine is used for CAMS) and a set of chemical and physical transformation modules for the troposphere and the stratosphere (Carslaw et al., 1995; Damski et al., 2007; Yarwood. G. et al., 2005; Sofiev, 2000; Sofiev et al., 2010). Apart from the transport and physico-chemical cores described below, SILAM includes a set of supplementary tools including a meteorological pre-processor, input-output converters, reprojection and interpolation routines, etc. In the operational forecasts, these enabled direct forcing of the model by the ECMWF IFS meteorological fields.

SILAM has been extensively evaluated in a variety of regional and global air quality projects (Brasseur et al., 2019; Huijnen et al., 2010; Kouznetsov et al., 2020; Petersen et al., 2019; Sofiev et al., 2015b; Xian et al., 2019) and health impact assessment studies (Korhonen et al., 2008; Kukkonen et al., 2020; Lehtomäki et al., 2018).

3.11.2 Model geometry

The centre points of the model grid cover 25.05°W to 44.95°E and 30.05°N to 71.95°N on a regular latitude longitude grid of 0.1°resolution. Following (Sofiev, 2002), SILAM uses a multi-vertical approach with the meteorology-resolving grid corresponding to the tropospheric part of the IFS vertical: hybrid levels from 69 to 137. The chemical transformations and vertical fluxes are computed based on 10 thick staggered layers, with the thickness increasing from 25 m for the lowest layer to 1000-2000 m in the free troposphere. The layer tops are located at 25, 75, 175, 375, 775, 1500, 2700, 4700, 6700 and 8700m above the surface. Within the thick layers, the sub-grid information is used to evaluate the weighted averages of the high-resolution meteorological parameters and effective diffusion coefficients after (Sofiev, 2002).

3.11.3 Forcing Meteorology

Meteorological forcing is the ECMWF IFS operational forecasts taken from the 12:00UTC forecast of the previous day extracted at a resolution of 0.1° and temporal frequency of one hour for the first 72 hours and three hours for the last day of the forecast. The list of meteorological parameters extracted is: U and V components of 10m wind [m/s], 2m temperature [K], dew point temperature 2m [K] accumulated large scale rain [kg/m^2], accumulated convective rain [kg/m^2], surface roughness [m], total cloud cover [fract], convective available potential energy [J/kg], U and V -wind components at model levels [m/s],

temperature at model levels [K], cloud water at model levels [kg/kg], cloud ice at model levels [kg/kg], specific humidity at model levels [kg/kg], cloud cover at model levels[fract], logarithm of surface pressure.

3.11.4 Chemical initial and boundary conditions

Boundary conditions are taken from the C-IFS (see Table 2). The full fields are imported every 3 hours; in-between, the linear interpolation is applied. The forecasts are initialised with the SILAM forecast of the previous day.

3.11.5 Emissions

The common annual anthropogenic emissions CAMS-REG are implemented as explained in Section 3.2. The PM$_{2.5}$ emissions are split into EC, OC and mineral components, and OC is mapped to the volatility bins according to (Shrivastava et al., 2008). Emissions of biogenic VOCs, wind-blown dust, and sea salt are computed online in dedicated SILAM modules (Poupkou et al., 2010; Sofiev et al., 2011; Soares et al., 2016; Sofieva et al., 2022). GFAS hourly emissions from wild-land fires are replicated from D-2 to D+1 for forecast and shut down after; in the analysis mode it is used as is.

Emissions of 6 pollen species are computed online following the heat-sum approach for trees (Sofiev et al., 2015b), climatological season for grasses and mugwort species, and multi-criteria hybrid model for ragweed (Prank et al., 2013).

3.11.6 Solver, advection and mixing

The SILAM Eulerian transport core (Sofiev et al., 2015a) is based on the coupled developments: refined advection scheme of (Galperin and Sofiev, 1994) and vertical diffusion and dry deposition algorithm of (Sofiev, 2002)and (Kouznetsov and Sofiev, 2012). The methods are compatible, in a sense that both use the same set of variables to determine the sub-grid distribution of tracer mass. The approach, in particular, allows computing correct vertical exchange using high-resolution input data but low-resolution chemistry and diffusion grids. The later feature is used in the vertical setup with thick layers.

Diffusion is parameterised following the first-order K-theory based closure. Horizontal diffusion is embedded into the advection routine, which itself has zero numerical viscosity, thus allowing full control over the diffusion fluxes. The vertical diffusivity parameterisation follows the approach suggested by (Groisman and Genikhovich, 1997) and (Sofiev et al., 2010). The procedure diagnoses all the similarity theory parameters using the profiles of the basic meteorological quantities: wind, temperature and humidity. Output includes the value of eddy diffusivity for scalars at some reference height (taken to be 1m).

The model uses process-wise splitting and 1-D advection implementation flipping the order of processes every other time step.

3.11.7 Deposition

Dry deposition parameterisation for gases generally follows the resistive analogy of (Wesely, 1989). Deposition velocities for aerosols are evaluated using the original (Kouznetsov and Sofiev, 2012) algorithm. Wet deposition parameterisation is based on the scavenging coefficient after (Sofiev, 2000) for gas species and follows the generalised formulations of (Kouznetsov and Sofiev, 2012) for aerosols.

3.11.8 Chemistry and aerosols

The main gas-phase chemical mechanism is CB05 with additions for SOx from (Sofiev, 2000) and organics from VBS (Volatility-Basis Set, (Shrivastava et al., 2008)). The heterogeneous scheme is an updated version of the DMAT model scheme (Sofiev, 2000). The formation pathways of secondary inorganic aerosols follow the VBS approach extended with the feedback to the main gas-phase chemical module. The aerosol size distribution is represented via sectional approach, with species-specific bin selections. Each bin is characterised with its lower and upper borders, as well as the mass-mean diameter, which is precomputed / predefined for each bin and species from its size spectrum. Primary anthropogenic aerosols are emitted into bins with mass-mean diameter of 0.5 µm (fine aerosol, dry size) and 6 µm (coarse aerosols, dry size). Secondary inorganic aerosols were put into 0.2 and 0.7 µm bins, plus a separate 3 µm bin for coarse nitrates formed on the sea salt surface. The dust size spectrum is described with 4 bins from 0.3 µm up to 20 µm. Finally, the seasalt spectrum is represented with 5 bins, from 0.05 µm up to 20 µm of mass-mean nominal diameter. Throughout computations, the particles are transported in accordance with their mass-mean diameter corrected with regard to actual humidity and the particle solubility. External mixing is assumed.

3.11.9 Assimilation system

The embedded data assimilation is based on the 3d- and 4d-dimensional variational approach, as well as with the EnKF (Vira and Sofiev, 2012, 2015). Tangent-linear (if needed) and adjoint formulations exist for the transport module, the transformation schemes and for the deposition modules. The assimilation procedure has been tested for both initialising the concentration fields and for refinement of the emission (Sofiev, 2019). The observation operators exist for in-situ observations and for the vertically integrated columns observed by the nadir-looking satellites. For the near-real time operational analyses in CAMS, the previous-day observations are used in a 3D-VAR data assimilation suite. That routine assimilates in-situ observations of NO_2, O_3 and $PM_{2.5}$, PM_{10}, SO_2 and CO.

4   Post-processing

4.1   ENSEMBLE model

All eleven individual operational model results deliver their results to the CRPU (Météo-France for NRT/FC and NRT/AN, and INERIS for IRA and VRA, using the product definition introduced in Section 2.2). An ENSEMBLE model is subsequently computed as a median of all available operational models. As explicated in Section 3, there are slight differences in the individual model geometry even if they are as close as possible to the common requirement to deliver model output on the same grid. The ENSEMBLE is computed across all models at each horizontal and vertical grid point of the common grid and for each species.

Relying on 11 different models offer a very comprehensive view on the various possible representations of key atmospheric processes relevant to air quality (see the wide range of modelling design detailed in Section 3) and thus a characterisation of the intrinsic modelling uncertainty. The flipside of this diversity is a relatively higher risk of one model not being able to deliver in a timely basis. A median ENSEMBLE is computed everyday no matter how many models are successfully delivered for that given day. A Key Performance Indicator is documented to track the number of models which have delivered on time to be included in the ENSEMBLE for either the analyses or the forecasts (Figure 1).

Using the median to compute such an ensemble is a very robust approach to cope with potential missing members, and it has been shown to outperform individual models for average performances (Galmarini et al., 2004). It is however a very conservative approach and developments are ongoing, in particular to improve the skills of the system to capture air quality exceedance detections by making use of machine learning algorithm coupled to the raw CAMS regional forecasts (Bertrand et al., 2022).
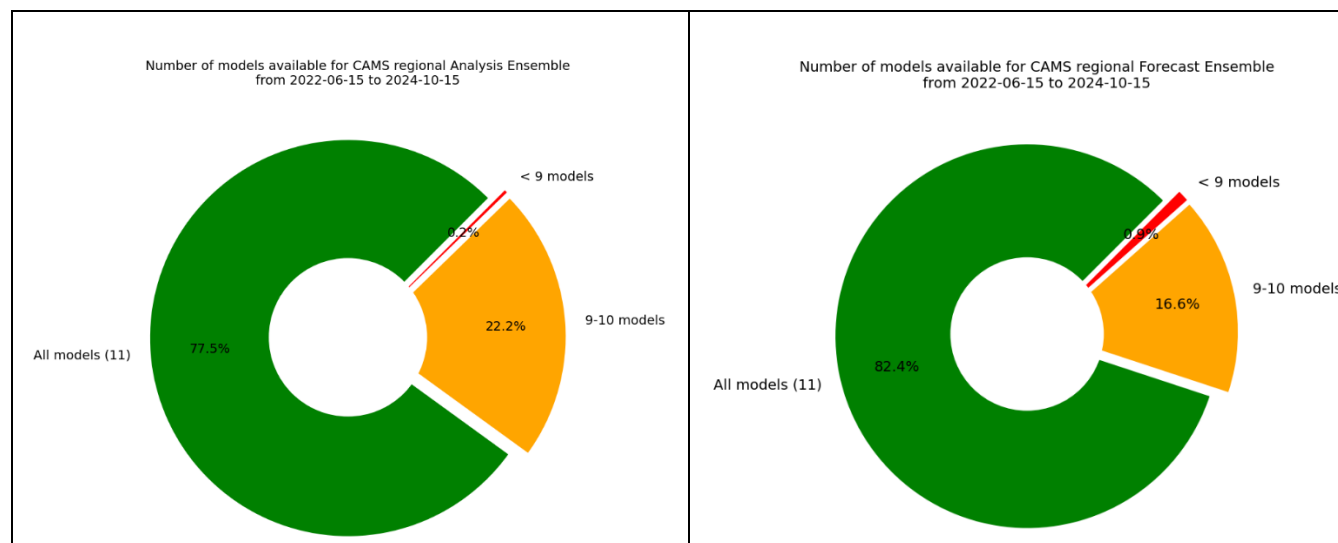
Figure 2: Distribution of the number of operational models having delivered on time to be included in the ENSEMBLE computation for the period 15/06/2022-15/10/2024: left NRT/AN (analysis) and right: NRT/FC (forecasts).

4.2   Evaluation and Quality Control (EQC)

Evaluation and quality control is an essential part of CAMS in order to ensure the reliability and transparency of the products. For all the chemical species where a dense enough monitoring network allows a recurrent and statistically significant evaluation, synthetic performance reports are produced and made available on the CAMS website[6]. These evaluations focus primarily on the surface in-situ air quality regulatory monitoring networks for O_3, NO_2, PM_{10}, $PM_{2.5}$. For the assimilated products, the evaluation is performed on about one third of the stations, deliberately left out of the assimilation workflow (Section 2.3). The forecasts are evaluated using all available surface stations whose spatial representativity ranges from rural to urban background air quality. The skill scores are updated on a daily frequency and available publicly through an interactive interface on the CAMS EQC pages for the ENSEMBLE and individual models. Quarterly summaries are produced in publicly available reports. They also include an evaluation of the models in the troposphere against above-surface measurements (aircraft and space borne remote sensing and profiling). For the Interim and Validated reanalyses, the evaluation reports are produced on an annual basis.

The present article is essentially a description of the system rather than a detailed analysis of its performance. Nevertheless, we present here a couple of evaluation diagnostics for illustration purposes. Therefore, the performances of individual models contributing to the ENSEMBLE are anonymised as it would be too complex to enter here in the details of the performances of each model, which relate to intrinsic parametrisations.

In Figure 3 we show the root mean square error for surface ozone and PM_{10} taken as the median over each quarter since the beginning of the CAMS production at the end of 2014 and over hundreds of European air quality monitoring stations. The figure is divided in two parts as urban background stations were only included in the evaluation as of fall 2018 (note also that the vertical scales differ). It appears clearly that while the spread of the models was still substantial in the first part of the period, the system has reached a level of maturity since 2017 with more homogeneous performances between the various models and very few outliers. The ENSEMBLE model appears to give better scores overall. It can be surpassed in terms of RMSE in some occasions but not always by the same model, therefore still illustrating the added value of the multi-model ensemble approach. The range of performances is today about 12-18µg/m³ for the RMSE of daily maxima ozone, so that the Key Performance Indicator of 18µg/m³ is not always met depending on the models and the season. For PM_{10}, the RMSE is between 5 to 8µg/m³ so that the same KPI of 18µg/m³ is usually met. Without entering in a more detailed analysis, it is visible

---

[6] https://atmosphere.copernicus.eu/regional-services, last accessed 30/10/2024

1249   that the scores are still gradually improving over the 2018-2023 period. Over the recent years, the median ENSEMBLE seems

1250   to produce more systematically better performances and becomes more difficult to beat.

1251
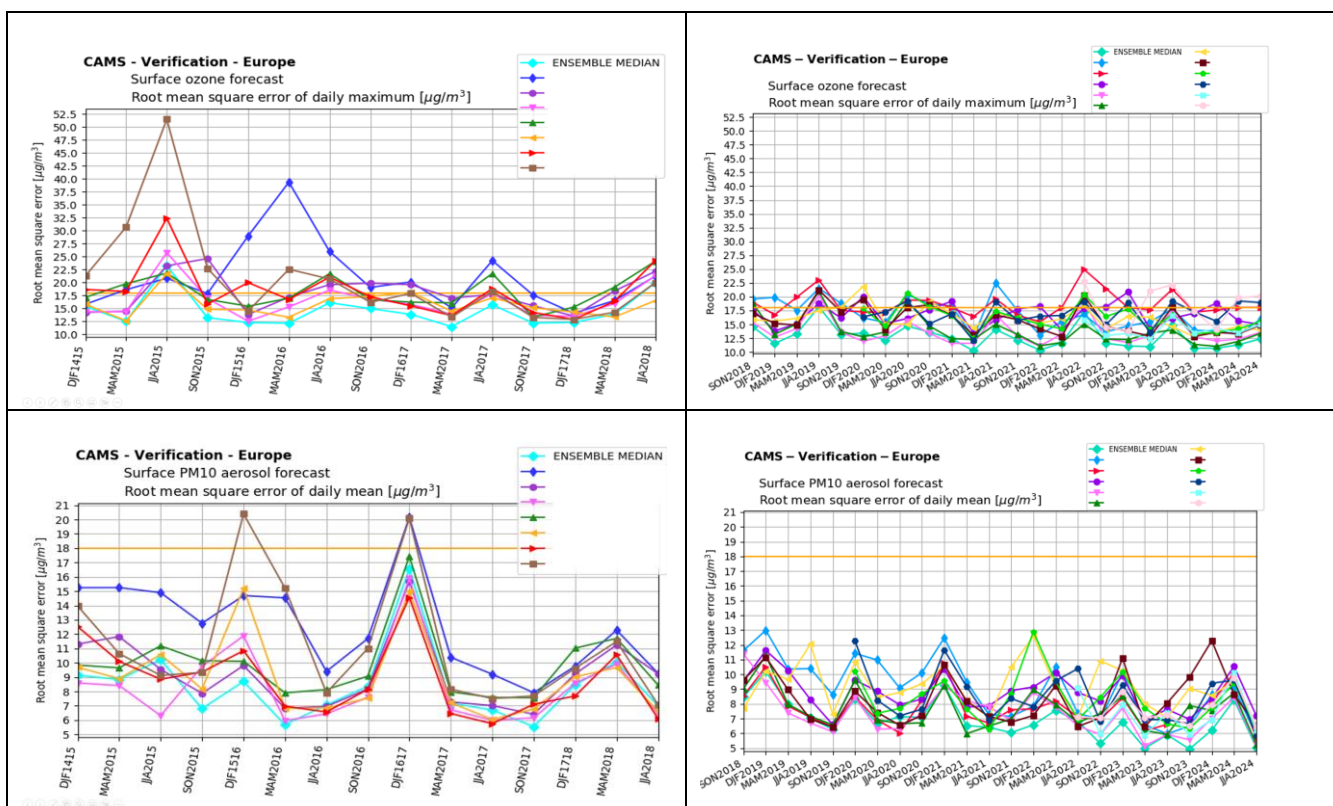
1252   *Figure 3: Evolution of the skill scores of the CAMS Regional Air Quality Forecasts (individual models and ENSEMBLE median) between*
1253   *2014 and 2024 (divided in two parts: before and after 2018 as urban background stations were not included in the evaluation over the first*
1254   *period, and fewer models were available) Each point is the quarterly median of the RMSE (µg/m³) computed at regulatory air quality*
1255   *monitoring stations for top: daily maximum ozone and bottom: daily mean PM₁₀. The straight yellow line corresponds to the Key*
1256   *Performance Indicator for RMSE of 18µg/m³.*

1257   In the European Air Quality regulation, detrimental air quality situations are identified in terms of various exceedance levels

1258   depending on the air pollutants. For PM_{10}, the daily mean concentrations should not exceed 50µg/m³ more than 35 days (EC,

1259   2008). The performance of the CAMS Regional reanalyses in capturing that threshold can be assessed through the performance

1260   diagram presented in Figure 4. On the x-axis the success ratio is the number of hits divided by the number of hits and false

1261   alarms. On the y-axis, the probability of detection is the number of hits divided by the number of hits and misses. For this

1262   example, for the year 2021, the ENSEMBLE median has the best success ratio, but some individual models outperform in

1263   terms of probability of detection.
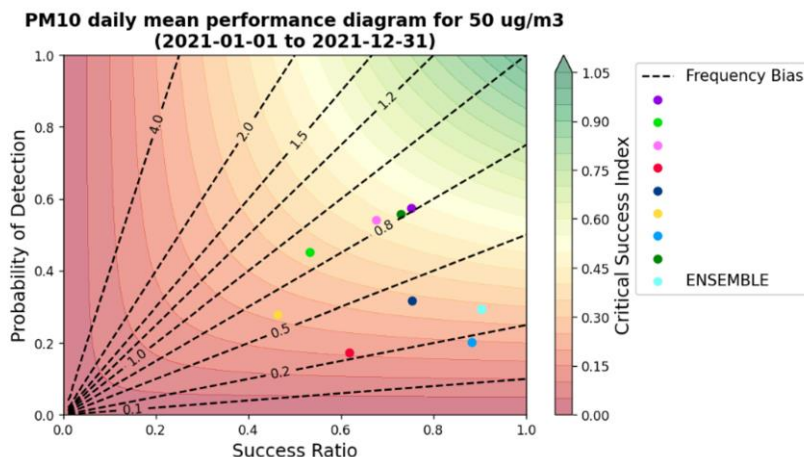
Figure 4: Performance of the CAMS Regional ENSEMBLE and individual models reanalyses in capturing air quality threshold detection for daily mean PM$_{10}$ above 50µg/m^3 in 2021.

An illustration of the evaluation above the surface is provided in Figure 5. The total column of NO$_2$ in the CAMS regional ENSEMBLE forecast is compared to the TROPOMI instrument on board the Sentinel 5P satellite. The higher spatial resolution (approximately 5km) available since the launch of the instrument allows reaching out to urban level NO$_2$ concentrations therefore providing an excellent opportunity for the evaluation of spatial patterns of air pollution. Beyond surface and total columns, it is also essential to assess the performances of the vertical structure as illustrated for the comparison with ozone soundings in Belgium (Uccle). Here both the regional forecast and analyses are compared to assess the impact of surface assimilation of air quality measurement on the vertical profiles. The CAMS global model forecast is also included along with the CAMS regional ensemble range for the forecast and the analysis. A more detailed analysis of the comparison with satellite data can be found in (Douros et al., 2022).
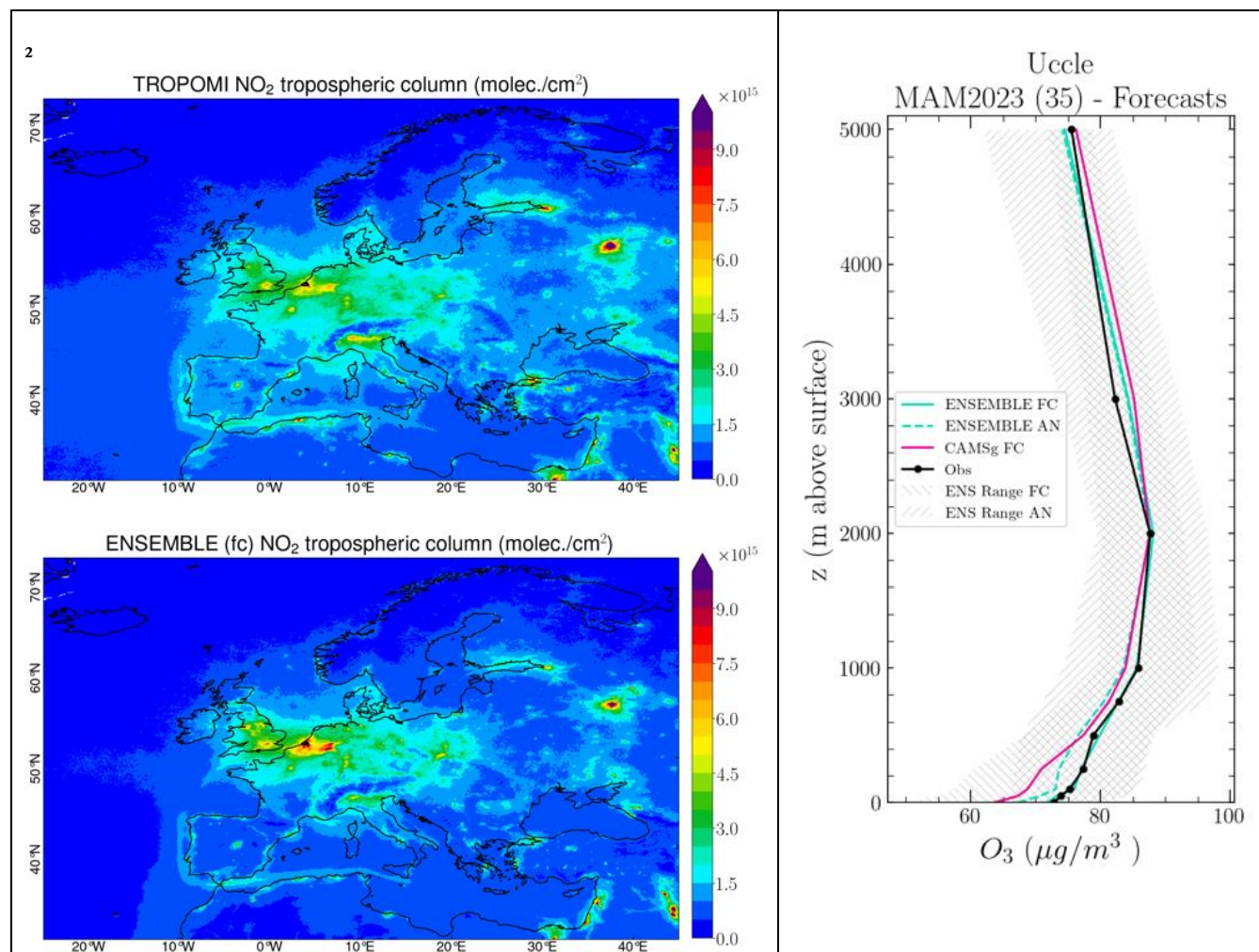
Figure 5: Left: Evaluation over MAM-2023 of the CAMS Regional ensemble forecasts against TROPOMI satellite NO_2 tropospheric columns (10^{15} molecules/cm²). The CAMS NO_2 profiles have been multiplied with the TROPOMI kernels to remove the dependency on the retrieval a-priori profile shape. Right: Regional and global CAMS forecast and regional analyses of ozone compared to vertical profiles measured with ozone sondes over Uccle, Brussels, Belgium for MAM-2023 (µg/m³). source: CAMS2_83 Evaluation and Quality Control Service, https://atmosphere.copernicus.eu/regional-services

4.3   Dissemination and further use of the CAMS Regional Products

The results of the CAMS regional production system are made available publicly on the website https://atmosphere.copernicus.eu/european-air-quality-forecast-plots where maps and time series of the various air pollutant and pollen species can be displayed. The results of the median ENSEMBLE as well as each individual model are available for both forecast and analysis products. Daily means, daily maxima, and hourly fields are available. The list of vertical levels available for interactive plotting on the website is: surface, 100m, 1000m, 3000m and 5000m (note that more vertical levels

1287   are available on the ADS). The model spread can also be assessed by selecting any grid point in the map to display the time

1288   series of the 4 day forecast including modelled dispersion (Figure 6).

1289
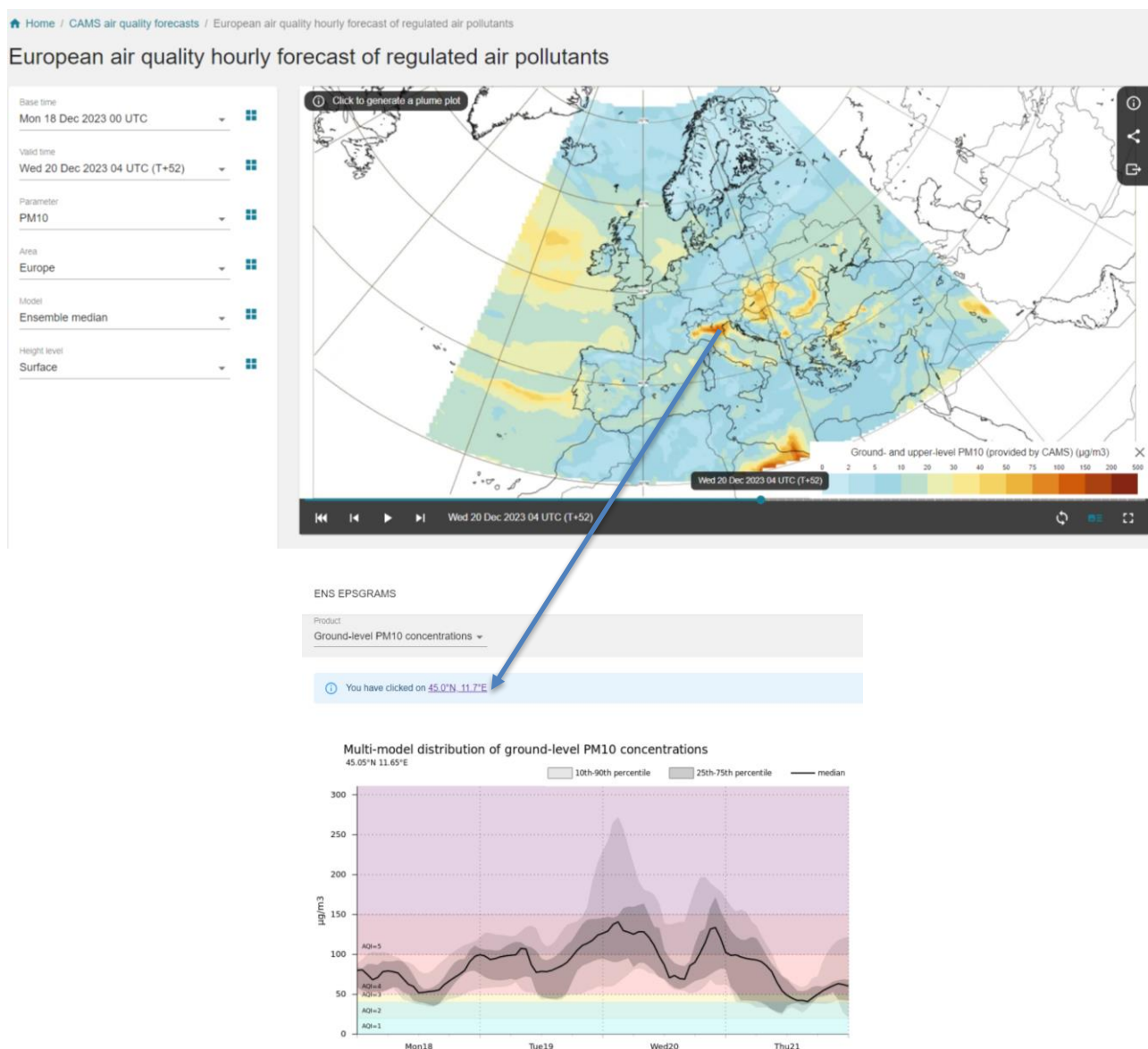
1290   *Figure 6: Screenshot of the CAMS Regional Production website displaying air quality forecasts over Europe (atmosphere.copernicus.eu6)*

The Copernicus Atmosphere Data Store (ADS) constitutes an important dissemination pathway for the CAMS Regional production system. All the numerical data can be freely retrieved through the website ads.atmosphere.copernicus.eu where automated requests can be built to download entire fields or custom extractions in either grib or netcdf formats.

The typical use of CAMS Regional forecast product is for national and local air quality management agencies to understand the day-to-day air quality situation and anticipate major air pollution events. This can be done either by a qualitative analysis of quicklooks available on the CAMS website or external companies that have developed alternative visualisation tools.

The numerical data obtained on the ADS can also be used as background information for national or local scale air quality modelling applications. Such uses range from the nesting of a Chemistry Transport Model as three-dimensional and hourly concentrations of several chemical species are available in the CAMS Regional Forecast. They can also be used to feed gaussian city-scale surface air quality models. There are also reported use of the CAMS Regional Forecast to inform machine-learning air quality statistical prediction tools (Bertrand et al., 2022; Petetin et al., 2022).

The use of CAMS Regional reanalyses is rather to inform longer term air quality applications. They can be used as background information for land-use regression models used in air quality policy products or exposure assessment for health impact studies (Horálek et al., 2022). They are also the primary source of information for the Interim Assessment Report produced annually by the CAMS Policy Service and serves as background information for European Member States in the Regulatory Air Quality reporting obligations (Hamer et al., 2023).

5   Conclusion & Perspectives

The regional production of the Copernicus Atmosphere Monitoring Service is today a well-established reference for air quality forecast and analysis in European and beyond. It is constituted of a unique ensemble of eleven European Chemistry-Transport models operated in ten countries under the management of a Centralised Regional Production Unit. The system follows strict requirements in order to produce consistent air quality products through the ensemble of individual CTM. Those requirements include in particular forcing fields such as meteorology, chemical hemispheric boundary conditions, and surface fluxes of anthropogenic and wildfire emissions. But the added value of the use of an ensemble of models also lies in the diversity of the modelling strategy. As of today, the ensemble offers a very wide array of choices in terms of model design and structure, as well as regarding the formulation of underlying physical and chemical processes or forcing and coupling at the interfaces (land, sea, biosphere, …).

In the present paper, we provide a comprehensive scientific documentation of the technical characteristics for the common forcing requirements as well as the diversity in modelling design brought about by the individual contributing modelling

1319   groups. We also explained how the billions of data produced on a daily basis are aggregated centrally, evaluated and

1320   disseminated for a wide range of air quality applications. The CAMS Service has been operational since the end of 2014 and

1321   has reached today a high level of performance and stability. Since 2017 the spread of model performances has converged and

1322   it continues to improve gradually over the years.

1323   As an operational service, the Regional Production of CAMS follows closely the research developments in the field of air

1324   quality modelling. A substantial part of the model development is undertaken independently by the modelling teams through

1325   various research projects and PhD work at national level. The international benchmarking activities (such as the AQMEII or

1326   Eurodelta initiatives, (Galmarini et al., 2017; Colette et al., 2017)) are also an important source of information to identify

1327   model development priorities. More recently, the European Union has launched a series of research projects devoted to the

1328   Evolution of Copernicus in the Horizon Europe Programme[7].

1329   In order to ensure a continuous improvement, the system follows a regular development cycle. The individual models are

1330   improved in time so that they remain in the state of the art of chemistry transport modelling. When the progress becomes

1331   mature enough, system upgrades are scheduled on a bi-annual basis to allow individual modelling groups to bring their

1332   development into the operational model version. These bi-annual upgrades are also the opportunity to carry coordinated

1333   changes, such as the regular update of anthropogenic emission fluxes. Through these upgrades, the portfolio of products is also

1334   continuously expanding. For instance, in addition to the 19 chemical species already being delivered, the current plan at the

1335   time of submission of the present article (i.e. for the year 2024) is to include new PM species such as ammonium nitrate and a

1336   tracer of shipping emissions.

1337   A large part of the research effort in relation to the Regional Production is related to Chemistry-Transport deterministic

1338   modelling. But there are also interesting prospects in the coupling between machine learning and physical and chemical

1339   modelling. The Regional Service is about to launch operational forecasts at station level on the basis of Model Output Statistics

1340   or any other Machine Learning Postprocessing which promises to open unprecedented performance in particular for air quality

1341   threshold detection (Bertrand et al., 2022). Novel methodologies to compute the ENSEMBLE model from the eleven individual

1342   production and move away from the conservative median approach are also under consideration.

1343   Besides the modelling developments, the uptake of innovative observations is also instrumental in the long-term perspective

1344   of CAMS. The production of deposition fluxes is a good illustration of the need to make the best of available observations.

1345   While CTMs are producing by nature deposition fluxes, they are not systematically quality checked and therefore the output

1346   products are limited at present to ambient air concentrations. A mid-term development is therefore ongoing to benchmark wet

---

[7] https://atmosphere.copernicus.eu/copernicus-research-whats-horizon

1347   and dry deposition fluxes to ensure their robustness. To achieve this, CAMS relies on the network of deposition data collected
1348   in the EMEP network of rural supersites in Europe. But there are also promising prospects in the uptake of near-real-time
1349   advanced observations of atmospheric composition at the supersites of the ACTRIS European Research Infrastructure, in
1350   particular with regards to particulate matter chemical composition and source apportionment. Lastly, in the outlook of the
1351   future perspectives there are also high expectations regarding the uptake of geostationary satellite retrievals with the
1352   perspective of the launch of the Sentinel 4 satellite which will bring unprecedented high-frequency atmospheric composition
1353   information over Europe.

6   Data Availability

1355   Copernicus is funded under the Copernicus Regulation and operated by ECMWF under the ECMWF Agreement. Access to
1356   all Copernicus (previously known as GMES or Global Monitoring for Environment and Security) Information and Data is
1357   regulated under Regulation (EU) No 1159/2013 of the European Parliament and of the Council of 12 July 2013 on the European
1358   Earth monitoring programme, under the ECMWF Agreement and under the European Commission's Terms and Conditions.
1359   Access to all Copernicus information is regulated under Regulation (EU) No 1159/2013 and under the ECMWF Agreement.

1360   The Copernicus Licence is free of charge, worldwide, non-exclusive, royalty free and perpetual. Access to Copernicus Products
1361   is given for any purpose in so far as it is lawful, whereas use may include, but is not limited to: reproduction; distribution;
1362   communication to the public; adaptation, modification and combination with other data and information; or any combination
1363   of the foregoing.

1364   The full terms of the Copernicus Licence are available at: https://ads.atmosphere.copernicus.eu/api/v2/terms/static/licence-to-
1365   use-copernicus-products.pdf

7   Code Availability

1367   Following the Copernicus Programme Data Policy, the Regional Production data and information are available on a full, open,
1368   and free-of-charge basis, subject to limitations concerning registration, dissemination formats, and access restrictions. The
1369   Copernicus Atmosphere Data Store is located at: https://ads.atmosphere.copernicus.eu/.

1370   The CHIMERE v2020 model is available on its dedicated website at https://www.lmd.polytechnique.fr/chimere/ and for
1371   download at https://doi.org/10.14768/8afd9058-909c-4827-94b8-69f05f7bb46d.

1372   The DEHM model is available for collaborative requests to J. H. Christensen; jc@envs.au.dk.

The EMEP model is available at https://github.com/metno/emep-ctm under the GPLv3 licence. The model version for CAMS is updated once or twice a year in the frame of the regular updates in the CAMS regional service. The current version is close to the one archived on https://doi.org/10.5281/zenodo.4230110

The EURAD-IM source code is not publicly available for download, but code and data are available on request by e-mail.

The air quality part of the GEM-AQ model code is available upon request from the Institute of Environmental Protection. The meteorological part of the GEM-AQ model is available from Environment and Climate Change Canada (https://github.com/ECCC-ASTD-MRD).

The LOTOS-EUROS model is available upon user request from the website https://airqualitymodeling.tno.nl/lotos-euros/open-source-version/.

Access for implementation is only granted to the extent it is needed for the Parties concerned to carry out their tasks in the CAMS2_40 project and provided that SMHI can grant Access Rights to the MATCH CTM (Chemistry Transport Model), including version control, build environment, scripting system for production, and the legal restrictions or limits. This includes limitations imposed on licenses of software and data. Access Rights are subject to written request. The Access Rights are granted for the purpose of the CAMS Project only and may be restricted if this results in the infringement of third-party rights. All commercial and third-party software are excluded and no Access Rights are granted.

The FARM code embedded in the MINNI System is available at https://hpc-forge.cineca.it/projects/open/20

The MOCAGE source code is not publicly available for download, but code and data are available on request by e-mail.

The MONARCH model is available at https://earth.bsc.es/gitlab/es/monarch under the GPLv3 licence.

The SILAM code is available at https://github.com/fmidev/silam-model under the GPLv3 licence. The model is updated several times a year, including two CAMS-related updates. The GitHub release follows the most-recent operational release.

8   Author Contribution

AC designed and drafted the overall manuscript and coordinated all contributions.

GC, FB, EB, VG, FM, AR, VP, CM, OF, AJ, VHP and LR contributed to drafting the centralised production specifics and general review of the draft.

MA, JA, AB, RB, DB, JB, GB, AC, JHC, FC, IDE, MDI, GD, EDT, JD, JE, HF, YF, JF, EF, LF, MG, CG, GG, MG, AG, JG, RH, MK, JWK, RKo, RKr, ACL, JL, VL, FM, AM, MM, AN, MO, CPGP, JP, AP, BR, LR, AS, MS, PS, DS, MS, AS, JS, CT, RT, TT, ST, ST, AUn, AUp, AV, PvV, LV, ZY contributed to draft the specificities of individual model description.

HE contributed to draft the text on model evaluation

JK, HdvG: contributed to draft the text on emissions.

MR, OF, VP, AR, EB, provided plots and figures

9   Competing Interest

The authors declare that they have no conflict of interest.

10   Acknowledgements

The activities described in this paper have been funded by the Copernicus Atmosphere Monitoring Service. ECMWF implements the Copernicus Atmosphere Monitoring Service and the Copernicus Climate Change Service with funding from the European Union on behalf of the European Commission.

INERIS acknowledged the support of the French Ministry in Charge of Ecology for continuous support in developing the CHIMERE model and related air quality forecasting activities.

FMI acknowledges the support of Academy of Finland projects PS4A (grant 318194) and ALL-Impress (grant 329215) for the pollen module developments.

The computing resources and the related technical support for MINNI forecast are provided by CRESCO/ENEAGRID High Performance Computing infrastructure and its staff. CRESCO/ENEAGRID High Performance Computing infrastructure is funded by ENEA, the Italian National Agency for New Technologies, Energy and Sustainable Economic Development and by Italian and European research programmes (see http://www.cresco.enea.it/english).

1421   *Table 1: Overview of the main characteristics and configurations of the eleven chemistry-transport models as used in the CAMS Regional*
1422   *Production*

		CHIMERE	DEHM	EMEP	EURAD-IM	GEM-AQ	LOTOS-EUROS	MATCH	MINNI	MOCAGE	MONARCH	SILAM
Discretisation	**Horizontal resolution**	0.1° x 0.1° regular lat-lon	0.1° x 0.1° regular lat-lon	0.1° x 0.1° regular lat-lon	9x9 km Lambert conformal	0.1° x 0.1° lat-lon spherical grid	0.1° x 0.1° regular lat-lon	0.1° x 0.1° regular lat-lon	0.15° x 0.1° regular lat-lon	0.1° x 0.1° regular lat-lon	0.15° x 0.15° rotated regular lat-lon	0.1° x 0.1° regular lat-lon
	number of vertical levels	9	29	20	23	28	12	26	14	47	24	10
	top altitude	500hPa	100hPa	100hPa	100hPa	10hPa	200hPa	8000m	7040m	5hPa	50hPa	8700m
	depth of lowermost layer	20m	20m	50m	35m	20m	20m	45m	40m	40m	40m	25m
	number of lower layers	7 below 2km	12 below 1km	10 in PBL	15 below 2km	14 below 5km	7 below 1km	10 below 850hPa	8 below 1km	8 below 2km	7 below 2km	5 below 1km
Initial & boundary conditions & meteorology	**Meteorological driver**	D-1 00:00 UTC IFS, 3hrly	D-1 12:00 UTC IFS, 3hrly	D-1 12:00 UTC IFS, 3hrly	D-1 12:00 UTC IFS for FC, IFS analysis for AN, 3hrly for FC, 6hrly for AN, downscaled with WRF	D-1 12:00 UTC IFS, 3hrly	D-1 00:00/12:00 UTC IFS, 3hrly	D-1 12:00 UTC IFS, 3hrly	D-1 12:00 UTC IFS, 1hrly	D-1 12:00 UTC IFS for FC, 1hrly (from +00h to +72h), 3hrly (from +72h to +96h) ; D00:00 UTC IFS for AN, 1hrly	D-1 12:00 UTC IFS, 6hrly, downscaled with NMMB	D-1 12:00 UTC IFS, 1hrly (from +00h to +72h), 3hrly (from +72h to +96h)

		CHIMERE	DEHM	EMEP	EURAD-IM	GEM-AQ	LOTOS-EUROS	MATCH	MINNI	MOCAGE	MONARCH	SILAM
	Boundary values	CAMS-Global IFS	CAMS-Global IFS	CAMS-Global IFS	CAMS-Global IFS	CAMS-Global IFS	CAMS-Global IFS	CAMS-Global IFS	CAMS-Global IFS	CAMS-Global IFS + MOCAGE global for additional species	CAMS-Global IFS	CAMS-Global IFS & SILAM
	Initial values	Previous forecast	Previous forecast	Previous analysis	Previous forecast	Previous forecast	Previous forecast	Previous forecast	Previous forecast	Previous forecast	Previous forecast	Previous forecast
Emissions anthropogenic	**Inventory**	CAMS-REG v6.1 REF2 2022	CAMS-REG v6.1 REF2 2022	CAMS-REG v6.1 REF2 2022	CAMS-REG v6.1 REF2 2022	CAMS-REG v6.1 REF2 2022	CAMS-REG v6.1 REF2 2022	CAMS-REG v6.1 REF2 2022	CAMS-REG v6.1 REF2 2022	CAMS-REG v6.1 REF2 2022	CAMS-REG v6.1 REF2 2022	CAMS-REG v6.1 REF2 2022
	Temporal disaggregation	TNO	CAMS-REG-TEMPO_v4.1	CAMS-REG-TEMPO_v4.1	CAMS-REG-TEMPO_v4.1	CAMS-REG-TEMPO_v4.1	CAMS-REG-TEMPO_v4.1	GENEMIS	CAMS-REG-TEMPO_v3.2	GENEMIS	CAMS-REG-TEMPO_v4.1	TNO
Emissions: natural & biogenic	**in-domain soil and road dust emissions**	(Marticorena and Bergametti, 1995)	none	(Marticorena and Bergametti, 1995; Marticorena et al., 1997; Dabdub and Seinfeld, 1994; Gomes et al., 2003; Fécan et al., 1998) Road dust emissions currently switched off.	Based on DREAM model	(Marticorena and Bergametti, 1995)	(Marticorena and Bergametti, 1995) and soil moisture inhibition as in (Fécan et al., 1998)	Road dust from (Schaap et al., 2009) and (Omstedt et al., 2005) and mineral dust based on the DEAD model of (Zender et al., 2003) (mainly attributed to the Mediterranean area).	Erosion and resuspension from (Vautard et al., 2005), soil suitable for mobilization parameterized following (Zender et al., 2003)	(Ginoux et al., 2001) and ECOCLIMAP database	Mineral dust scheme based on (Klose et al., 2021) and (Pérez et al., 2011)	SILAM dust source, SILAM sea salt source, Silam BIO-VOC source

		CHIMERE	DEHM	EMEP	EURAD-IM	GEM-AQ	LOTOS-EUROS	MATCH	MINNI	MOCAGE	MONARCH	SILAM
	in-domain sea-salt emissions	(Martensson et al., 2003) (Monahan, 1986)	(Martensson et al., 2003) (Monahan, 1986)	(Martensson et al., 2003) (Monahan, 1986; Tsyro et al., 2011)	(Sofiev et al., 2011)	(Gong et al., 2003)	(Martensson et al., 2003) {Monahan, 1986 #822	(Sofiev et al., 2011)	(Zhang et al., 2005)	(Sič et al., 2015)	(Jaeglé et al., 2011)	(Sofiev et al., 2011)
	Birch, Grass, Olive, Ragweed,	yes	yes	yes	yes	yes	yes	yes	yes	yes	yes	yes
	Biogenic emissions	MEGAN V2.10 (Guenther et al., 2012)	MEGAN v2.04 (Guenther et al., 2006)	(Simpson et al., 2012)	MEGAN V2.10 (Guenther et al., 2012)	MEGAN-MACC climatology	(Guenther et al., 1993) with detailed tree types for Europe	(Simpson et al., 2012)	MEGAN v2.04 (Guenther et al., 2006)	CAMS-GLOB-BIOv3.1 (Sinderalova et al, 2022) isoprene from MEGAN v2.04 (Guenther et al., 2006)	MEGAN v2.04 (Guenther et al., 2006)	Dynamic biogenic, (Poupkou et al., 2010)
	Soil NOx	MEGAN V2.10 (Guenther et al., 2012)	GEIA (Yienger and Levy, 1995)	CAMS-GLOB-SOIL	MEGAN V2.10 (Guenther et al., 2012)	none	(Yienger and Levy, 1995)	none	(Williams et al., 1992)	CAMS-GLOB-SOILv2.2 (Simpson et al, 2021)	MEGAN v2.04 (Guenther et al., 2006)	none
	Wildfires emissions	Hourly emissions from D-2 cycled for AN (D-1) and FC (D+0 and D+1, zero for the remaining days)	last available 24h cycle over D-2 and D-1 cycled for AN (D-1) and FC (D+0 and D+1, zero for the remaining days)	Hourly emissions from D-2 cycled for AN (D-1) and FC (D+0 and D+1, zero for the remaining days)	last available 24h cycle over D-2 and D-1 cycled for AN (D-1) and FC (D+0 and D+1, zero for the remaining days)	last available 24h cycle over D-2 and D-1 cycled for AN (D-1) and FC (D+0 and D+1, zero for the remaining days)	Hourly emissions from D-2 cycled for AN (D-1) and FC (D+0 and D+1, zero for the remaining days)	Hourly emissions from D-1 for AN (D-1) and last available 24h from D-2 and D-1 cycled for FC (D+0 to D+4)	Hourly emissions from D-1 for AN (D-1) and last available 24h from D-2 and D-1 cycled for FC (D+0 to D+4)	Hourly emissions from D-2 cycled for AN (D-1) and FC (D+0 and D+1, zero for the remaining days)	Hourly emissions from D-2 cycled for AN (D-1) and FC (D+0 and D+1, zero for the remaining days)	Hourly emissions from D-2 cycled for AN (D-1) and FC (D+0 and D+1, zero for the remaining days)

		CHIMERE	DEHM	EMEP	EURAD-IM	GEM-AQ	LOTOS-EUROS	MATCH	MINNI	MOCAGE	MONARCH	SILAM
Chemistry/Physics	**Gas phase chemistry**	MELCHIOR2 (Derognat et al., 2003), 44 gaseous species and 120 reactions	Modified (Strand and Hov, 1994), 74 species and 158 reactions	EmChem 19a, 127 species and 198 reactions (Simpson et al., 2020a)	RACM-MM (Geiger et al., 2003)	Modified ADOM IIB mechanism, 51 species and 120 reactions	Modified CBM-IV (Schaap et al., 2004)	EmChem 09 (Simpson et al., 2012) and (Langner et al., 1998)	SAPRC 99 (Carter, 2000)	RACM (tropospheric) and REPROBUS (stratospheric)	CB05 (Yarwood. G. et al., 2005)	CBM-IV
	Heterogeneous chemistry	Conversion of NO2 into HNO3 and N2O5 and Conversion of HO2 into H2O2	Oxidation of NO2 by O3 on aerosols	Aerosol-uptake of HNO3, HO2 and O3	Hydrolysis of N2O5	Hydrolysis of N2O5	Hydrolysis of N2O5	Hydrolysis of N2O5, aerosol uptake of HNO3 and CH3O2H	none	only relevant for polar stratospheric clouds	Hydrolysis of N2O5 and aerosol uptake of HNO3 on dust and sea salt	Sofiev (2000)
	Aerosol size distribution	10 bins from 10 nm to 40 µm	2 size fractions: PM2.5 and coarse fraction of PM10	2 size fractions: PM2.5 and coarse fraction of PM10	3 log-normal modes: 2 fine + 1 coarse	12 bins from 10nm to 20.5µm	5 size bins for dust and sea-salt, 2 size bins for other aerosols	2 size fractions: PM2.5 and coarse fraction of PM10	3 log-normal model: Aitken, accumulation and coarse	6 bins	8 bins for dust and sea salt. Fine mode for BC, OM, SO4 and NH4. Coarse and fine mode for NO3	2 bins, except for dust (4 bins from 10nm to 30µm) and sea salt (5 bins from 10nm to 30µm)
	Inorganic aerosols	(Couvidat et al., 2018): Thermodynamic equilibrium for particles under 1 µm and a dynamic approach for particles above 1 µm. Thermodynamic for the H+-NH4+-SO42--NO3--Na+-Cl--H2O system is based on ISORROPIA 2.1.	(Frohn, 2004)	MARS (Binkowski and Shankar, 1995), thermodynamic equilibrium for the SO4-HNO3-NO3-NH3-NH4-H2O system	thermodynamic equilibrium for the H+-NH4+-SO42--NO3--H2O system (Friese and Ebel, 2010)	(Gong et al., 2003)	ISORROPIA-2 (Fountoukis and Nenes, 2007)	(Mozurkewich, 1993)	ISORROPIA v1.7 (Nenes et al., 1998)	ISORROPIA-2 (Guth et al., 2016)	EQSAM (Metzger et al., 2002)	(Sofiev, 2000)

		CHIMERE	DEHM	EMEP	EURAD-IM	GEM-AQ	LOTOS-EUROS	MATCH	MINNI	MOCAGE	MONARCH	SILAM
	Secondary organic aerosols	(Bessagnet et al., 2009)	VBS approach (NPAS scheme of (Bergström et al., 2012a))	VBS approach (NPAS scheme, (Bergström et al., 2012a; Simpson et al., 2012))	updated SORGAM module (Li et al., 2013)	(Jiang, 2003)	not included	VBS schemes for ASOA and BSOA (Bergström et al., 2012a)) (Hodzic et al., 2016)	SORGAM (Schell et al., 2001b)	(Castro et al., 1999)	non-volatile scheme for anthropogenic, biogenic and pyrogenic precursors (Pai et al., 2020)	VBS
	Aqueous phase chemistry	SO2 oxidation by O3 and H2O2	SO2 oxidation by O3 and H2O2 (Jonson et., 2000)	SO2 oxidation by ozone and H2O2 and metal ion-catalyzed O2	10 gas/aqueous phase equilibria, 5 irreversible S(IV) -> S(VI) transformations	SO2 oxidation	SO2 oxidation	SO2 oxidation	SO2 oxidation (Seinfeld and Pandis, 1998)	SO2 oxidation	SO2 oxidation by ozone and H2O2	SO2 oxidation, nitrate formation (Sofiev, 2000), heterogeneous nitrate formation on sea salt particles
	Dry deposition: gases	resistance approach (Wesely, 1989)	resistance approach (Simpson et al., 2003; Emberson et al., 2000a)	resistance approach, including non-stomatal deposition of NH3	resistance approach (Zhang et al., 2003)	resistance approach	resistance approach (Erisman et al., 1994)	resistance approach (Simpson et al., 2012)	resistance approach (Wesely, 1989)	resistance approach (Michou et al., 2005)	resistance approach (Wesely, 1989)	resistance approach (Wesely, 1989)
	Dry deposition: aerosols	gravitational settling	gravitational settling (Simpson et al., 2003; Emberson et al., 2000a)	(Simpson et al., 2012)	resistance approach (Petroff and Zhang, 2010)	gravitational settling	(Zhang et al., 2001)	resistance approach (Simpson et al., 2012)	gravitational settling (Binkowski and Shankar, 1995)	(Sič et al., 2015)	(Zhang et al., 2001; Pérez et al., 2011)	(Kouznetsov and Sofiev, 2012)

		CHIMERE	DEHM	EMEP	EURAD-IM	GEM-AQ	LOTOS-EUROS	MATCH	MINNI	MOCAGE	MONARCH	SILAM
	Wet deposition	In-cloud scavenging for all gas/aerosols is taken into account. Below cloud by rain and snow falls is taken into account for soluble gas (HNO3, H2O2) and particles	(Simpson et al., 2003)	In-cloud and sub-cloud scavenging ratios for gases; in-cloud scavenging ratios and sub-cloud scavenging efficiencies for aerosols.	CMAQ (Salameh et al., 2007)	Below cloud scavenging for soluble gas species and aerosols	(Banzhaf et al., 2012)	gases: species dependent in-cloud and sub-cloud scavenging ratios; particles: in-cloud scavenging ratio, sub-cloud scavenging (Berge, 1993) and (Simpson et al., 2012)	(Simpson et al., 2003)	Convective: (Mari et al., 2000) Stratiform: (Giorgi and Chameides, 1986),(Slinn et al., 1978; Slinn, 1983)	(Foley et al., 2010; Pérez et al., 2011)	SILAM
Assimilation	Assimilation method	Kriging-based analysis	3D-Var	Intermittent 3d-var	Intermittent 3d-var	Optimal Interpolation	ENKF	Intermittent 3d-var	Optimal Interpolation	3D VAR	LETKF (Di Tomaso et al., 2017)	Intermittent 3d-var
	Assimilated surface pollutants	NO2, O3, PM2.5, PM10, CO, SO2	NO2, O3, CO, SO2, PM2.5, PM10	NO2, O3, SO2, CO, PM2.5, PM10	NO2, O3, CO, PM2.5, PM10	NO2, O3, CO, PM2.5, PM10, CO, SO2	NO2, O3, PM2.5, PM10	NO2, O3, CO, SO2, PM2.5, PM10	NO2, O3, CO, SO2, PM2.5, PM10	NO2, O3, PM2.5, PM10	NO2, O3, CO, SO2, PM2.5, PM10	NO2, O3, CO, SO2, PM2.5, PM10
	assimilated satellite	none	none	NO2 (OMI) until 2021, currently disabled	currently none	none	NO2 (OMI) until 2021	none	none	ground-based lidars from French network, ceilometers from e-profile, SO2 Tropomi	none	none
	Frequency of assimilation	Hourly	Hourly	Hourly	Hourly	Hourly	Hourly	Hourly	Hourly	Hourly	Hourly	Hourly

1423

1424   *Table 2: Overview of the matching between chemical species used as boundary conditions from the global IFS model and the eleven regional*
1425   *models of the CAMS Regional production*

IFS	CHIMERE	DEHM	EMEP	EURAD	GEM-AQ	LOTOS EUROS	MATCH	MINNI	MOCAGE	MONARCH	SILAM
aermr01 (wet) (sea salt 0.03-0.5 µm radius)	sea salt bins 3 to 5	SS_25= aermr01/4.3+ 0.5*aermr02/4.3	SS_25= aermr01/4.3+ 0.5*aermr02/4.3	not used	not used	SS bins 1=aermr01/4.3 (where SS_25 = SS bin 1 and 2)	SS_25=aermr01/4.3+0.4*aermr02/4.3	SS bin [1-2.5µm] = aermr01/4.3+0.40*aermr02/4.3	SS bins 1-6 = aermr01/4.3	SS bin 1=0.34*aermr01/4.3 SS bin 2=0.30*aermr01/4.3 + 0.02*aermr02/4.3	SS bin 0.5µm = aermr01/4.3
aermr02 (wet) (sea salt 0.5-5 µm radius)	sea salt bins 6 to 8	SS_co= 0.5*aermr02/4.3	SS_co=0.5*aermr02/4.3	not used	not used	SS bins 2=0.1*aermr02/4.3 SS bins 3=0.2*aermr02/4.3 SS bins 4=0.4*aermr02/4.3 SS bins 5=0.3*aermr02/4.3	SS_co=0.6*aermr02/4.3	SS bin [2.5-10µm] = 0.60*aermr02/4.3	SS bins 1-6 = aermr02/4.3	SS bin 3=0.13*aermr02/4.3 SS bin 4=0.18*aermr02/4.3 SS bin 5=0.35*aermr02/4.3 SS bin 6=0.32*aermr02/4.3+ 0.06*aermr03/4.3	SS bin 3µm = aermr02/4.3
aermr03 (wet) (sea salt 5-20 µm radius)	sea salt bin 9	not used	not used	not used	not used	not used	not used	not used	SS bins 1-6 = aermr03/4.3	SS bin 7=0.40*aermr03/4.3 SS bin 8=0.54*aermr03/4.3	SS bin 9µm = 0.5*aermr02/4.3 SS bin 20µm = 0.5*aermr02/4.3
aermr04 (dust 0.03-0.55 µm radius)	dust bins 4 to 6	DUST_25=aermr04+ aermr05	DUST_25= aermr04+ aermr05	DUST_acc=0.05 total IFS dust, DUST_coa=0.95 total IFS dust	dust bins 3-7	dust bin 1 = 0.2*aermr04+ 0.2*aermr05 dust bin 2 = 0.8*aermr04+ 0.8*aermr05	dust_25=aermr04+ aermr05+ 0.11*aermr06	dust bin [1-2.5µm] = aermr04+ aermr05+ aermr06*0,11	Dust bins 1-6	DUST bin 1 = 0.03 * aermr04 DUST bin 2 = 0.14 * aermr04	Dust 0.3µm = 0.4*aermr04 Dust 1.5µm = 0.6*aermr04

aermr05 (dust 0.55-0.9 µm radius)	dust bin 7	not used	DUST_25= aermr04+ aermr05	DUST_acc=0.05 total IFS dust, DUST_coa=0.95 total IFS dust	dust bins 8		dust_25= aermr04+ aermr05+ 0.11*aermr06	used above in dust bin [1-2.5um]	Dust bins 1-6	DUST bin 3 = 0.82 * aermr04 + 0.11 * aermr05	Dust 6µm = aermr05
aermr06 (dust 0.9-20 µm radius)	dust bins 7 to 10	DUST_co = 0,4*aermr06	DUST_co =0,4*aermr06	DUST_acc=0.05 total IFS dust, DUST_coa=0.95 total IFS dust	dust bins 9-12	dust bin 3 = 0.08*aermr06 dust bin 4 = 0.16*aermr06 dust bin 5 = 0.16*aermr06	dust_co= 0.44*aermr06	dust bin [2.5-10µm] = aermr06* 0,44	Dust bins 1-6	DUST bin 4 = 0.89 * aermr06 + 0.01 * aermr06 DUST bin 5 = 0.11 * aermr06 DUST bin 6 = 0.23 * aermr06 DUST bin 7 = 0.50 * aermr06 DUST bin 8 = 0.14 * aermr06	Dust 6µm = 0.4*aermr06 Dust 20µm = 0.6*aermr06
aermr07 hydrophilic OM	PPM bins 3 to 6	not used	not used	80% accumulation mode, 20% Aitken mode	OC bins 1-12	POM_25	EC_25=0.7*aermr07; EC_co=0.15*aermr07	AORPA bin 0-1µm = 0,00050* aermr07+ 0,00050* aermr08 AORPA bin 1-2.5µm = 0,44955* aermr07+ 0,44955* aermr08 AORA bin 0-1µm = 0,00050* aermr07 + 0,00050* aermr08 AORA bin 1-2.5µm = 0,49950* aermr07	OC bins 1-6	hydrophilic POM	Non-volatile bin of organic aerosol

								+ 0,49950* aermr08			
aermr08 hydrophobic OM	PPM bins 3 to 6	not used	not used	80% accumulation mode, 20% Aitken mode	OC bins 1-12	POM_25	EC_25=0.7*aermr08; EC_co=0.15*aermr08	AORB bin 0-1µm = 0,00010*aermr07 + 0,00010*aermr08 AORB bin 1-2.5µm = 0,09990*aermr07 + 0,09990*aermr08	OC bins 1-6	hydrophobic POM	Non-volatile bin of organic aerosol
aermr09 hydrophilic BC	PPM bins 3 to 6	BCfresh	not used	70% accumulation mode, 30% Aitken mode	BC bins 1-12	EC_25	OC_25=0.7*aermr09 OC_co=0.15*aermr09	AEC bin 0-1µm = 0,0011*aermr09+0,001*aermr10	BC bins 1-6	hydrophilic BC	EC
aermr10 hydrophobic BC	PPM bins 3 to 6	BCaged	not used	70% accumulation mode, 30% Aitken mode	BC bins 1-12	EC_25	OC_25=0.7*aermr10 OC_co=0.15*aermr10	AEC bin 1-2.5µm = 0,999*aermr09+0,999*aermr10	BC bins 1-6	hydrophobic BC	EC
aermr11 Sulphate Aerosol	SO4 bins 3 to 6	SO4	SO4	90% accumulation mode, 10% Aitken mode	SO4 bins 1-12	SO4_25	SO4	SO4 bin 0-1µm = 0,001*aermr11 SO4 bin 1-2,5µm = 0,999*aermr11	MOCAGE-global	SO4	SO4 split equaly on 2 modes
aermr16 Nitrate fine mode	not used	not used	NO3_F (0-2.5 µm)	90% accumulation mode, 10%	not used	NO3_25	NO3_f	NO3 bin 0-1µm = 0,001*aermr16 NO3 bin	MOCAGE-global	not used	not used

			Aitken mode					1-2,5µm = 0,999*aermr16 + 0,55*aermr17			
aermr17 Nitrate coarse mode	not used	not used	NO3_C (2.5-10 µm)	not used	not used	NO3_co	NITRATE(coarse)	Corse unspecified =0.45*aermr17	MOCAGE-global	not used	not used
aermr18 Ammonium	not used	not used	NH4_F (0-2.5 µm)	90% accumulation mode, 10% Aitken mode	not used	NH4_25	NH4_f	NH4 bin 0-1µm = 0,001*aermr18 NH4 bin 1-2,5µm = 0,999*aermr18	MOCAGE-global	not used	not used
aerm19 Biogenic SOA	OM	OM	not used	not used	BSOA	not used	SOA	BSOA	BSOA	not used	BSOA
aerm20 Anthropogenic SOA	OM	OM	not used	not used	ASOA	not used	SOA	ASOA	ASOA	not used	ASOA
CHOCHO (Glyoxal)	CHOCHO	not used	CHOCHO	CHOCHO	CHOCHO	not used	CHOCHO	CHOCHO	CHOCHO	not used	CHOCHO
C2H6 (ethane)	C2H6	C2H6	C2H6	C2H6	C2H6	not used	C2H6	ALK1	MOCAGE-global	C2H6	2xPAR5
C5H8 (isoprene)	C5H8	C5H8	C5H8	C5H8	C5H8	C5H8	C5H8	C5H8	MOCAGE-global	C5H8	C5H8
CH4_c (methane)	CH4	not used	CH4	not used	CH4	CH4	CH4	CH4	MOCAGE-global	not used	not used

CO (carbon monoxide)	CO	CO	CO	CO	CO	CO	CO	CO	CO	CO	CO
GO3 (ozone)	O3	O3	O3	O3	O3	O3	O3	O3	O3	O3	O3
H2O2 (hydrpogen peroxyde)	not used	not used	not used	H2O2	H2O2	not used	seasonal climatological conc used	not used	MOCAGE-global	H2O2	not used
HCHO (formaldehyde)	HCHO	HCHO	HCHO	HCHO	HCHO	HCHO	HCHO	HCHO	MOCAGE-global	HCHO	HCHO
HNO3 (nitric acid)	HNO3	HNO3	HNO3	HNO3	HNO3	HNO3	HNO3	HNO3	MOCAGE-global	HNO3	HNO3
NO (nitrogen monoxide)	not used	NO	NO	NO	NO	NO	NO	NO	MOCAGE-global	NO	NO
NO2 (nitrogen dioxide)	NO2	NO2	NO2	NO2	NO2	NO2	NO2	NO2	MOCAGE-global	NO2	NO2
PAN (Peroxyacetyl nitrate)	PAN	PAN	PAN	PAN	PAN	PAN	PAN	PAN	MOCAGE-global	PAN	PAN
SO2 (Sulphur dioxide)	SO2	SO2	SO2	SO2	SO2	SO2	SO2	SO2	SO2	SO2	SO2

1426

1427

1428

1429 **References**

1430

1431 Aamaas, B., Peters, G. P., and Fuglestvedt, J. S.: Simple emission metrics for climate impacts, Earth Syst. Dynam., 4, 145-
1432 170, 2013.

1433 Ackermann, I. J., Hass, H., Memmesheimer, M., Ebel, A., Binkowski, F. S., and Shankar, U.: Modal aerosol dynamics
1434 model for Europe: development and first applications, Atmospheric Environment, 32, 2981-2999,
1435 http://dx.doi.org/10.1016/S1352-2310(98)00006-5, 1998.

1436 Adani, M. and Uboldi, F.: Data assimilation experiments over Europe with the Chemical Transport Model FARM,
1437 Atmospheric Environment, 306, 119806, 2023.

1438 Alfaro, S. C. and Gomes, L.: Modeling mineral aerosol production by wind erosion: Emission intensities and aerosol size
1439 distributions in source areas, Journal of Geophysical Research: Atmospheres, 106, 18075-18084, 2001.

1440 Andersson-Sköld, Y. and Simpson, D.: Comparison of the chemical schemes of the EMEP MSC-W and IVL photochemical
1441 trajectory models, Atmospheric Environment, 33, 1111-1129, 1999.

1442 Atkinson, R., Baulch, D. L., Cox, R. A., Crowley, J. N., Hampson, R. F., Hynes, R. G., Jenkin, M. E., Rossi, M. J., and Troe,
1443 J.: Evaluated kinetic and photochemical data for atmospheric chemistry: Volume I - gas phase reactions of Ox, HOx, NOx
1444 and SOx species, Atmos. Chem. Phys., 4, 1461-1738, 10.5194/acp-4-1461-2004, 2004.

1445 Badia, A. and Jorba, O.: Gas-phase evaluation of the online NMMB/BSC-CTM model over Europe for 2010 in the
1446 framework of the AQMEII-Phase2 project, Atmospheric Environment, 115, 657-669, 2015.

1447 Badia, A., Jorba, O., Voulgarakis, A., Dabdub, D., Pérez García-Pando, C., Hilboll, A., Gonçalves, M., and Janjic, Z.:
1448 Description and evaluation of the Multiscale Online Nonhydrostatic AtmospheRe CHemistry model (NMMB-MONARCH)
1449 version 1.0: gas-phase chemistry at global scale, Geoscientific Model Development, 10, 609-638, 2017.

1450 Baklanov, A. and Sørensen, J.: Parameterisation of radionuclide deposition in atmospheric long-range transport modelling,
1451 Physics and Chemistry of the Earth, Part B: Hydrology, Oceans and Atmosphere, 26, 787-799, 2001.

1452 Banzhaf, S., Schaap, M., Kerschbaumer, A., Reimer, E., Stern, R., van der Swaluw, E., and Builtjes, P. J. H.:
1453 Implementation and evaluation of pH-dependent cloud chemistry and wet deposition in the chemical transport model REM-
1454 Calgrid, Atmos. Environ., 49, 2012.

1455 Barbu, A., Segers, A., Schaap, M., Heemink, A., and Builtjes, P.: A multi-component data assimilation experiment directed
1456 to sulphur dioxide and sulphate over Europe, Atmospheric Environment, 43, 1622-1631, 2009.

1457 Bechtold, P., Bazile, E., Guichard, F., Mascart, P., and Richard, E.: A mass-flux convection scheme for regional and global
1458 models, Quarterly Journal of the Royal Meteorological Society, 127, 869-886, 2001.

1459 Berge, E.: Coupling of wet scavenging of sulphur to clouds in a numerical weather prediction model, Tellus B: Chemical and
1460 Physical Meteorology, 45, 1-22, 1993.

1461 Bergström, R., Hayman, G. D., Jenkin, M. E., and Simpson, D.: Update and comparison of atmospheric chemistry
1462 mechanisms for the EMEP MSC-W model system — EmChem19a, EmChem19X, CRIv2R5Em, CB6r2Em, and
1463 MCMv3.3Em, The Norwegian Meteorological Institute, Oslo, Norway, 2022.

1464 Bergström, R., Denier Van Der Gon, H., Prévôt, A. S., Yttri, K. E., and Simpson, D.: Modelling of organic aerosols over
1465 Europe (2002–2007) using a volatility basis set (VBS) framework: application of different assumptions regarding the
1466 formation of secondary organic aerosol, Atmospheric Chemistry and Physics, 12, 8499-8527, 2012a.

1467 Bergström, R., Denier van der Gon, H. A. C., Prévôt, A. S. H., Yttri, K. E., and Simpson, D.: Modelling of organic aerosols
1468 over Europe (2002–2007) using a volatility basis set (VBS) framework: application of different assumptions regarding the
1469 formation of secondary organic aerosol, Atmos. Chem. Phys., 12, 8499-8527, doi:10.5194/acp-12-8499-2012, 2012b.

1470 Bertrand, J. M., Meleux, F., Ung, A., Descombes, G., and Colette, A.: Technical note: Improving the European air quality
1471 forecast of Copernicus Atmosphere Monitoring Service using machine learning techniques, Atmos. Chem. Phys. Discuss.,
1472 2022, 1-28, 10.5194/acp-2022-767, 2022.

1473 Bessagnet, B., Brignon, J.-M., Le Gall, A.-C., Meleux, F., Schucht, S., and Rouïl, L.: Politiques combinées de gestion de la
1474 qualité de l'air et du changement climatique (partie 1): enjeux, synergies et antagonismes, INERIS, Verneuil en Halatte,
1475 2009.

1476 Bessagnet, B., Hodzic, A., Vautard, R., Beekmann, M., Cheinet, S., Honore, C., Liousse, C., and Rouil, L.: Aerosol
1477 modeling with CHIMERE - preliminary evaluation at the continental scale, Atmospheric Environment, 38, 2803-2817,
1478 10.1016/j.atmosenv.2004.02.034, 2004.

1479 Bessagnet, B., Menut, L., Colette, A., Couvidat, F., Dan, M., Mailler, S., Létinois, L., Pont, V., and Rouïl, L.: An Evaluation
1480 of the CHIMERE Chemistry Transport Model to Simulate Dust Outbreaks across the Northern Hemisphere in March 2014,
1481 Atmosphere, 8, 251, 2017.

1482 Bessagnet, B., Menut, L., Curci, G., Hodzic, A., Guillaume, B., Liousse, C., Moukhtar, S., Pun, B., Seigneur, C., and Schulz,
1483 M.: Regional modeling of carbonaceous aerosols over Europe—focus on secondary organic aerosols, Journal of
1484 Atmospheric Chemistry, 61, 175-202, 2008.

1485 Binkowski, F. and Shankar, U.: The Regional Particulate Matter Model .1. Model description and preliminary results, J.
1486 Geophys. Res., 100, 26191–26209, 1995.

1487 Binkowski, F. S.: The aerosol portion of Models-3 CMAQ. In Science Algorithms of the EPA Models-3 Community
1488 Multiscale Air Quality (CMAQ) Modeling System. Part II: Chapters 9-18, National Exposure Research Laboratory, U.S.
1489 Environmental Protection Agency, Research Triangle Park, NC, 1999.

1490 Bott, A.: A Positive Definite Advection Scheme Obtained by Nonlinear Renormalization of the Advective Fluxes, Mon.
1491 Wea. Rev., 117, 1006-1015, 1989.

1492 Brandt, J., Silver, J. D., Frohn, L. M., Geels, C., Gross, A., Hansen, A. B., Hansen, K. M., Hedegaard, G. B., Skjoth, C. A.,
1493 Villadsen, H., Zare, A., and Christensen, J. H.: An integrated model study for Europe and North America using the Danish

Eulerian Hemispheric Model with focus on intercontinental transport of air pollution, Atmospheric Environment, 53, 156-176, 2012.

Brasseur, G. P., Xie, Y., Petersen, A. K., Bouarar, I., Flemming, J., Gauss, M., Jiang, F., Kouznetsov, R., Kranenburg, R., and Mijling, B.: Ensemble forecasts of air quality in eastern China–Part 1: Model description and implementation of the MarcoPolo–Panda prediction system, version 1, Geoscientific Model Development, 12, 33-67, 2019.

Burridge, D.: THE METEOROLOGICAL OFFICE OPERATIONAL 10-LEVEL NUMERICAL WEATHER PREDICTION MODEL (DECEMBER 1975), 1977.

Carslaw, K. S., Luo, B., and Peter, T.: An analytic expression for the composition of aqueous HNO3-H2SO4 stratospheric aerosols including gas phase removal of HNO3, Geophysical Research Letters, 22, 1877-1880, 1995.

Carson, D.: The development of a dry inversion-capped convectively unstable boundary layer, Quarterly Journal of the Royal Meteorological Society, 99, 450-467, 1973.

Carter, W. P. L.: Condensed atmospheric photooxidation mechanisms for isoprene, Atmospheric Environment, 30, 4275-4290, http://dx.doi.org/10.1016/1352-2310(96)00088-X, 1996.

Carter, W. P. L.: Documentation of the SAPRC-99 Chemical Mechanism for VOC Reactivity Assessment, 2000.

Castro, L., Pio, C., Harrison, R. M., and Smith, D.: Carbonaceous aerosol in urban and rural European atmospheres: estimation of secondary organic carbon concentrations, Atmospheric Environment, 33, 2771-2781, 1999.

Chang, T.: Rain and snow scavenging of HNO3 vapor in the atmosphere, Atmospheric Environment (1967), 18, 191-197, 1984.

Christensen, J., Brandt, J., Frohn, L., and Skov, H.: Modelling of mercury in the Arctic with the Danish Eulerian Hemispheric Model, Atmospheric Chemistry and Physics, 4, 2251-2257, 2004.

Christensen, J. H.: The Danish Eulerian hemispheric model—A three-dimensional air pollution model used for the Arctic, Atmospheric Environment, 31, 4169-4191, 1997.

Colella, P. and Woodward, P. R.: The piecewise parabolic method (PPM) for gas-dynamical simulations, Journal of computational physics, 54, 174-201, 1984.

Colette, A., Bessagnet, B., Meleux, F., Terrenoire, E., and Rouïl, L.: Frontiers in air quality modelling, Geosci. Model Dev., 7, 203-210, 2014.

Colette, A., Bessagnet, B., Vautard, R., Szopa, S., Rao, S., Schucht, S., Klimont, Z., Menut, L., Clain, G., Meleux, F., Curci, G., and Rouïl, L.: European atmosphere in 2050, a regional air quality and climate perspective under CMIP5 scenarios, Atmos. Chem. Phys., 13, 7451-7471, 2013.

Colette, A., Andersson, C., Baklanov, A., Bessagnet, B., Brandt, J., Christensen, J. H., Doherty, R., Engardt, M., Geels, C., Giannakopoulos, C., Hedegaard, G. H., Katragkou, E., Langner, J., Lei, H., Manders, A., Melas, D., Meleux, F., Rouïl, L., Sofiev, M., Soares, J., Stevenson, D. S., Tombrou-Tzella, M., Varotsos, K. V., and Young, P.: Is the ozone climate penalty robust in Europe?, Environmental Research Letters, 10, 084015, 2015.

Colette, A., Andersson, C., Manders, A., Mar, K., Mircea, M., Pay, M. T., Raffort, V., Tsyro, S., Cuvelier, C., Adani, M., Bessagnet, B., Bergström, R., Briganti, G., Butler, T., Cappelletti, A., Couvidat, F., D'Isidoro, M., Doumbia, T., Fagerli, H., Granier, C., Heyes, C., Klimont, Z., Ojha, N., Otero, N., Schaap, M., Sindelarova, K., Stegehuis, A. I., Roustan, Y., Vautard, R., van Meijgaard, E., Vivanco, M. G., and Wind, P.: EURODELTA-Trends, a multi-model experiment of air quality hindcast in Europe over 1990–2010, Geosci. Model Dev., 10, 3255-3276, 10.5194/gmd-10-3255-2017, 2017.

Côté, J., Gravel, S., Méthot, A., Patoine, A., Roch, M., and Staniforth, A.: The operational CMC–MRB global environmental multiscale (GEM) model. Part I: Design considerations and formulation, Monthly Weather Review, 126, 1373-1395, 1998a.

Côté, J., Desmarais, J.-G., Gravel, S., Méthot, A., Patoine, A., Roch, M., and Staniforth, A.: The operational CMC–MRB global environmental multiscale (GEM) model. Part II: Results, Monthly Weather Review, 126, 1397-1418, 1998b.

Couvidat, F., Bessagnet, B., Garcia-Vivanco, M., Real, E., Menut, L., and Colette, A.: Development of an inorganic and organic aerosol model (CHIMERE 2017β v1.0): seasonal and spatial evaluation over Europe, Geosci. Model Dev., 11, 165-194, 10.5194/gmd-11-165-2018, 2018.

Curier, R., Timmermans, R., Calabretta-Jongen, S., Eskes, H., Segers, A., Swart, D., and Schaap, M.: Improving ozone forecasts over Europe by synergistic use of the LOTOS-EUROS chemical transport model and in-situ measurements, Atmospheric environment, 60, 217-226, 2012.

D'Elia, I., Briganti, G., Vitali, L., Piersanti, A., Righini, G., D'Isidoro, M., Cappelletti, A., Mircea, M., Adani, M., and Zanini, G.: Measured and modelled air quality trends in Italy over the period 2003–2010, Atmospheric Chemistry and Physics, 21, 10825-10849, 2021.

Dabdub, D. and Seinfeld, J. H.: Numerical advective schemes used in air quality models—sequential and parallel implementation, Atmospheric Environment, 28, 3369-3385, 1994.

Damski, J., Thölix, L., Backman, L., Taalas, P., and Kulmala, M.: FinRose--middle atmospheric chemistry transport model, Boreal environment research, 12, 2007.

Denier van der Gon, H. A. C., Bergström, R., Fountoukis, C., Johansson, C., Pandis, S. N., Simpson, D., and Visschedijk, A. J. H.: Particulate emissions from residential wood combustion in Europe – revised estimates and an evaluation, Atmos. Chem. Phys., 15, 6503-6519, 10.5194/acp-15-6503-2015, 2015.

Derognat, C., Beekmann, M., Baeumle, M., Martin, D., and Schmidt, H.: Effect of biogenic volatile organic compound emissions on tropospheric chemistry during the Atmospheric Pollution Over the Paris Area (ESQUIF) campaign in the Ile-de-France region, Journal of Geophysical Research: Atmospheres, 108, 2003.

Di Tomaso, E., Schutgens, N. A. J., Jorba, O., and Pérez García-Pando, C.: Assimilation of MODIS Dark Target and Deep Blue observations in the dust aerosol component of NMMB-MONARCH version 1.0, Geoscientific Model Development, 10, 1107-1129, 2017.

Di Tomaso, E., Escribano, J., Basart, S., Ginoux, P., Macchia, F., Barnaba, F., Benincasa, F., Bretonnière, P. A., Buñuel, A., Castrillo, M., Cuevas, E., Formenti, P., Gonçalves, M., Jorba, O., Klose, M., Mona, L., Montané Pinto, G., Mytilinaios, M., Obiso, V., Olid, M., Schutgens, N., Votsis, A., Werner, E., and Pérez García-Pando, C.: The MONARCH high-resolution reanalysis of desert dust aerosol over Northern Africa, the Middle East and Europe (2007–2016), Earth Syst. Sci. Data, 14, 2785-2816, 10.5194/essd-14-2785-2022, 2022.

1563 Douros, J., Eskes, H., van Geffen, J., Boersma, K. F., Compernolle, S., Pinardi, G., Blechschmidt, A. M., Peuch, V. H.,
1564 Colette, A., and Veefkind, P.: Comparing Sentinel-5P TROPOMI NO2 column observations with the CAMS-regional air
1565 quality ensemble, EGUsphere, 2022, 1-40, 10.5194/egusphere-2022-365, 2022.

1566 Ebel, A., Friedrich, R., and Rodhe, H.: GENEMIS: Assessment, improvement, and temporal and spatial disaggregation of
1567 European emission data, in: Tropospheric modelling and emission estimation, Springer, 181-214, 1997.

1568 EC: Directive 2008/50/EC of the European Parliament and of the Council of 21 May 2008 on ambient air quality and cleaner
1569 air for Europe, European Commission, Brussels, 2008.

1570 ECMWF: IFS Documentation CY47R3 - Part IV Physical processes, Reading, doi: 10.21957/eyrpir4vj, 2021.

1571 Elbern, H., Strunk, A., Schmidt, H., and Talagrand, O.: Emission rate and chemical state estimation by 4-dimensional
1572 variational inversion, Atmospheric Chemistry and Physics, 7, 3749-3769, 2007.

1573 Emberson, L., Ashmore, M., Cambridge, H., Simpson, D., and Tuovinen, J.-P.: Modelling stomatal ozone flux across
1574 Europe, Environmental Pollution, 109, 403-413, 2000a.

1575 Emberson, L. D., Ashmore, M. R., Simpson, D., Tuovinen, J.-P., and Cambridge, H. M.: Towards a model of ozone
1576 deposition and stomatal uptake over Europe, Norwegian Meteorological Institute, Oslo, Norway, 57, 2000b.

1577 EMEP: Transboundary particulate matter, photo-oxydants, acidifying and eutrophying components, EMEP, Oslo, Norway,
1578 2023.

1579 Erisman, J. W., Van Pul, A., and Wyers, P.: Parametrization of surface resistance for the quantification of atmospheric
1580 deposition of acidifying pollutants and ozone, Atmospheric Environment, 28, 2595-2607, http://dx.doi.org/10.1016/1352-
1581 2310(94)90433-2, 1994.

1582 Escribano, J., Di Tomaso, E., Jorba, O., Klose, M., Gonçalves Ageitos, M., Macchia, F., Amiridis, V., Baars, H., Marinou,
1583 E., Proestakis, E., Urbanneck, C., Althausen, D., Bühl, J., Mamouri, R. E., and Pérez García-Pando, C.: Assimilating
1584 spaceborne lidar dust extinction can improve dust forecasts, Atmos. Chem. Phys., 22, 535-560, 10.5194/acp-22-535-2022,
1585 2022.

1586 Fécan, F., Marticorena, B., and Bergametti, G.: Parametrization of the increase of the aeolian erosion threshold wind friction
1587 velocity due to soil moisture for arid and semi-arid areas, Annales Geophysicae, 149-157,

1588 Flemming, J., Huijnen, V., Arteta, J., Bechtold, P., Beljaars, A., Blechschmidt, A. M., Diamantakis, M., Engelen, R. J.,
1589 Gaudel, A., Inness, A., Jones, L., Josse, B., Katragkou, E., Marecal, V., Peuch, V. H., Richter, A., Schultz, M. G., Stein, O.,
1590 and Tsikerdekis, A.: Tropospheric chemistry in the Integrated Forecasting System of ECMWF, Geosci. Model Dev., 8, 975-
1591 1003, 10.5194/gmd-8-975-2015, 2015.

1592 Foley, K., Roselle, S., Appel, K., Bhave, P., Pleim, J., Otte, T., Mathur, R., Sarwar, G., Young, J., and Gilliam, R.:
1593 Incremental testing of the Community Multiscale Air Quality (CMAQ) modeling system version 4.7, Geoscientific Model
1594 Development, 3, 205-226, 2010.

1595 Forester, C.: Higher order monotonic convective difference schemes, Journal of Computational Physics, 23, 1-22, 1977.

Fountoukis, C. and Nenes, A.: ISORROPIA II: a computationally efficient thermodynamic equilibrium model for K+−Ca2+−Mg2+−NH4+−Na+−SO42−−NO3−−Cl−−H2O aerosols, Atmos. Chem. Phys., 7, 4639-4659, doi:10.5194/acp-7-4639-2007, 2007.

Friese, E. and Ebel, A.: Temperature dependent thermodynamic model of the system H+− NH4+− Na+− SO42− NO3−−Cl−− H2O, The Journal of Physical Chemistry A, 114, 11595-11631, 2010.

Frohn, L.: A study of long-term high-resolution air pollution modelling, Ministry of the Environment, National Environmental Research Institute, Roskilde, Denmark, 2004.

Galmarini, S., Kioutsioukis, I., and Solazzo, E.: E pluribus unum*: ensemble air quality predictions, Atmos. Chem. Phys., 13, 7153-7182, 10.5194/acp-13-7153-2013, 2013.

Galmarini, S., Bianconi, R., Addis, R., Andronopoulos, S., Astrup, P., Bartzis, J., Bellasio, R., Buckley, R., Champion, H., and Chino, M.: Ensemble dispersion forecasting—Part II: Application and evaluation, Atmospheric Environment, 38, 4619-4632, 2004.

Galmarini, S., Koffi, B., Solazzo, E., Keating, T., Hogrefe, C., Schulz, M., Benedictow, A., Griesfeller, J. J., Janssens-Maenhout, G., Carmichael, G., Fu, J., and Dentener, F.: Technical note: Coordination and harmonization of the multi-scale, multi-model activities HTAP2, AQMEII3, and MICS-Asia3: simulations, emission inventories, boundary conditions, and model output formats, Atmos. Chem. Phys., 17, 1543-1555, 10.5194/acp-17-1543-2017, 2017.

Galperin, M. and Sofiev, M.: Errors in the validation of models for long-range transport and critical loads stipulated by stochastic properties of pollution fields., EMEP Chemical Coordinating Centre, Lillestrom, Passau, 162–179, 1994.

Geels, C., Winther, M., Andersson, C., Jalkanen, J.-P., Brandt, J., Frohn, L. M., Im, U., Leung, W., and Christensen, J. H.: Projections of shipping emissions and the related impact on air pollution and human health in the Nordic region, Atmospheric Chemistry and Physics, 21, 12495-12519, 2021.

Geiger, H., Barnes, I., Bejan, I., Benter, T., and Spittler, M.: The tropospheric degradation of isoprene: an updated module for the regional atmospheric chemistry mechanism, Atmospheric Environment, 37, 1503-1519, 2003.

Gery, M. W., Whitten, G. Z., Killus, J. P., and Dodge, M. C.: A photochemical kinetics mechanism for urban and regional scale computer modeling, Journal of Geophysical Research: Atmospheres, 94, 12925-12956, 1989.

Ginoux, P., Chin, M., Tegen, I., Prospero, J. M., Holben, B., Dubovik, O., and Lin, S. J.: Sources and distributions of dust aerosols simulated with the GOCART model, Journal of Geophysical Research: Atmospheres, 106, 20255-20273, 2001.

Giorgi, F. and Chameides, W. L.: Rainout lifetimes of highly soluble aerosols and gases as inferred from simulations with a general circulation model, Journal of Geophysical Research: Atmospheres, 91, 14367-14376, 1986.

Gomes, L., Rajot, J., Alfaro, S., and Gaudichet, A.: Validation of a dust production model from measurements performed in semi-arid agricultural areas of Spain and Niger, Catena, 52, 257-271, 2003.

Gong, S., Barrie, L., Blanchet, J. P., Von Salzen, K., Lohmann, U., Lesins, G., Spacek, L., Zhang, L., Girard, E., and Lin, H.: Canadian Aerosol Module: A size-segregated simulation of atmospheric aerosol processes for climate and air quality models 1. Module development, Journal of Geophysical Research: Atmospheres, 108, AAC 3-1-AAC 3-16, 2003.

1630   Granier, C., Darras, S., van der Gon, H. D., Doubalova, J., Elguindi, N., Galle, B., Gauss, M., Guevara, M., Jalkanen, J. P.,
1631   and Kuenen, J.: The Copernicus Atmosphere Monitoring Service global and regional emissions (April 2019 version),
1632   Copernicus Atmosphere Monitoring Service, 10.24380/d0bn-kx16, 2019.

1633   Groisman, P. Y. and Genikhovich, E. L.: Assessing surface–atmosphere interactions using former Soviet Union standard
1634   meteorological network data. Part I: Method, Journal of climate, 10, 2154-2183, 1997.

1635   Guenther, A., Zimmerman, P., Harley, P., Monson, R., and Fall, R.: Isoprene and monoterpene rate variability: model
1636   evaluations and sensitivity analyses, J. Geophys. Res., 98, 12609–12617, 1993.

1637   Guenther, A., Karl, T., Harley, P., Wiedinmyer, C., Palmer, P. I., and Geron, C.: Estimates of global terrestrial isoprene
1638   emissions using MEGAN (Model of Emissions of Gases and Aerosols from Nature), Atmos. Chem. Phys., 6, 3181-3210,
1639   2006.

1640   Guenther, A., Jiang, X., Heald, C. L., Sakulyanontvittaya, T., Duhl, T. a., Emmons, L., and Wang, X.: The Model of
1641   Emissions of Gases and Aerosols from Nature version 2.1 (MEGAN2. 1): an extended and updated framework for modeling
1642   biogenic emissions, Geoscientific Model Development, 5, 1471-1492, 2012.

1643   Guevara, M., Tena, C., Porquet, M., Jorba, O., and Pérez García-Pando, C.: HERMESv3, a stand-alone multi-scale
1644   atmospheric emission modelling framework–Part 1: global and regional module, Geoscientific Model Development, 12,
1645   1885-1907, 2019.

1646   Guevara, M., Jorba, O., Tena, C., Denier van der Gon, H., Kuenen, J., Elguindi, N., Darras, S., Granier, C., and Pérez
1647   García-Pando, C.: Copernicus Atmosphere Monitoring Service TEMPOral profiles (CAMS-TEMPO): global and European
1648   emission temporal profile maps for atmospheric chemistry modelling, Earth Syst. Sci. Data, 13, 367-404, 10.5194/essd-13-
1649   367-2021, 2021.

1650   Guth, J., Josse, B., Marécal, V., Joly, M., and Hamer, P.: First implementation of secondary inorganic aerosols in the
1651   MOCAGE version 2.15.0 chemistry transport model, Geosci. Model Dev., 9, 137-160, 10.5194/gmd-9-137-2016, 2016.

1652   Hamer, P., Fjaeraa, A.-M., Soarez, J., Meleux, F., Colette, A., Ung, A., Raux, B., and Tarrason, L.: Copernicus Atmosphere
1653   Monitoring Service Interim Annual Assessment Report on European Air Quality in 2022, ECMWF, Bonn,
1654   https://policy.atmosphere.copernicus.eu/reports/CAMS271_2021SCx_D1.1.1._202306_2022_Interim_Assessment_Report_v
1655   1.pdf, 2023.

1656   Hansen, K. M., Christensen, J. H., Brandt, J., Frohn, L. M., Geels, C., Skjøth, C. A., and Li, Y. F.: Modeling short-term
1657   variability of α-hexachlorocyclohexane in Northern Hemispheric air, Journal of Geophysical Research: Atmospheres, 113,
1658   2008.

1659   Hass, H., Jakobs, H., and Memmesheimer, M.: Analysis of a regional model (EURAD) near surface gas concentration
1660   predictions using observations from networks, Meteorology and Atmospheric Physics, 57, 173-200, 1995.

1661   Heidam, N. Z., Christensen, J., Wåhlin, P., and Skov, H.: Arctic atmospheric contaminants in NE Greenland: levels,
1662   variations, origins, transport, transformations and trends 1990–2001, Science of the Total Environment, 331, 5-28, 2004.

1663   Heimann, M. and Keeling, C. D.: A three-dimensional model of atmospheric CO2 transport based on observed winds: 2.
1664   Model description and simulated tracer experiments, Max-Planck-Institut für Meteorologie1989.

1665 Hendriks, C., Forsell, N., Kiesewetter, G., Schaap, M., and Schöpp, W.: Ozone concentrations and damage for realistic
1666 future European climate and air quality scenarios, Atmospheric Environment, 144, 208-219, 2016.

1667 Hertel, O., Christensen, J., Runge, E. H., Asman, W. A., Berkowicz, R., Hovmand, M. F., and Hov, Ø.: Development and
1668 testing of a new variable scale air pollution model—ACDEP, Atmospheric Environment, 29, 1267-1290, 1995.

1669 Hervig, M. E., Russell III, J. M., Gordley, L. L., Park, J. H., and Drayson, S. R.: Observations of aerosol by the HALOE
1670 experiment onboard UARS: A preliminary validation, Geophysical research letters, 20, 1291-1294, 1993.

1671 Hicks, B., Baldocchi, D., Meyers, T., Hosker, R., and Matt, D.: A preliminary multiple resistance routine for deriving dry
1672 deposition velocities from measured quantities, Water, Air, and Soil Pollution, 36, 311-330, 1987.

1673 Hodzic, A., Kasibhatla, P. S., Jo, D. S., Cappa, C. D., Jimenez, J. L., Madronich, S., and Park, R. J.: Rethinking the global
1674 secondary organic aerosol (SOA) budget: stronger production, faster removal, shorter lifetime, Atmospheric Chemistry and
1675 Physics, 16, 7917-7941, 2016.

1676 Hollingsworth, A.: Toward a monitoring and forecasting system for atmospheric composition: The GEMS Project, Bull.
1677 Amer. Meteor. Soc., 89, 1147-1164, https://doi.org/10.1175/2008BAMS2355.1, 2008.

1678 Hollingsworth, A. and Lönnberg, P.: The statistical structure of short-range forecast errors as determined from radiosonde
1679 data. Part I: The wind field, Tellus A, 38, 111-136, 1986.

1680 Holtslag, A., Van Meijgaard, E., and De Rooy, W.: A comparison of boundary layer diffusion schemes in unstable
1681 conditions over land, Boundary-Layer Meteorology, 76, 69-95, 1995.

1682 Holtslag, A. A. and Nieuwstadt, F. T.: Scaling the atmospheric boundary layer, Boundary-Layer Meteorology, 36, 201-209,
1683 1986.

1684 Horálek, J., Schreiberová, M., Vlasáková, L., Hamer, P., Schneider, P., and Marková, J.: Interim European air quality maps
1685 for 2020. PM10, NO2 and ozone spatial estimates based on non-validated UTD data., NILU, Oslo,
1686 https://www.eionet.europa.eu/etcs/etc-atni/products/etc-atni-report-19-2021-interim-european-air-quality-maps-for-2020-
1687 pm10-no2-and-ozone-spatial-estimates-based-on-non-validated-utd-data, 2022.

1688 Huang, G., Brook, R., Crippa, M., Janssens-Maenhout, G., Schieberle, C., Dore, C., Guizzardi, D., Muntean, M., Schaaf, E.,
1689 and Friedrich, R.: Speciation of anthropogenic emissions of non-methane volatile organic compounds: a global gridded data
1690 set for 1970–2012, Atmospheric Chemistry and Physics, 17, 7683-7701, 2017.

1691 Huijnen, V., Eskes, H., Poupkou, A., Elbern, H., Boersma, K., Foret, G., Sofiev, M., Valdebenito, A., Flemming, J., and
1692 Stein, O.: Comparison of OMI NO 2 tropospheric columns with an ensemble of global and European regional air quality
1693 models, Atmospheric Chemistry and Physics, 10, 3273-3296, 2010.

1694 Hunt, B. R., Kostelich, E. J., and Szunyogh, I.: Efficient data assimilation for spatiotemporal chaos: A local ensemble
1695 transform Kalman filter, Physica D: Nonlinear Phenomena, 230, 112-126, https://doi.org/10.1016/j.physd.2006.11.008,
1696 2007.

1697 Jaeglé, L., Quinn, P. K., Bates, T. S., Alexander, B., and Lin, J.-T.: Global distribution of sea salt aerosols: new constraints
1698 from in situ and remote sensing observations, Atmospheric Chemistry and Physics, 11, 3137, 2011.

1699 Janjic, Z. and Gall, L.: Scientific documentation of the NCEP nonhydrostatic multiscale model on the B grid (NMMB). Part
1700 1 Dynamics, NCAR/TN-489+STR, 2012.

1701 Jöckel, P., Tost, H., Pozzer, A., Brühl, C., Buchholz, J., Ganzeveld, L., Hoor, P., Kerkweg, A., Lawrence, M., and Sander,
1702 R.: The atmospheric chemistry general circulation model ECHAM5/MESSy1: consistent simulation of ozone from the
1703 surface to the mesosphere, Atmospheric Chemistry and Physics, 6, 5067-5104, 2006.

1704 Joly, M. and Peuch, V.-H.: Objective classification of air quality monitoring sites over Europe, Atmospheric Environment,
1705 47, 111-123, 2012.

1706 Jorba, O., Dabdub, D., Blaszczak-Boxe, C., Pérez, C., Janjic, Z., Baldasano, J., Spada, M., Badia, A., and Gonçalves, M.:
1707 Potential significance of photoexcited NO2 on global air quality with the NMMB/BSC chemical transport model, Journal of
1708 Geophysical Research: Atmospheres, 117, 2012.

1709 Kahnert, M.: Variational data analysis of aerosol species in a regional CTM: background error covariance constraint and
1710 aerosol optical observation operators, Tellus B: Chemical and Physical Meteorology, 60, 753-770, 2008.

1711 Kain, J. S. and Fritsch, J. M.: A one-dimensional entraining/detraining plume model and its application in convective
1712 parameterization, Journal of Atmospheric Sciences, 47, 2784-2802, 1990.

1713 Kaiser, J., Heil, A., Andreae, M., Benedetti, A., Chubarova, N., Jones, L., Morcrette, J.-J., Razinger, M., Schultz, M., and
1714 Suttie, M.: Biomass burning emissions estimated with a global fire assimilation system based on observed fire radiative
1715 power, Biogeosciences, 9, 527-554, 2012.

1716 Kawka, M., Struzewska, J., and Kaminski, J. W.: Spatial and Temporal Variation of NO 2 Vertical Column Densities
1717 (VCDs) over Poland: Comparison of the Sentinel-5P TROPOMI Observations and the GEM-AQ Model Simulations,
1718 Atmosphere, 12, 896, 2021.

1719 Klose, M., Jorba, O., Gonçalves Ageitos, M., Escribano, J., Dawson, M. L., Obiso, V., Di Tomaso, E., Basart, S., Montané
1720 Pinto, G., and Macchia, F.: Mineral dust cycle in the Multiscale Online Nonhydrostatic AtmospheRe CHemistry model
1721 (MONARCH) version 2.0, Geoscientific Model Development, 14, 6403-6444, 2021.

1722 Köble, R. and Seufert, G.: Novel maps for forest tree species in Europe, Proceedings of the 8th European symposium on the
1723 physico-chemical behaviour of air pollutants:"a changing atmosphere, 17-20,

1724 Korhonen, H., Carslaw, K. S., Spracklen, D. V., Mann, G. W., and Woodhouse, M. T.: Influence of oceanic dimethyl sulfide
1725 emissions on cloud condensation nuclei concentrations and seasonality over the remote Southern Hemisphere oceans: A
1726 global model study, Journal of Geophysical Research: Atmospheres, 113, 2008.

1727 Kouznetsov, R. and Sofiev, M.: A methodology for evaluation of vertical dispersion and dry deposition of atmospheric
1728 aerosols, Journal of Geophysical Research: Atmospheres, 117, 2012.

1729 Kouznetsov, R., Sofiev, M., Vira, J., and Stiller, G.: Simulating age of air and the distribution of SF 6 in the stratosphere
1730 with the SILAM model, Atmospheric Chemistry and Physics, 20, 5837-5859, 2020.

1731 Kuenen, J., Visschedijk, A., Jozwicka, M., and Denier Van Der Gon, H.: TNO-MACC_II emission inventory; a multi-year
1732 (2003–2009) consistent high-resolution European emission inventory for air quality modelling, Atmospheric Chemistry and
1733 Physics, 14, 10963-10976, 2014.

1734 Kuenen, J., Dellaert, S., Visschedijk, A., Jalkanen, J.-P., Super, I., and Denier van der Gon, H.: CAMS-REG-v4: a state-of-
1735 the-art high-resolution European emission inventory for air quality modelling, Earth System Science Data, 14, 491-515,
1736 2022.

1737 Kukkonen, J., Savolahti, M., Palamarchuk, Y., Lanki, T., Nurmi, V., Paunu, V.-V., Kangas, L., Sofiev, M., Karppinen, A.,
1738 and Maragkidou, A.: Modelling of the public health costs of fine particulate matter and results for Finland in 2015,
1739 Atmospheric Chemistry and Physics, 20, 9371-9391, 2020.

1740 Kylling, A., Stamnes, K., and Tsay, S.-C.: A reliable and efficient two-stream algorithm for spherical radiative transfer:
1741 Documentation of accuracy in realistic layered media, Journal of Atmospheric Chemistry, 21, 115-150, 1995.

1742 Lahoz, W., Geer, A., Bekki, S., Bormann, N., Ceccherini, S., Elbern, H., Errera, Q., Eskes, H., Fonteyn, D., and Jackson, D.:
1743 The Assimilation of Envisat data (ASSET) project, Atmospheric Chemistry and Physics, 7, 1773-1796, 2007.

1744 Lambert, J. D.: Numerical methods for ordinary differential systems, Wiley New York1991.

1745 Lana, A., Bell, T., Simó, R., Vallina, S., Ballabrera-Poy, J., Kettle, A., Dachs, J., Bopp, L., Saltzman, E., and Stefels, J.: An
1746 updated climatology of surface dimethlysulfide concentrations and emission fluxes in the global ocean, Global
1747 Biogeochemical Cycles, 25, 2011.

1748 Landgraf, J. and Crutzen, P.: An efficient method for online calculations of photolysis and heating rates, Journal of the
1749 atmospheric sciences, 55, 863-878, 1998.

1750 Lange, R.: Transferability of a three-dimensional air quality model between two different sites in complex terrain, Journal of
1751 Applied Meteorology and Climatology, 28, 665-679, 1989.

1752 Langner, J., Bergström, R., and Pleijel, K.: European scale modeling of sulphur, oxidized nitrogen and photochemical
1753 oxidants. Model development and evaluation for the 1994 growing season, Swedish Met. and Hydrol. Inst., Norrköping,
1754 Sweden, 1998.

1755 Lansø, A. S., Smallman, T. L., Christensen, J. H., Williams, M., Pilegaard, K., Sørensen, L.-L., and Geels, C.: Simulating the
1756 atmospheric CO 2 concentration across the heterogeneous landscape of Denmark using a coupled atmosphere–biosphere
1757 mesoscale model system, Biogeosciences, 16, 1505-1524, 2019.

1758 Lefevre, F., Brasseur, G., Folkins, I., Smith, A., and Simon, P.: Chemistry of the 1991–1992 stratospheric winter: Three-
1759 dimensional model simulations, Journal of Geophysical Research: Atmospheres, 99, 8183-8195, 1994.

1760 Lehtomäki, H., Korhonen, A., Asikainen, A., Karvosenoja, N., Kupiainen, K., Paunu, V.-V., Savolahti, M., Sofiev, M.,
1761 Palamarchuk, Y., and Karppinen, A.: Health impacts of ambient air pollution in Finland, International journal of
1762 environmental research and public health, 15, 736, 2018.

1763 Li, Y., Elbern, H., Lu, K., Friese, E., Kiendler-Scharr, A., Mentel, T. F., Wang, X., Wahner, A., and Zhang, Y.: Updated
1764 aerosol module and its application to simulate secondary organic aerosols during IMPACT campaign May 2008,
1765 Atmospheric chemistry and physics, 13, 6289-6304, 2013.

1766 Liu, D. C. and Nocedal, J.: On the limited memory BFGS method for large scale optimization, Mathematical programming,
1767 45, 503-528, 1989.

1768 Louis, J.-F.: A parametric model of vertical eddy fluxes in the atmosphere, Boundary-Layer Meteorology, 17, 187-202,
1769 1979.

1770 Lurmann, F. W., Lloyd, A. C., and Atkinson, R.: A chemical mechanism for use in long-range transport/acid deposition
1771 computer modeling, Journal of Geophysical Research: Atmospheres, 91, 10905-10936, 1986.

1772 Maas, R. and Grennfelt , P.: Towards Cleaner Air - Scientific Assessment Report 2016, EMEP-Steering body and Working
1773 Group on Effects - Convention on Long-Range Transboundary Air Pollution 2016.

1774 Madronich, S.: Photodissociation in the atmosphere: 1. Actinic flux and the effects of ground reflections and clouds, Journal
1775 of Geophysical Research: Atmospheres, 92, 9740-9752, 1987.

1776 Madronich, S. and Weller, G.: Numerical integration errors in calculated tropospheric photodissociation rate coefficients,
1777 Journal of atmospheric chemistry, 10, 289-300, 1990.

1778 Manders, A. M. M., Builtjes, P. J. H., Curier, L., Denier van der Gon, H. A. C., Hendriks, C., Jonkers, S., Kranenburg, R.,
1779 Kuenen, J., Segers, A. J., Timmermans, R. M. A., Visschedijk, A., Wichink Kruit, R. J., Van Pul, W. A. J., Sauter, F. J., van
1780 der Swaluw, E., Swart, D. P. J., Douros, J., Eskes, H., van Meijgaard, E., van Ulft, B., van Velthoven, P., Banzhaf, S., Mues,
1781 A., Stern, R., Fu, G., Lu, S., Heemink, A., van Velzen, N., and Schaap, M.: Curriculum Vitae of the LOTOS-EUROS (v2.0)
1782 chemistry transport model, Geosci. Model Dev. Discuss., 2017, 1-53, 10.5194/gmd-2017-88, 2017.

1783 Marécal, V., Peuch, V. H., Andersson, C., Andersson, S., Arteta, J., Beekmann, M., Benedictow, A., Bergstrom, R.,
1784 Bessagnet, B., Cansado, A., Chéroux, F., Colette, A., Coman, A., Curier, R. L., Denier van der Gon, H. A. C., Drouin, A.,
1785 Elbern, H., Emili, E., Engelen, R. J., Eskes, H. J., Foret, G., Friese, E., Gauss, M., Giannaros, C., Guth, J., Joly, M.,
1786 Jaumouilla, E., Josse, B., Kadygrov, N., Kaiser, J. W., Krajsek, K., Kuenen, J., Kumar, U., Liora, N., Lopez, E., Malherbe,
1787 L., Martinez, I., Melas, D., Meleux, F., Menut, L., Moinat, P., Morales, T., Parmentier, J., Piacentini, A., Plu, M., Poupkou,
1788 A., Queguiner, S., Robertson, L., Rouil, L., Schaap, M., Segers, A., Sofiev, M., Tarasson, L., Thomas, M., Timmermans, R.,
1789 Valdebenito, A., van Velthoven, P., van Versendaal, R., Vira, J., and Ung, A.: A regional air quality forecasting system over
1790 Europe: the MACC-II daily ensemble production, Geosci. Model Dev., 8, 2777-2813, 2015.

1791 Mari, C., Jacob, D. J., and Bechtold, P.: Transport and scavenging of soluble gases in a deep convective cloud, Journal of
1792 Geophysical Research: Atmospheres, 105, 22255-22267, 2000.

1793 Martensson, E., Nilsson, E., de Leeuw, G., Cohen, L., and Hansson, H.-C.: Laboratory simulations and parameterisation of
1794 the primary marine aerosol production, J. Geophys. Res., 108, 4297, doi:10.1029/2002JD002263, 2003.

1795 Martet, M., Peuch, V., Laurent, B., Marticorena, B., and Bergametti, G.: Evaluation of long-range transport and deposition
1796 of desert dust with the CTM MOCAGE, Tellus B: Chemical and Physical Meteorology, 61, 449-463, 2009.

1797 Marticorena, B. and Bergametti, G.: Modeling the atmospheric dust cycle: 1. Design of a soil-derived dust emission scheme,
1798 Journal of geophysical research: atmospheres, 100, 16415-16430, 1995.

1799 Marticorena, B., Bergametti, G., Aumont, B., Callot, Y., N'Doumé, C., and Legrand, M.: Modeling the atmospheric dust
1800 cycle: 2. Simulation of Saharan dust sources, Journal of Geophysical Research: Atmospheres, 102, 4387-4404, 1997.

1801 Maul, P., Barber, F., and Martin, A.: Some observations of the meso-scale transport of sulphur compounds in the rural East
1802 Midlands, Atmospheric Environment (1967), 14, 339-354, 1980.

1803   McRae, G. J., Goodin, W. R., and Seinfeld, J. H.: Numerical solution of the atmospheric diffusion equation for chemically
1804   reacting flows, Journal of Computational Physics, 45, 1-42, 1982.

1805   Meleux, F., Solmon, F., and Giorgi, F.: Increase in summer European ozone amounts due to climate change, Atmospheric
1806   Environment, 41, 7577-7587, 2007.

1807   Memmesheimer, M., Friese, E., Ebel, A., Jakobs, H., Feldmann, H., Kessler, C., and Piekorz, G.: Long-term simulations of
1808   particulate matter in Europe on different scales using sequential nesting of a regional model, International Journal of
1809   Environment and Pollution, 22, 108-132, 2004.

1810   Ménégoz, M., Salas y Melia, D., Legrand, M., Teyssèdre, H., Michou, M., Peuch, V.-H., Martet, M., Josse, B., and
1811   Dombrowski-Etchevers, I.: Equilibrium of sinks and sources of sulphate over Europe: comparison between a six-year
1812   simulation and EMEP observations, Atmospheric Chemistry and Physics, 9, 4505-4519, 2009.

1813   Menut, L., Bessagnet, B., Briant, R., Cholakian, A., Couvidat, F., Mailler, S., Pennel, R., Siour, G., Tuccella, P., and
1814   Turquety, S.: The CHIMERE v2020r1 online chemistry-transport model, Geoscientific Model Development, 14, 6781-6811,
1815   2021.

1816   Metzger, S., Dentener, F., Pandis, S., and Lelieveld, J.: Gas/aerosol partitioning: 1. A computationally efficient model, J.
1817   Geophys. Res., 107, 4312, 2002.

1818   Michou, M., Laville, P., Serça, D., Fotiadi, A., Bouchou, P., and Peuch, V.-H.: Measured and modeled dry deposition
1819   velocities over the ESCOMPTE area, Atmospheric Research, 74, 89-116, 2005.

1820   Mircea, M., Ciancarella, L., Briganti, G., Calori, G., Cappelletti, A., Cionni, I., Costa, M., Cremona, G., D'Isidoro, M.,
1821   Finardi, S., Pace, G., Piersanti, A., Righini, G., Silibello, C., Vitali, L., and Zanini, G.: Assessment of the AMS-MINNI
1822   system capabilities to simulate air quality over Italy for the calendar year 2005, Atmospheric Environment, 84, 178-188,
1823   https://doi.org/10.1016/j.atmosenv.2013.11.006, 2014.

1824   Miyoshi, T. and Yamane, S.: Local Ensemble Transform Kalman Filtering with an AGCM at a T159/L48 Resolution,
1825   Monthly Weather Review, 135, 3841-3861, 10.1175/2007MWR1873.1, 2007.

1826   Monahan, E. C.: The ocean as a source of atmospheric particles, in: The Role of Air-Sea Exchange in Geochemical Cycling,
1827   Kluwer Academic Publishers, Dordrecht, Holland, 129–163, 1986.

1828   Morcrette, J. J., Boucher, O., Jones, L., Salmond, D., Bechtold, P., Beljaars, A., Benedetti, A., Bonet, A., Kaiser, J., and
1829   Razinger, M.: Aerosol analysis and forecast in the European Centre for medium-range weather forecasts integrated forecast
1830   system: Forward modeling, Journal of Geophysical Research: Atmospheres, 114, 2009.

1831   Mozurkewich, M.: The dissociation constant of ammonium nitrate and its dependence on temperature, relative humidity and
1832   particle size, Atmospheric Environment. Part A. General Topics, 27, 261-270, http://dx.doi.org/10.1016/0960-
1833   1686(93)90356-4, 1993.

1834   Nenes, A., Pandis, S., and Pilinis, C.: ISORROPIA: A New Thermodynamic Equilibrium Model for Multiphase
1835   Multicomponent Inorganic Aerosols, Aquatic Geochemistry, 4, 123-152, 1998.

1836   Nho-Kim, E.-Y., Michou, M., and Peuch, V.-H.: Parameterization of size-dependent particle dry deposition velocities for
1837   global modeling, Atmospheric Environment, 38, 1933-1942, 2004.

Nho-Kim, E., Peuch, V., and Oh, S.: Estimation of the global distribution of Black Carbon aerosols with MOCAGE, the CTM of Météo-France, J. Korean Meteor. Soc, 41, 587-598, 2005.

Nieradzik, L.: Application of a high dimensional model representation on the atmospheric aerosol module MADE of the EURAD-CTM, Institut fur Geophysik und Meteorologie der Universitat zu Koln, 2005.

Nieuwstadt, F.: The steady-state height and resistance laws of the nocturnal boundary layer: Theory compared with Cabauw observations, Boundary-Layer Meteorology, 20, 3-17, 1981.

Nocedal, J.: Updating quasi-Newton matrices with limited storage, Mathematics of computation, 35, 773-782, 1980.

Noilhan, J. and Planton, S.: A simple parameterization of land surface processes for meteorological models, Monthly weather review, 117, 536-549, 1989.

Omstedt, G., Bringfelt, B., and Johansson, C.: A model for vehicle-induced non-tailpipe emissions of particles along Swedish roads, Atmospheric environment, 39, 6088-6097, 2005.

Pai, S. J., Heald, C. L., Pierce, J. R., Farina, S. C., Marais, E. A., Jimenez, J. L., Campuzano-Jost, P., Nault, B. A., Middlebrook, A. M., Coe, H., Shilling, J. E., Bahreini, R., Dingle, J. H., and Vu, K.: An evaluation of global organic aerosol schemes using airborne observations, Atmos. Chem. Phys., 20, 2637-2665, 10.5194/acp-20-2637-2020, 2020.

Parrish, D. F. and Derber, J. C.: The National Meteorological Center's spectral statistical-interpolation analysis system, Monthly Weather Review, 120, 1747-1763, 1992.

Passant, N.: Speciation of UK emissions of non-methane volatile organic compounds, AEA Technology2002.

Pepper, D., Kern, C., and Long Jr, P.: Modeling the dispersion of atmospheric pollution using cubic splines and chapeau functions, Atmospheric Environment (1967), 13, 223-237, 1979.

Pérez, C., Haustein, K., Jorba, O., Janjic, Z., Huneeus, N., Baldasano, J. M., Black, T., Basart, S., Nickovic, S., Miller, R. L., Perlwitz, J., Schulz, M., and Thomson, M.: Atmospheric dust modeling from meso to global scales with the online NMMB/BSC-Dust model–Part 1: Model description, annual simulations and evaluation, Atmospheric Chemistry and Physics, 11, 13001-13027, 2011.

Petersen, A. K., Brasseur, G. P., Bouarar, I., Flemming, J., Gauss, M., Jiang, F., Kouznetsov, R., Kranenburg, R., Mijling, B., and Peuch, V.-H.: Ensemble forecasts of air quality in eastern China–Part 2: Evaluation of the MarcoPolo–Panda prediction system, version 1, Geoscientific Model Development, 12, 1241-1266, 2019.

Peterson, J. T.: Calculated actinic fluxes (290-700 nm) for air pollution photochemistry applications, US Environmental Protection Agency, Office of Research and Development …1976.

Petroff, A. and Zhang, L.: Development and validation of a size-resolved particle dry deposition scheme for application in aerosol transport models, Geoscientific Model Development, 3, 753-769, 2010.

Peuch, V.-H., Engelen, R., Rixen, M., Dee, D., Flemming, J., Suttie, M., Ades, M., Agustí-Panareda, A., Ananasso, C., Andersson, E., Armstrong, D., Barré, J., Bousserez, N., Dominguez, J. J., Garrigues, S., Inness, A., Jones, L., Kipling, Z., Letertre-Danczak, J., Parrington, M., Razinger, M., Ribas, R., Vermoote, S., Yang, X., Simmons, A., Garcés de Marcilla, J.,

and Thépaut, J.-N.: The Copernicus Atmosphere Monitoring Service: From Research to Operations, Bulletin of the American Meteorological Society, 103, E2650-E2668, https://doi.org/10.1175/BAMS-D-21-0314.1, 2022.

Peuch, V., Engelen, R., Simmons, A., Lahoz, W., Laj, P., and Galmarini, S.: Monitoring atmospheric composition and climate, research in support of the Copernicus/GMES atmospheric service, Special Issue, Atmos. Chem. Phys., http://www. atmos-chem-phys. net/special_issue310. html, 2014.

Poupkou, A., Giannaros, T., Markakis, K., Kioutsioukis, I., Curci, G., Melas, D., and Zerefos, C.: A model for European Biogenic Volatile Organic Compound emissions: Software development and first validation, Environmental Modelling & Software, 25, 1845-1856, 2010.

Prank, M., Chapman, D. S., Bullock, J. M., Belmonte, J., Berger, U., Dahl, A., Jäger, S., Kovtunenko, I., Magyar, D., and Niemelä, S.: An operational model for forecasting ragweed pollen release and dispersion in Europe, Agricultural and forest meteorology, 182, 43-53, 2013.

Rabitz, H. and Aliş, Ö. F.: General foundations of high-dimensional model representations, Journal of Mathematical Chemistry, 25, 197-233, 1999.

Rappenglück, B., Lubertino, G., Alvarez, S., Golovko, J., Czader, B., and Ackermann, L.: Radical precursors and related species from traffic as observed and modeled at an urban highway junction, Journal of the Air & Waste Management Association, 63, 1270-1286, 2013.

Rémy, S., Kipling, Z., Flemming, J., Boucher, O., Nabat, P., Michou, M., Bozzo, A., Ades, M., Huijnen, V., Benedetti, A., Engelen, R., Peuch, V. H., and Morcrette, J. J.: Description and evaluation of the tropospheric aerosol scheme in the European Centre for Medium-Range Weather Forecasts (ECMWF) Integrated Forecasting System (IFS-AER, cycle 45R1), Geosci. Model Dev., 12, 4627-4659, 10.5194/gmd-12-4627-2019, 2019.

Robertson, L., Langner, J., and Engardt, M.: An Eulerian limited-area atmospheric transport model, Journal of Applied Meteorology and Climatology, 38, 190-210, 1999.

Robichaud, A. and Ménard, R.: Multi-year objective analyses of warm season ground-level ozone and PM 2.5 over North America using real-time observations and Canadian operational air quality models, Atmospheric Chemistry and Physics, 14, 1769-1800, 2014.

Roselle, S. J. and Binkowski, F. S.: Cloud dynamics and chemistry, Science algorithms of the EPA Models-3 Community multiscale air quality (CMAQ) modeling system, 1999.

Rouïl, L., Honore, C., Vautard, R., Beekmann, M., Bessagnet, B., Malherbe, L., Meleux, F., Dufour, A., Elichegaray, C., Flaud, J. M., Menut, L., Martin, D., Peuch, A., Peuch, V. H., and Poisson, N.: PREV'AIR An Operational Forecasting and Mapping System for Air Quality in Europe, Bulletin of the American Meteorological Society, 90, 73-83, 10.1175/2008bams2390.1, 2009.

Salameh, T., Drobinski, P., Menut, L., Bessagnet, B., Flamant, C., Hodzic, A., and Vautard, R.: Aerosol distribution over the western Mediterranean basin during a Tramontane/Mistral event, Annales Geophysicae, 25, 2271-2291, 2007.

Sander, S., Golden, D., Kurylo, M., Moortgat, G., Wine, P., Ravishankara, A., Kolb, C., Molina, M., Finlayson-Pitts, B., and Huie, R.: Chemical kinetics and photochemical data for use in atmospheric studies evaluation number 15, Pasadena, CA: Jet Propulsion Laboratory, National Aeronautics and Space …, 2006.

Sandu, A. and Sander, R.: Simulating chemical systems in Fortran90 and Matlab with the Kinetic PreProcessor KPP-2.1, Atmospheric Chemistry and Physics, 6, 187-195, 2006.

Sarwar, G., Simon, H., Bhave, P., and Yarwood, G.: Examining the impact of heterogeneous nitryl chloride production on air quality across the United States, Atmospheric Chemistry and Physics, 12, 6455-6473, 2012.

Schaap, M., Van Loon, M., Ten Brink, H., Dentener, F., and Builtjes, P.: Secondary inorganic aerosol simulations for Europe with special attention to nitrate, Atmospheric Chemistry and Physics, 4, 857-874, 2004.

Schaap, M., Kranenburg, R., Curier, L., Jozwicka, M., Dammers, E., and Timmermans, R.: Assessing the sensitivity of the OMI-NO2 product to emission changes across Europe, Remote Sensing, 5, 4187-4208, 2013.

Schaap, M., Manders, A. M. M., Hendriks, E. C. J., Cnossen, J. M., Segers, A. J. S., Denier van der Gon, H., Jozwicka, M., Sauter, F. J., Velders, G. J. M., Matthijsen, J., and Builtjes, P. J. H.: Regional Modelling of Particulate Matter for the Netherlands Netherlands Research Program on Particulate Matter, ISSN: 1875-2314, 2009.

Schell, B., Ackermann, I. J., Hass, H., Binkowski, F. S., and Ebel, A.: Modeling the formation of secondary organic aerosol within a comprehensive air quality model system, Journal of Geophysical Research: Atmospheres, 106, 28275-28293, 2001a.

Schell, B., Ackermann, I. J., Hass, H., Binkowski, F. S., and Ebel, A.: Modelling the formation of secondary organic within a comprehensive air quality model system, J. Geophys. Res., 106, 28275-28293, 2001b.

Schutgens, N. A. J., Miyoshi, T., Takemura, T., and Nakajima, T.: Applying an ensemble Kalman filter to the assimilation of AERONET observations in a global aerosol transport model, Atmos. Chem. Phys., 10, 2561-2576, 10.5194/acp-10-2561-2010, 2010.

Seinfeld, J. H. and Pandis, S. N.: Atmospheric Chemistry and Physics, From Air Pollution to Climate Change., New York, USA.1998.

Shaddick, G., Salter, J. M., Peuch, V.-H., Ruggeri, G., Thomas, M. L., Mudu, P., Tarasova, O., Baklanov, A., and Gumy, S.: Global air quality: An inter-disciplinary approach to exposure assessment for burden of disease analyses, Atmosphere, 12, 48, 2020.

Shrivastava, M. K., Lane, T. E., Donahue, N. M., Pandis, S. N., and Robinson, A. L.: Effects of gas particle partitioning and aging of primary emissions on urban and regional organic aerosol concentrations, Journal of Geophysical Research: Atmospheres, 113, 2008.

Sič, B., El Amraoui, L., Marécal, V., Josse, B., Arteta, J., Guth, J., Joly, M., and Hamer, P.: Modelling of primary aerosols in the chemical transport model MOCAGE: Development and evaluation of aerosol physical parameterizations, Geoscientific Model Development, 8, 381-408, 2015.

Silibello, C., Calori, G., Brusasca, G., Giudici, A., Angelino, E., Fossati, G., Peroni, E., and Buganza, E.: Modelling of PM10 concentrations over Milano urban area using two aerosol modules, Environmental Modelling & Software, 23, 333-343, 2008.

1940 Silver, J. D., Christensen, J. H., Kahnert, M., Robertson, L., Rayner, P. J., and Brandt, J.: Multi-species chemical data
1941 assimilation with the Danish Eulerian hemispheric model: system description and verification, Journal of Atmospheric
1942 Chemistry, 73, 261-302, 2016.

1943 Simpson, D., Guenther, A., Hewitt, C., and Steinbrecher, R.: Biogenic emissions in Europe 1. Estimates and uncertainties, J.
1944 Geophys. Res., 100, 22875–22890, 1995.

1945 Simpson, D., Fagerli, H., Jonson, J., Tsyro, S., Wind, P., and Tuovinen, J.-P.: The EMEP Unified Eulerian Model. Model
1946 Description, The Norwegian Meteorological Institute, EMEP, Oslo, 2003.

1947 Simpson, D., Bergström, R., Briolat, A., Imhof, H., Johansson, J., Priestley, M., and Valdebenito, A.: GenChem v1. 0–a
1948 chemical pre-processing and testing system for atmospheric modelling, Geoscientific Model Development, 13, 6447-6465,
1949 2020a.

1950 Simpson, D., Benedictow, A., Berge, H., Bergstrom, R., Emberson, L. D., Fagerli, H., Flechard, C. R., Hayman, G. D.,
1951 Gauss, M., Jonson, J. E., Jenkin, M. E., Nyiri, A., Richter, C., Semeena, V. S., Tsyro, S., Tuovinen, J. P., Valdebenito, A.,
1952 and Wind, P.: The EMEP MSC-W chemical transport model - technical description, Atmos. Chem. Phys., 12, 7825-7865,
1953 2012.

1954 Simpson, D., Fagerli, H., Colette, A., Denier van der Gon, H., Dore, C., Hallquist, M., Hansson, H.-C., Maas, R., Rouil, L.,
1955 Allemand, N., Bergström, B., Bessagnet, B., Couvidat, F., El Haddad, I., Genberg Safont, J., Goile, F., Grieshop, A.,
1956 Fraboulet, I., Hallquist, A., Hamilton, J., Juhrich, K., Klimont, Z., Kregar, Z., Mawdsely, I., Megaritis, A., Ntziachristos, L.,
1957 Pandis, S., Prévôt, A. S. H., Schindlbacher, S., Seljeskog, M., Sirina-Leboine, N., Sommers, J., and Åström, S.: How should
1958 condensables be included in PM emission inventories reported to EMEP/CLRTAP?, EMEP, Oslo, 2020b.

1959 Slinn, W., Hasse, L., Hicks, B., Hogan, A., Lal, D., Liss, P., Munnich, K., Sehmel, G., and Vittori, O.: Some aspects of the
1960 transfer of atmospheric trace constituents past the air-sea interface, Atmospheric Environment (1967), 12, 2055-2087, 1978.

1961 Slinn, W. G. N.: Precipitation scavenging, US. Department of Energy, Washington, D.C., 1983.

1962 Smagorinsky, J.: General circulation experiments with the primitive equations: I. The basic experiment, Monthly weather
1963 review, 91, 99-164, 1963.

1964 Soares, J., Sofiev, M., Geels, C., Christensen, J. H., Andersson, C., Tsyro, S., and Langner, J.: Impact of climate change on
1965 the production and transport of sea salt aerosol on European seas, Atmospheric Chemistry and Physics, 16, 13081-13104,
1966 2016.

1967 Sofiev, M.: A model for the evaluation of long-term airborne pollution transport at regional and continental scales,
1968 Atmospheric Environment, 34, 2481-2493, 2000.

1969 Sofiev, M.: Extended resistance analogy for construction of the vertical diffusion scheme for dispersion models, Journal of
1970 Geophysical Research: Atmospheres, 107, ACH 10-11-ACH 10-18, 2002.

1971 Sofiev, M.: On possibilities of assimilation of near-real-time pollen data by atmospheric composition models, Aerobiologia,
1972 35, 523-531, 2019.

1973 Sofiev, M., Galperin, M., and Genikhovich, E.: Construction and evaluation of Eulerian dynamic core for the air quality and
1974 emergency modelling system SILAM

1975   NATO Science for peace and security, Series C: Environmental Security, Air pollution modelling and its application, XIX,
1976   Springer, 699-701 pp.2008.

1977   Sofiev, M., Genikhovich, E., Keronen, P., and Vesala, T.: Diagnosing the surface layer parameters for dispersion models
1978   within the meteorological-to-dispersion modeling interface, Journal of applied meteorology and climatology, 49, 221-233,
1979   2010.

1980   Sofiev, M., Soares, J., Prank, M., de Leeuw, G., and Kukkonen, J.: A regional-to-global model of emission and transport of
1981   sea salt particles in the atmosphere, J. Geophys. Res., 116, doi:10.1029/2010JD014713, 2011.

1982   Sofiev, M., Vira, J., Kouznetsov, R., Prank, M., Soares, J., and Genikhovich, E.: Construction of an Eulerian atmospheric
1983   dispersion model based on the advection algorithm of M. Galperin: dynamic cores v. 4 and 5 of SILAM v. 5.5, Geoscientific
1984   Model Development Discussions, 8, 2015a.

1985   Sofiev, M., Siljamo, P., Ranta, H., Linkosalo, T., Jaeger, S., Rasmussen, A., Rantio-Lehtimaki, A., Severova, E., and
1986   Kukkonen, J.: A numerical model of birch pollen emission and dispersion in the atmosphere. Description of the emission
1987   module, International journal of biometeorology, 57, 45-58, 2013.

1988   Sofiev, M., Berger, U., Prank, M., Vira, J., Arteta, J., Belmonte, J., Bergmann, K. C., Chéroux, F., Elbern, H., Friese, E.,
1989   Galan, C., Gehrig, R., Khvorostyanov, D., Kranenburg, R., Kumar, U., Marécal, V., Meleux, F., Menut, L., Pessi, A. M.,
1990   Robertson, L., Ritenberga, O., Rodinkova, V., Saarto, A., Segers, A., Severova, E., Sauliene, I., Siljamo, P., Steensen, B. M.,
1991   Teinemaa, E., Thibaudon, M., and Peuch, V. H.: MACC regional multi-model ensemble simulations of birch pollen
1992   dispersion in Europe, Atmos. Chem. Phys., 15, 8115-8130, 10.5194/acp-15-8115-2015, 2015b.

1993   Sofieva, S., Asmi, E., Atanasova, N. S., Heikkinen, A. E., Vidal, E., Duplissy, J., Romantschuk, M., Kouznetsov, R.,
1994   Kukkonen, J., and Bamford, D. H.: Effects of temperature and salinity on sea-spray-aerosol formation simulated with a
1995   bubble-generating chamber, Atmospheric Measurement Techniques Discussions, 2022, 1-40, 2022.

1996   Spada, M.: Development and evaluation of an atmospheric aerosol module implemented within the NMMB/BSC-CTM,
1997   2015.

1998   Spada, M., Jorba, O., Pérez García-Pando, C., Janjic, Z., and Baldasano, J. M.: Modeling and evaluation of the global sea-
1999   salt aerosol distribution: sensitivity to size-resolved and sea-surface temperature dependent emission schemes, Atmos. Chem.
2000   Phys., 13, 11735-11755, 10.5194/acp-13-11735-2013, 2013.

2001   Stockwell, W. R., Kirchner, F., Kuhn, M., and Seefeld, S.: A new mechanism for regional atmospheric chemistry modeling,
2002   Journal of Geophysical Research: Atmospheres, 102, 25847-25879, 1997.

2003   Strand, A. and Hov, O.: A two-dimensional global study of tropospheric ozone production, J Geophys Res 99, 22877-22895,
2004   1994.

2005   Struzewska, J. and Kaminski, J.: Formation and transport of photooxidants over Europe during the July 2006 heat wave–
2006   observations and GEM-AQ model simulations, Atmospheric Chemistry and Physics, 8, 721-736, 2008.

2007   Struzewska, J. and Kaminski, J.: Impact of urban parameterization on high resolution air quality forecast with the GEM–AQ
2008   model, Atmospheric Chemistry and Physics, 12, 10387-10404, 2012.

2009 Struzewska, J., Kaminski, J., and Jefimow, M.: Application of model output statistics to the GEM-AQ high resolution air
2010 quality forecast, Atmospheric Research, 181, 186-199, 2016.

2011 Struzewska, J., Zdunek, M., Kaminski, J., Łobocki, L., Porebska, M., Jefimow, M., and Gawuc, L.: Evaluation of the GEM-
2012 AQ model in the context of the AQMEII Phase 1 project, Atmospheric Chemistry and Physics, 15, 3971-3990, 2015.

2013 Szymankiewicz, K., Kaminski, J. W., and Struzewska, J.: Interannual variability of tropospheric NO 2 column over Central
2014 Europe—Observations from SCIAMACHY and GEM-AQ model simulations, Acta Geophysica, 62, 915-929, 2014.

2015 Thürkow, M., Kirchner, I., Kranenburg, R., Timmermans, R., and Schaap, M.: A multi-meteorological comparison for
2016 episodes of PM10 concentrations in the Berlin agglomeration area in Germany with the LOTOS-EUROS CTM, Atmospheric
2017 Environment, 244, 117946, 2021.

2018 Tie, X., Madronich, S., Walters, S., Zhang, R., Rasch, P., and Collins, W.: Effect of clouds on photolysis and oxidants in the
2019 troposphere, Journal of Geophysical Research: Atmospheres, 108, 2003.

2020 Timmermans, R., van Pinxteren, D., Kranenburg, R., Hendriks, C., Fomba, K., Herrmann, H., and Schaap, M.: Evaluation of
2021 modelled LOTOS-EUROS with observational based PM10 source attribution, Atmospheric Environment: X, 14, 100173,
2022 2022.

2023 Troen, I. and Mahrt, L.: A simple model of the atmospheric boundary layer: Sensitivity to surface evaporation, Bound.-Layer
2024 Meteorol., 37, 129-148, 1986.

2025 Tsyro, S., Aas, W., Soares, J., Sofiev, M., Berge, H., and Spindler, G.: Modelling of sea salt concentrations over Europe: key
2026 uncertainties and comparison with observations, Atmos. Chem. Phys., 11, 10367–10388, doi:10.5194/acp-11-10367-2011,
2027 2011.

2028 Tuovinen, J.-P., Ashmore, M., Emberson, L., and Simpson, D.: Testing and improving the EMEP ozone deposition module,
2029 Atmos. Environ., 38, 2373–2385, 2004.

2030 van Leer, B.: Multidimensional explicit difference schemes for hyperbolic conservation laws, in: Computing Methods in
2031 Applied Sciences and Engineering VI, edited by: Lions, R. G. a. J. L., Elsevier, Amsterdam, 1984.

2032 Van Ulden, A. and Holtslag, A.: Estimation of atmospheric boundary layer parameters for diffusion applications, Journal of
2033 Applied Meteorology and Climatology, 24, 1196-1207, 1985.

2034 Van Zanten, M., Sauter, F., RJ, W. K., Van Jaarsveld, J., and Van Pul, W.: Description of the DEPAC module: Dry
2035 deposition modelling with DEPAC_GCN2010, RIVM rapport 680180001, 2010.

2036 Vautard, R., Bessagnet, B., Chin, M., and Menut, L.: On the contribution of natural Aeolian sources to particulate matter
2037 concentrations in Europe: Testing hypotheses with a modelling approach, Atmospheric Environment, 39, 3291-3303,
2038 https://doi.org/10.1016/j.atmosenv.2005.01.051, 2005.

2039 Venkatram, A.: Estimating the Monin-Obukhov length in the stable boundary layer for dispersion calculations, Boundary-
2040 Layer Meteorology, 19, 481-485, 1980.

2041 Venkatram, A., Karamchandani, P., and Misra, P.: Testing a comprehensive acid deposition model, Atmospheric
2042 Environment (1967), 22, 737-747, 1988.

Vira, J. and Sofiev, M.: On variational data assimilation for estimating the model initial conditions and emission fluxes for short-term forecasting of SOx concentrations, Atmospheric environment, 46, 318-328, 2012.

Vira, J. and Sofiev, M.: Assimilation of surface NO 2 and O 3 observations into the SILAM chemistry transport model, Geoscientific Model Development, 8, 191-203, 2015.

Wang, X., Zhang, L., and Moran, M. D.: Development of a new semi-empirical parameterization for below-cloud scavenging of size-resolved aerosol particles by both rain and snow, Geoscientific Model Development, 7, 799-819, 2014.

Weaver, A. and Courtier, P.: Correlation modelling on the sphere using a generalized diffusion equation, Quarterly Journal of the Royal Meteorological Society, 127, 1815-1846, 2001.

Wesely, M. L.: Parameterization of surface resistances to gaseous dry deposition in regional-scale numerical models, Atmospheric Environment (1967), 23, 1293-1304, 1989.

Wild, O., Zhu, X., and Prather, M. J.: Fast-J: Accurate Simulation of In- and Below-Cloud Photolysis in Tropospheric Chemical Models, Journal of Atmospheric Chemistry, 37, 245-282, 10.1023/A:1006415919030, 2000.

Williams, E., Guenther, A., and Fehsenfeldi, F.: An inventory of nitric oxide emissions from soils in the United States, Journal of Geophysical Research: Atmospheres, 97, 7511-7519, 1992.

Williamson, D. L. and Rasch, P. J.: Two-dimensional semi-Lagrangian transport with shape-preserving interpolation, Monthly Weather Review, 117, 102-129, 1989.

Willis, P. T. and Tattelman, P.: Drop-size distributions associated with intense rainfall, Journal of Applied Meteorology and Climatology, 28, 3-15, 1989.

Xian, P., Reid, J. S., Hyer, E. J., Sampson, C. R., Rubin, J. I., Ades, M., Asencio, N., Basart, S., Benedetti, A., and Bhattacharjee, P. S.: Current state of the global operational aerosol multi-model ensemble: An update from the International Cooperative for Aerosol Prediction (ICAP), Quarterly Journal of the Royal Meteorological Society, 145, 176-209, 2019.

Yamartino, R., Scire, J., Carmichael, G., and Chang, Y.: The CALGRID mesoscale photochemical grid model—I. Model formulation, Atmospheric Environment. Part A. General Topics, 26, 1493-1512, 1992.

Yamartino, R. J., Flemming, J., and Stern, R.: Adaptation of analytic diffusivity formulations to Eulerian grid model layers of finite thickness, in: Air Pollution Modeling and Its Application XVII, Springer, 468-477, 2007.

Yarwood. G., Rao, S., Yocke, M., and Whitten, G. Z.: Updates to the Carbon Bond chemical mechanism: CB05, http://www.camx.com/publ/pdfs/CB05_Final_Report_120805.pdf, 2005.

Yienger, J. and Levy, H.: Empirical model of global soil-biogenic NOχ emissions, Journal of Geophysical Research: Atmospheres, 100, 11447-11464, 1995.

Yuan, H., Dai, Y., Xiao, Z., Ji, D., and Shangguan, W.: Reprocessing the MODIS Leaf Area Index Products for Land Surface and Climate Modelling, Remote Sensing of Environment, 155, 1171–1187, doi:10.1016/j.rse.2011.01.001, 2011.

Zare, A., Christensen, J., Irannejad, P., and Brandt, J.: Evaluation of two isoprene emission models for use in a long-range air pollution model, Atmospheric Chemistry and Physics, 12, 7399-7412, 2012.

Zare, A., Christensen, J., Gross, A., Irannejad, P., Glasius, M., and Brandt, J.: Quantifying the contributions of natural emissions to ozone and total fine PM concentrations in the Northern Hemisphere, Atmospheric Chemistry and Physics, 14, 2735-2756, 2014.

Zender, C. S., Bian, H., and Newman, D.: Mineral Dust Entrainment and Deposition (DEAD) model: Description and 1990s dust climatology, Journal of Geophysical Research: Atmospheres, 108, 10.1029/2002jd002775, 2003.

Zhang, K. M., Knipping, E. M., Wexler, A. S., Bhave, P. V., and Tonnesen, G. S.: Size distribution of sea-salt emissions as a function of relative humidity, Atmospheric Environment, 39, 3373-3379, https://doi.org/10.1016/j.atmosenv.2005.02.032, 2005.

Zhang, L., Brook, J. R., and Vet, R.: A revised parameterization for gaseous dry deposition in air-quality models, Atmos. Chem. Phys., 3, 2067–2082, 2003.

Zhang, L., Gong, S., Padro, J., and Barrie, L.: A size-segregated particle dry deposition scheme for an atmospheric aerosol module, Atmospheric Environment, 35, 549-560, 2001.

Zhang, Y., Bocquet, M., Mallet, V., Seigneur, C., and Baklanov, A.: Real-time air quality forecasting, part I: History, techniques, and current status, Atmospheric Environment, 60, 632-655, 2012a.

Zhang, Y., Bocquet, M., Mallet, V., Seigneur, C., and Baklanov, A.: Real-time air quality forecasting, part II: State of the science, current research needs, and future prospects, Atmospheric Environment, 60, 656-676, https://doi.org/10.1016/j.atmosenv.2012.02.041, 2012b.

Zilitinkevich, S. and Mironov, D. V.: A multi-limit formulation for the equilibrium depth of a stably stratified boundary layer, Boundary-Layer Meteorology, 81, 325-351, 1996.